UNIVERSITA' DEGLI STUDI DI ROMA
"LA SAPIENZA"

FACOLTA' DI SCIENZE MATEMATICHE,
FISICHE E NATURALI

Dottorato di Ricerca in Scienze Chimiche
- Curriculum "Chimica macromolecolare e biologica" -

XVII CICLO (2001-2004)

"Polycyclic aromatic compounds able to induce and stabilize G-quadruplex DNA structures as new telomerase inhibitors: synthesis, physicochemical properties and biochemical studies"

Supervisori:

Prof. Giancarlo Ortaggi

Prof.ssa Maria Savino

Dottorando:

Dott. Marco Franceschin

INDEX

1. Introduction

1.1. Telomeres structure and function

Telomeres are terminal protein-DNA complexes forming capping structures that function to stabilize chromosomal ends and prevent them from being recognized by the cell as DNA double strand breaks. Functional telomeres require sufficient numbers of telomeric DNA repeats, as well as the proper repertoire and amounts of telomere associated proteins; mutation or loss of either can lead to "uncapping" and telomere dysfunction (Saldanha *et al.* **2003**, Karlseder **2003**). In particular, mammalian telomeres consist of tandem repeats of the six nucleotides TTAGGG, which are repeated for 5–25 kilobase pairs in length 5' to 3' toward the chromosome end (de Lange *et al.* **1990**). Several recent studies have suggested that the structure of the ends of telomeres may be more complex than originally thought. Griffith and colleagues have found that telomeres do not end in a linear manner (Griffith *et al.* **1999**). Instead, the end of the telomere can form a loop structure with the 3' G-rich strand (referred to as the T-loop), invading the duplex telomeric repeats and forming a displacement loop (D-loop, Fig. 1.1-1). Telomere-associated proteins may facilitate the formation and maintenance of both the T- and D-loops, suggesting the presence of a large DNA-protein structure at the end of each chromosome. In addition, most human telomeres appear to terminate in a single-stranded 3' GT-rich overhang, which is thought to play an important role in telomere structure and function (Wright *et al.* **1997**). The atomic-level structural details of the loop are not known, but the 3' overhang must be incorporated in some manner into the terminal part of the double-stranded telomeric region. Fig. 1.1-2 shows the T-loop/D-loop with the array of telomeric proteins that have been identified to date as having direct or indirect association

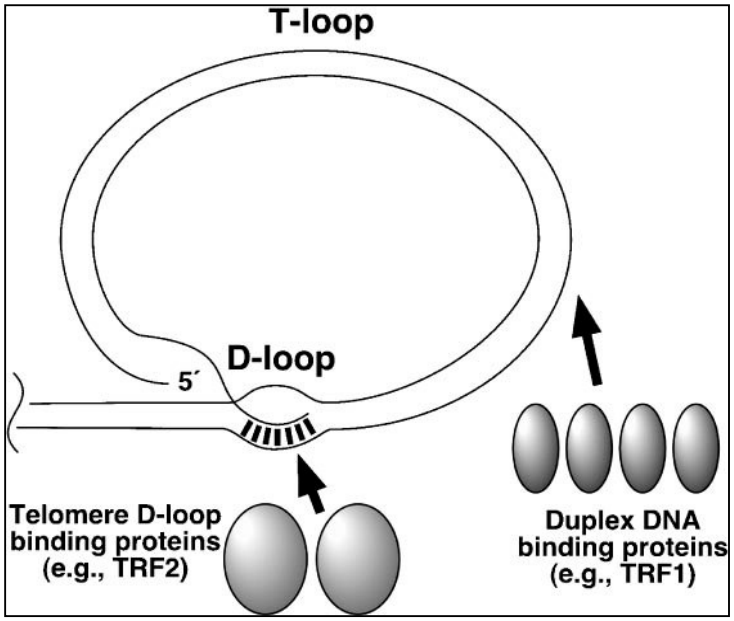

Fig. 1.1-1: Schematic representation of the T-loop/D-loop model for human telomeres capping structure (Rezler *et al.* **2003**).

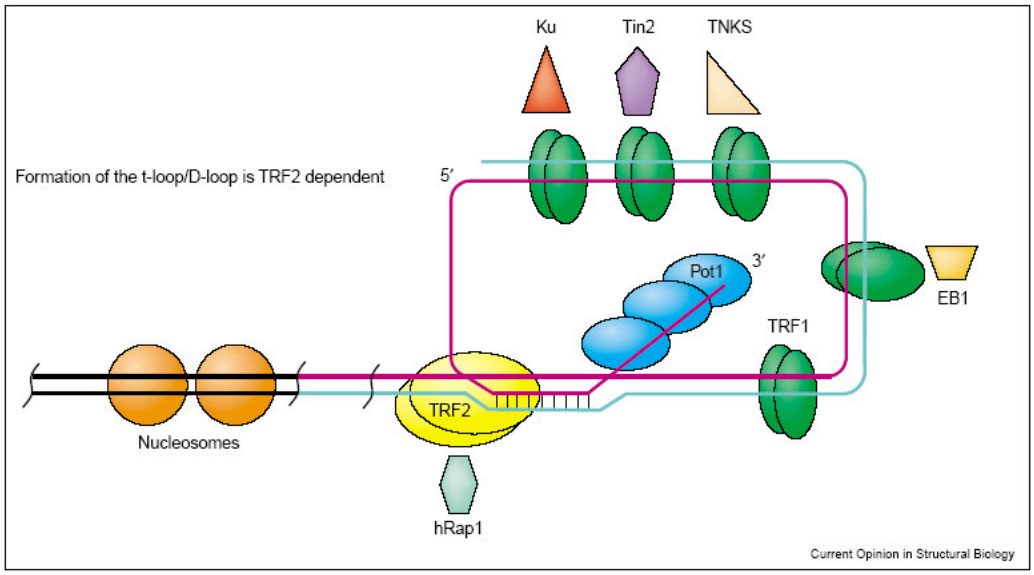

Fig. 1.1-2: The end of the human chromosome: the telomeric T-loop/D-loop model, showing known telomeric proteins (Neidle *et al.* **2003**).

with telomeric DNA (Neidle *et al.* **2003**). TRF1 and TRF2 are both associated with and critical to the formation of the T-loop and D-loop structures. They bind specifically to telomeric double-stranded DNA and the loss of functional TRF2 in human cells results in the generation of end-to-end chromosomal fusions (Stansel *et al.* **2001**). Of particular interest is the human protein hPot1, which has been shown to specifically bind to the single-stranded 3' overhang of the human telomeric sequence and has been identified in many species, playing an as yet undetermined role in the capping of chromosomes. However, deletion of the *pot1*$^{+}$ gene results in the loss of telomeric DNA and end-to-end chromosomal fusions (Baumann *et al.* **2001**).

In addition to protecting chromosomes from end-to-end fusion, telomeres are also thought to avoid the loss of DNA at the end of each chromosome upon the completion of DNA replication. In fact, dividing cells have been shown to undergo a progressive loss of 25–200 DNA base pairs following each cell division (Harley *et al.* **1990**). This loss of telomeric DNA is largely due to the "end replication problem" (Fig. 1.1-3), which refers to the inability of the DNA replication machinery to copy the final few base pairs of the lagging strand during DNA synthesis (Watson **1972**). Another possible cause for loss of telomeric sequence is by a 5' to 3' exonuclease activity that recesses the telomeric CA-rich strand (Makarov *et al.* **1997**). Because the telomere consists of a repetitive DNA sequence, its loss is thought to be less important to the cell than the loss of critical gene encoding sequences that may be near the end of a chromosome; therefore, repetitive telomeric sequences protect the cell from the loss of more critical gene encoding sequences (Rezler *et al.* **2003**).

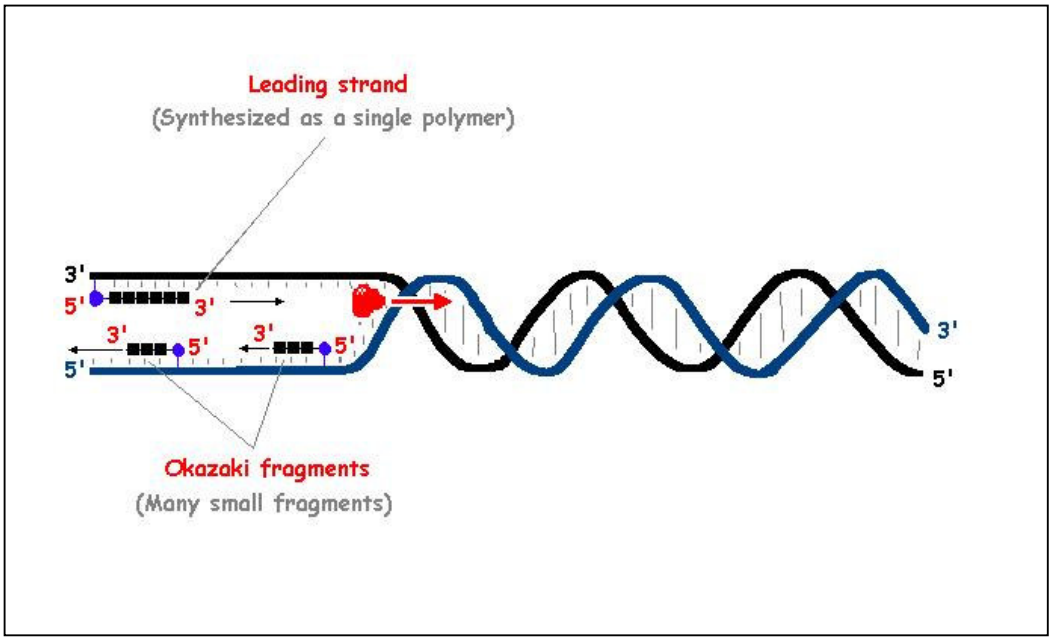

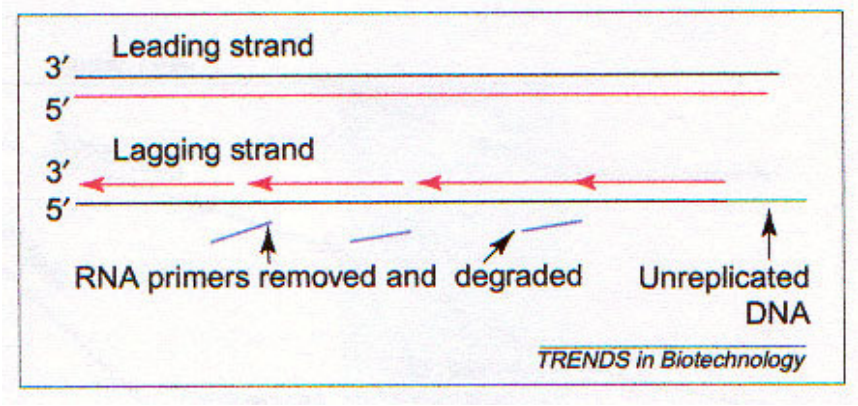

Fig. 1.1-3: End replication problem. DNA replication starts by the unwinding of double stranded DNA at the origin of replication. Synthesis of the new strands of DNA proceeds in the 5′ to 3′ direction. The leading strand is continuous, but the lagging strand is synthesized as a series of short segments of DNA (Okazaki fragments) onto the ends of RNA primers (top). The RNA primers are removed and DNA polymerase fills in the gaps, which are then ligated (not shown). The extreme 3′ end is not replicated leading to DNA loss and the 'end replication problem' (bottom, White *et al.* **2001**).

1.2. G-quadruplex DNA structures

Most of cellular DNA is known to be double stranded; several duplex DNA structures have been known so far (Watson *et al.* **1987**, Fig. 1.2-1). The single-stranded guanine-rich sequences of telomeric DNAs can assume non canonical structures, referred to as G-quadruplex (Neidle *et al.* **2003**). They are four-helices structures based on the G-quartet, in which four guanine bases associate with each other in a stable Hoogsteen hydrogen-bonded arrangement (Fig. 1.2-2). This arrangement, necessarily involving four DNA strands, can result in a variety of four-stranded G-quadruplex structural types, whose features depend on several factors, such as the number of separate strands, the pattern of strand orientation, the nature of the loops connecting the G-tetrads, the nature and concentration of monovalent cations stabilizing the structure and the glycosidic bond conformation (Fig. 1.2-2, Simonsson **2001**, Williamson **1994**). Alkali metal ions (typically sodium or potassium) are necessary for quadruplex stability, because they coordinate the O6 guanine atoms in a G-quartet (Fig. 1.2-3). In general, potassium ions, at physiological concentrations, provide optimal stability. Different metal ions can induce conformational change, which, depending on the quadruplex, can be profound, as in the case of the intramolecular quadruplex formed by the four-repeat sequence d[AGGG(TTAGGG)$_3$]. The NMR structure of the sodium form of the intramolecular quadruplex formed by (almost) four repeats of d(TTAGGG) in the 22-mer sequence d[AGGG(TTAGGG)$_3$] was reported several years ago (Wang *et al.* **1993**). It comprises a core of three G-quartets held together by strands in alternating orientations (Fig. 1.2-4(c,f)). This results in two lateral and one diagonal d(TTA) loop at the G-quartet ends. The crystal structure of the potassium form, crystallised under approximately physiological ionic conditions, shows a strikingly distinct arrangement, with all four strands parallel (Fig.

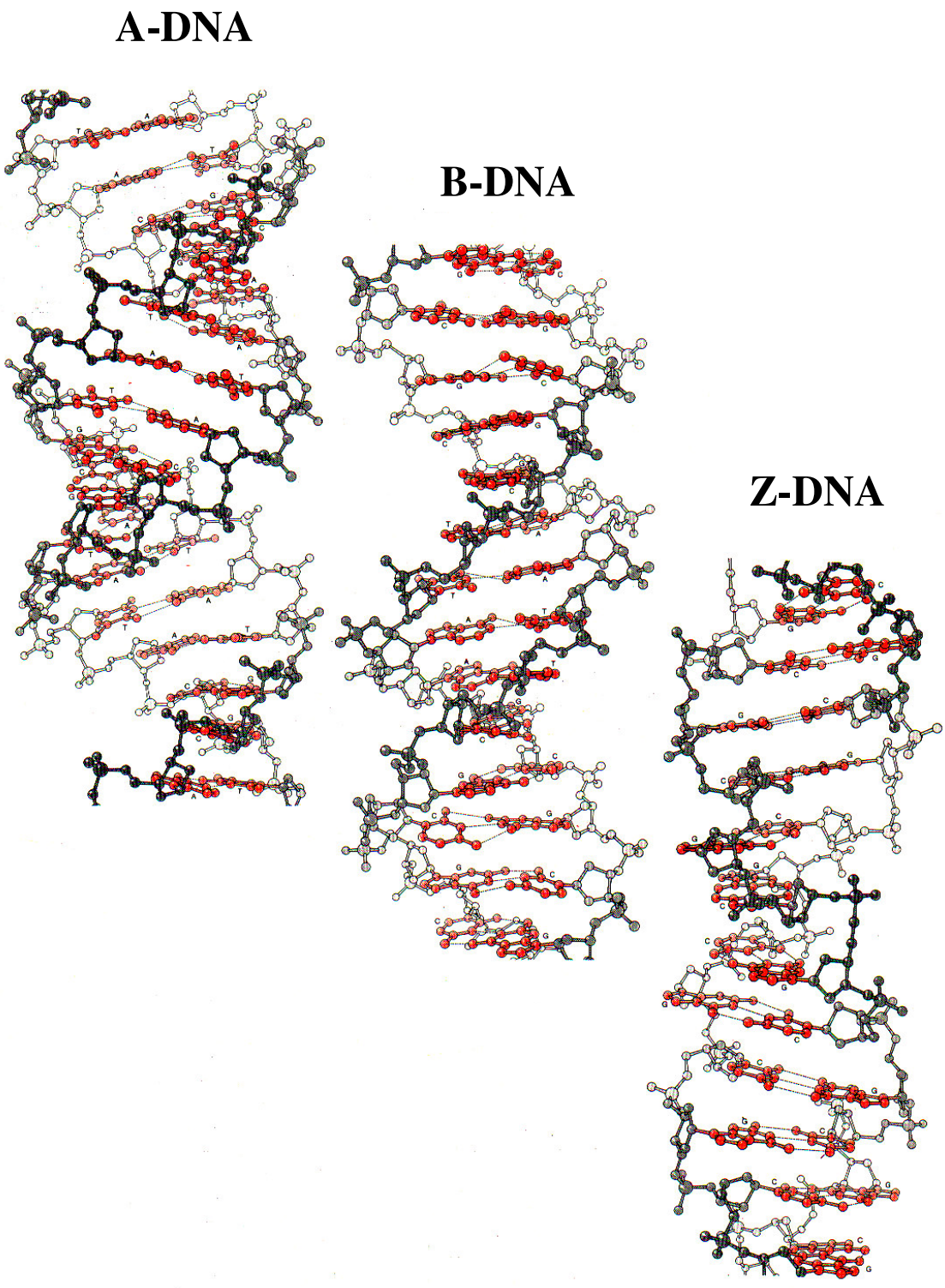

Fig. 1.2-1: A, B and Z-DNA double helix structures. Bases are red, while sugar-phosphate backbone is grey (Watson *et al.* **1987**).

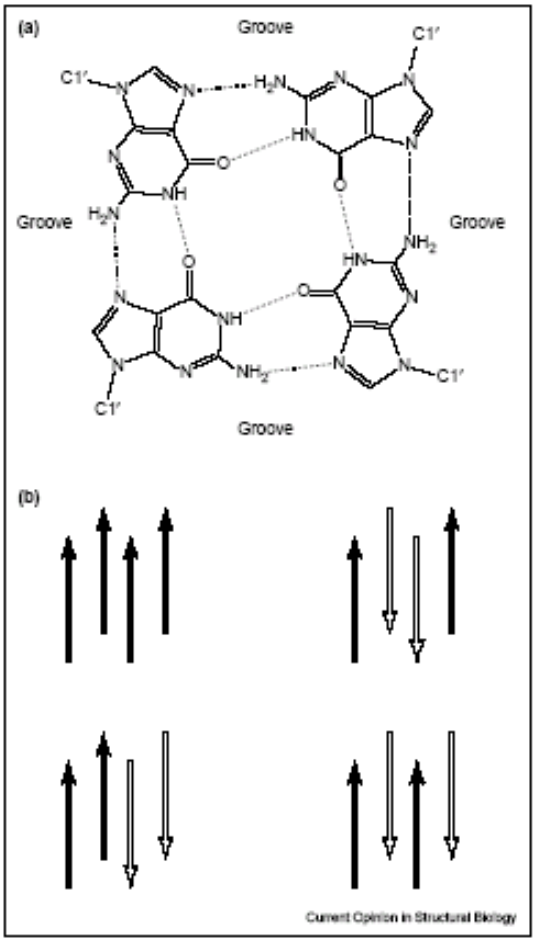

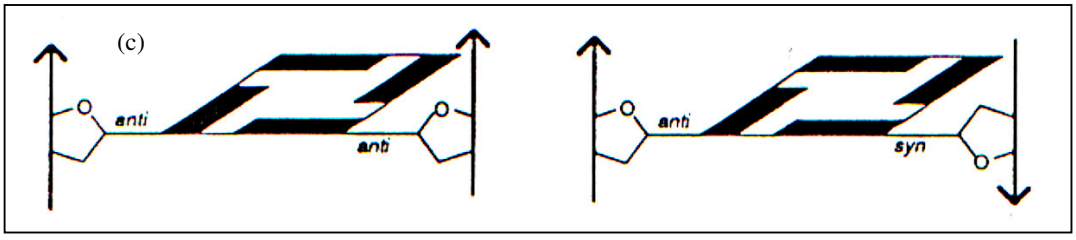

Fig. 1.2-2: The fundamental features of G-quadruplexes: the G-tetrad, strand orientations and glycosidic bond conformations. (a) The arrangement of hydrogen bonds between guanines in a G-tetrad. (b) The possible orientations of four DNA strands (Neidle *et al.* **2003**). (c) *Syn* and *anti* conformations of the glycosidic bond connecting the guanine base to the sugar-phosphate backbone (Williamson **1994**).

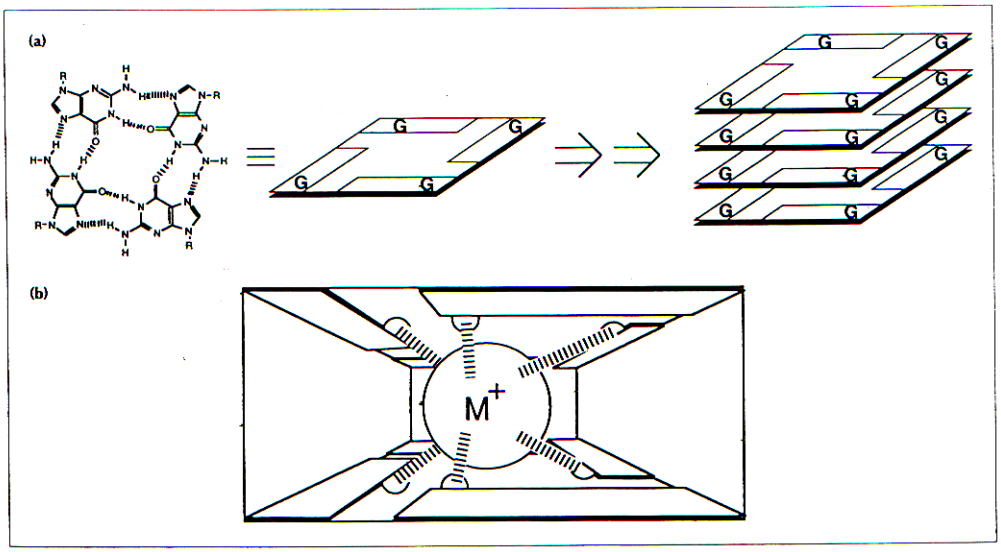

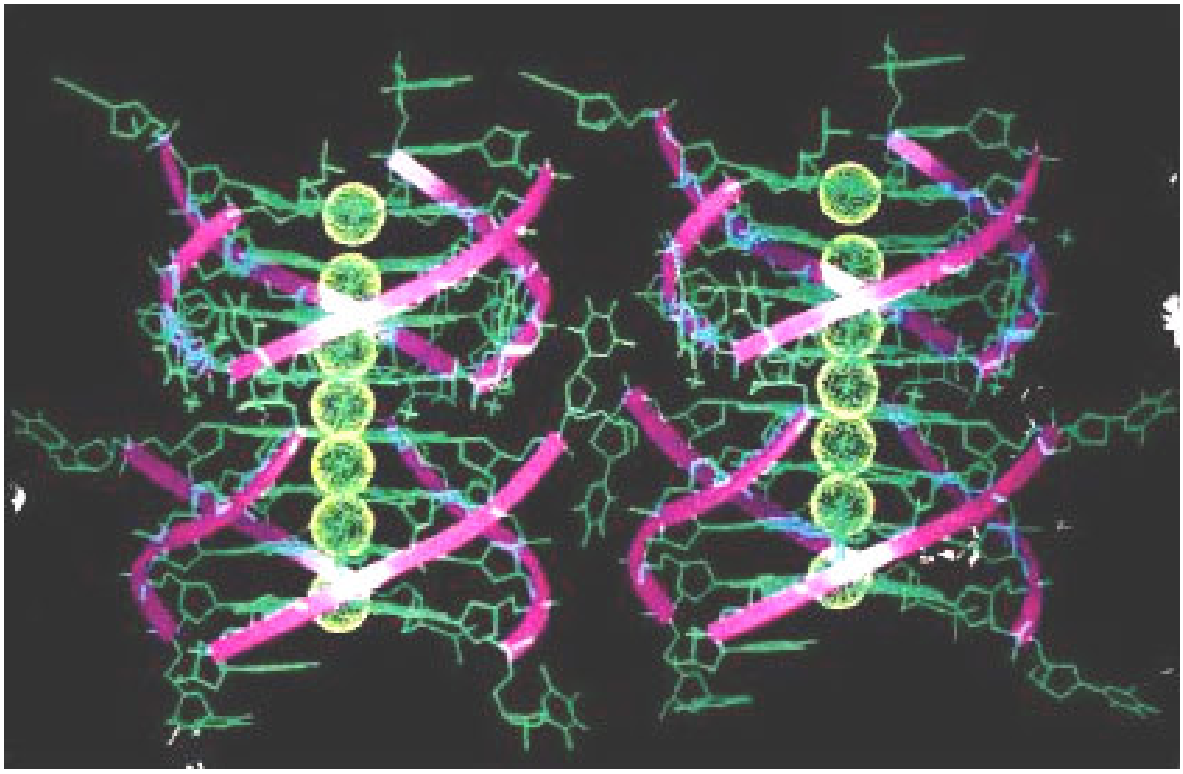

Fig. 1.2-3: Stabilization of G-quadruplex by monovalent cations. Alkali metal ions coordinate the O6 guanine atoms of two adjacent G-quartets (top, Williamson **1993**). X-ray derived G-quadruplex structure for d(TG_4T), in which sodium ions between G-quartets are shown as yellow spheres (bottom, Rhodes *et al.* **1995**).

1.2-4(d,g), Fig. 1.2-5, Parkinson *et al.* **2002**). This results in all three d(TTA) loops being external to the core and positioned alongside the grooves, rather than at the ends of the G-quartet stack. On the contrary, in the case of d(GGGGTTTTGGGG) from the telomeric sequence of *Oxytricha nova*, changes in alkali metal ions do not effect conformational change. In fact, both potassium and sodium forms show a G-quadruplex structure with parallel/antiparallel strand orientations and diagonal loops formed from opposite strands (Fig, 1.2-4(a), Haider *et al.* **2002**). On the other hand, the sequence with one fewer 3' guanine, d(GGGGTTTTGGG), also forms a dimeric quadruplex, but with a distinctive, asymmetric fold involving just three stacked G-quartets, rather than the four in the d(GGGGTTTTGGGG) structure. The two guanines not involved in the G-quartets are unpaired and are involved in stacking interactions with the G-quartet face and a thymine in the adjacent T4 loop (Fig. 1.2-4(b), Crnugelj *et al.* **2002**). This shows that even a minor sequence difference can result in major structural changes to the folding of G-quadruplex (Neidle *et al.* **2003**).

The complementary cytosine-rich strand, in duplex telomeric DNA or other non-telomeric G-rich sequences of the genome, can also form non-standard structures, built upon the i-motif. This category of four-stranded structure is only stable at low pH, as it involves C^+•C base pairs. The NMR structure of a 22-mer cytosine-rich telomere sequence (complementary to the guanine-rich d[$AG_3(T_2AG_3)_3$]) has been reported (Phan *et al.* **2000**). It shows an intramolecularly folded structure with six intercalated C^+•C base pairs (the i-motif part, Fig. 1.2-6) linked by three d(AAT) hairpin-type loops (Fig. 1.2-4(e)).

G-quadruplexes are usually thought to arise only from the folding of single-stranded telomeric DNA, that is, the 3' overhang. However, they may also be formed from duplex telomeric DNA under appropriate ionic and pH conditions (Phan *et al.* **2002**), as well as by the influence of appropriate proteins or ligands. This possibility has been demonstrated in a sequence analogous to that of the telomere, the guanine-rich nuclease hypersensitive promoter

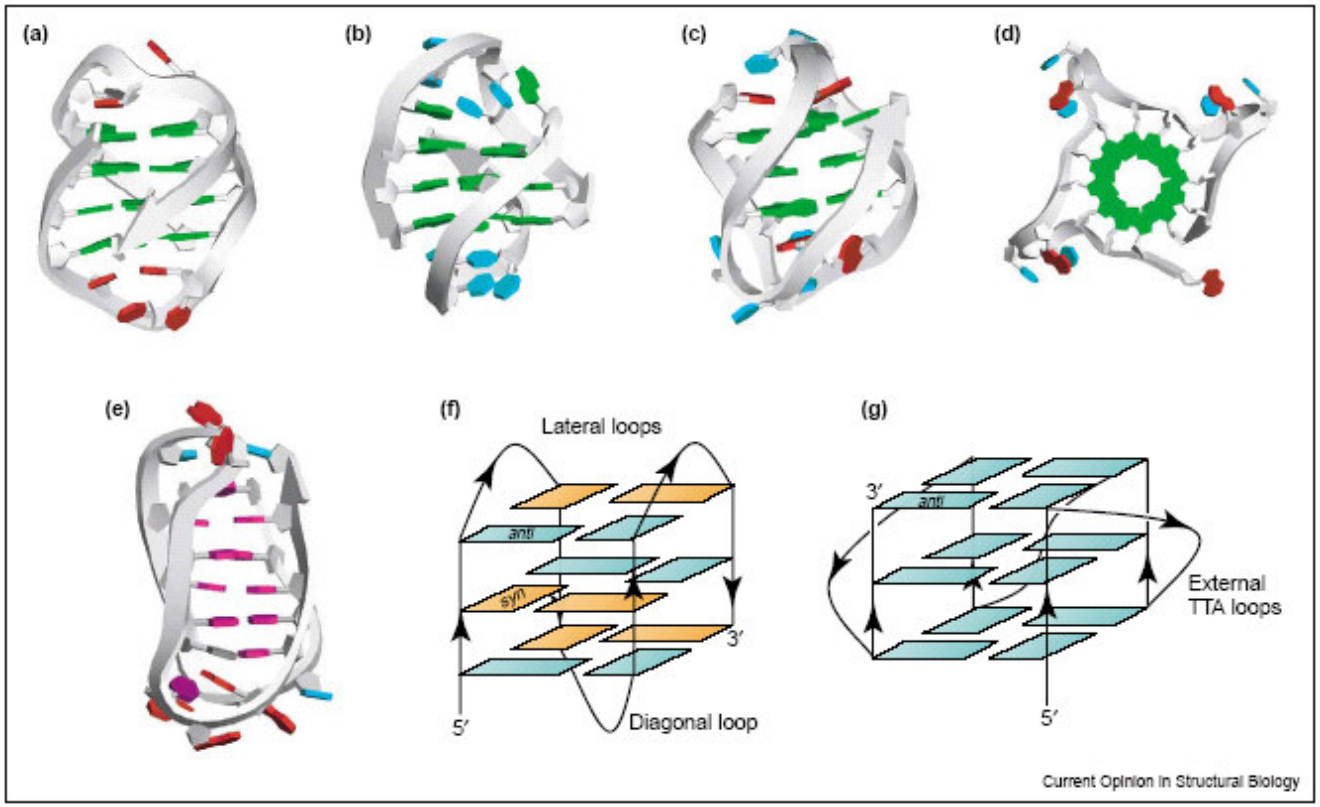

Fig. 1.2-4: Ribbon diagrams of various telomeric DNA quadruplex structures. (a) d($G_4T_4G_4$) from *Oxytricha* (Haider *et al.* **2002**). (b) d($G_4T_4G_3$) (Crnugelj *et al.* **2002**). (c) d[$AG_3(T_2AG_3)_3$] in Na^+ solution (Wang *et al.* **1993**). (d) d[$AG_3(T_2AG_3)_3$] with K^+ in the crystal (Parkinson *et al.* **2002**). (e) d($C_2AT_2C_2AT_2C_2T_3C_2$) in solution - the i-motif (Phan *et al.* **2000**). (f,g) Representations of the folds in structures (c,d), respectively (Neidle *et al.* **2003**).

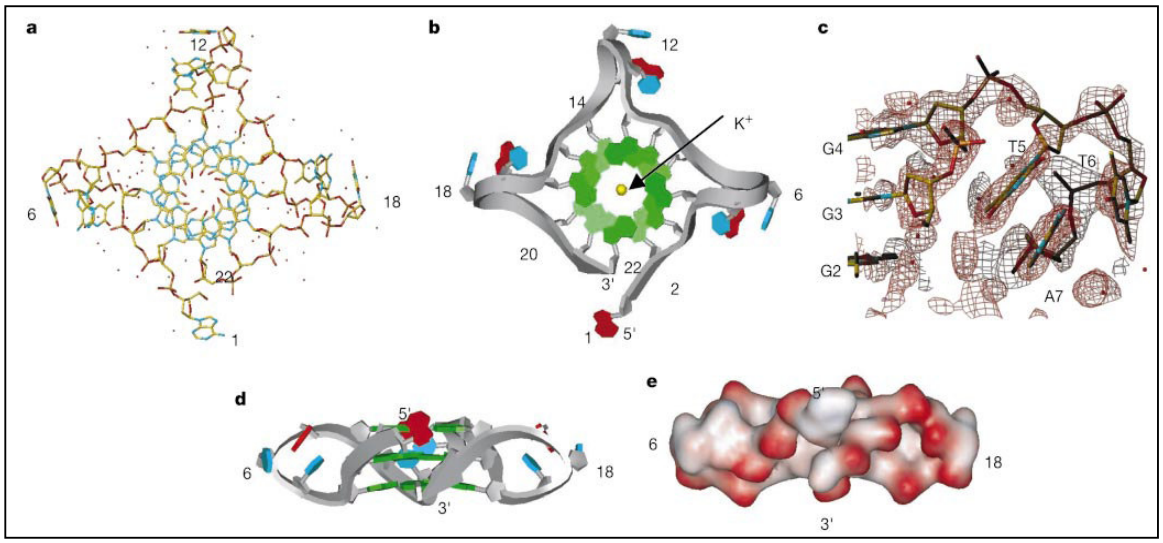

Fig. 1.2-5: Overall folding topology of the 22-mer intramolecular G-quadruplex formed by the sequence d[AGGG(TTTAGGG)$_3$]. (a) Stick representation coloured by atom type and viewed on the 5' face. The central potassium counter ion is coordinated in a bipyramidyl antiprismatic arrangement by the electronegative carbonyl groups of guanine O6. (b) View from the 3' end of the quadruplex looking down the helical axis with the phosphate sugar backbone drawn as a grey ribbon showing 5'-to-3' directionality. Guanines are green, thymines blue, and adenines red. (c) A representative part of the structure around the extended TTA loop region abutting the sides of the G-quadruplex. Overlaid is a ω_A-weighted map using data at 10–2.1 Å resolution contoured at 1.8σ . (d) Side view of the quadruplex highlighting its disc-like shape and positioning of the 3' and 5' strand ends. (e) Space-filling van der Waals contoured representation, coloured by charge, with red surfaces representing regions of negative charge (Parkinson *et al.* **2002**).

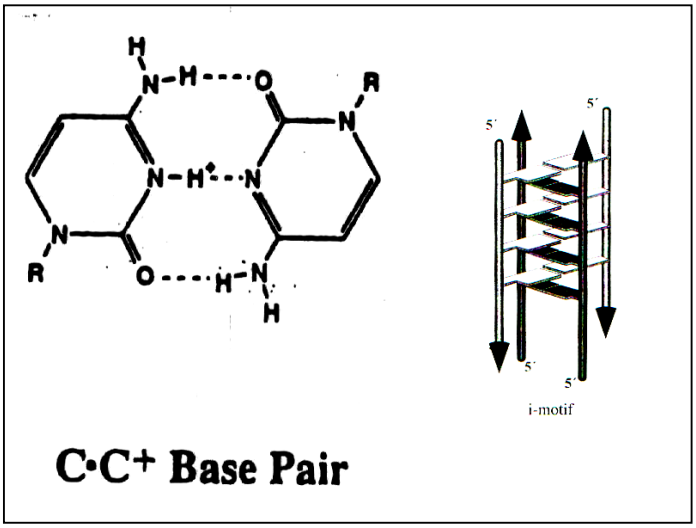

Fig. 1.2-6: C•C$^+$ base pair and schematic representation of the i-motif (Fedoroff *et al.* **2000**).

sequence of the c-*myc* oncogene. The formation of a quadruplex structure, driven by the presence of the quadruplex-binding porphyrin ligand TMPy4, was observed (par. 1.5, Siddiqui-Jain *et al.* **2002**).

The c-*myc* study has also answered the question of the biological existence of quadruplexes, at least in the special context of the c-*myc* promoter sequence. Recently, the existence of telomeric quadruplexes has been demonstrated in the macronuclei of the ciliate *Stylonychia lemnae* using specific antibodies generated against T_4G_4 sequences (Schaffitzel *et al.* **2001**). An analogous study has not yet been reported for human telomeres, although quadruplex-type structures may be involved in telomere loop regions (par. 1.1) and several telomere-associated proteins, such as Cdc13, do bind quadruplex DNA with high affinity (Neidle *et al.* **2003**).

1.3. Telomerase: its role in cellular senescence and cancer

Telomere maintenance is necessary for long-term cell proliferation. In the absence of a specific replication machinery at the telomere ends gradual sequence loss due to incomplete replication of the lagging strand would eventually lead to critically short telomeres and trimming of essential chromosomal sequences (Allsopp *et al.* **1995**). The mechanism whereby cells count divisions uses the gradual erosion of telomeres, which ultimately triggers replicative senescence in many cell types. In order to compensate for this loss, different mechanisms for the addition of new telomere sequences have evolved. In humans, telomere maintenance is mainly performed by a specific reverse transcriptase, telomerase (Mergny *et al.* **2002**). Human telomerase is a ribonucleoprotein (Morin **1989**) composed of a catalytic subunit, hTERT (Nakamura *et al.* **1997**), and a 451 nt long RNA (hTR; also known as hTER or hTERC) (Feng *et al.* **1995**), which contains an 11bp sequence that acts as the template on which telomeric repeats are added to the chromosome. Telomerase is active in the germline, as well as some stem cells, but is inactive in most somatic cells (Kim *et al.* **1994**). Furthermore, recent key experiments demonstrated that: (i) telomerase is sufficient for immortalisation of many cell types (Bodnar *et al.* **1998**) and sufficient to allow transformed cells to escape from crisis (Halvorsen *et al.* **1999**); (ii) inhibition of telomerase limits the growth of human cancer cells (Hahn *et al.* **1999**); (iii) ectopic expression of the telomerase catalytic subunit (hTERT; also known as hEST2 or hTRT) in combination with several oncogenes results in direct tumourigenic conversion of normal human epithelial and fibroblast cells. All these results point to a key role of telomerase in the tumourigenic process. Mutations leading to reactivation or up-regulation of the enzyme may represent a required event in the multistep development of many cancers (Mergny *et al.* **2002**). In some cases

(notably neuroblastomas, gastric and breast tumours), higher levels of telomerase activity are associated with poor prognosis, showing that telomerase could be used as a predictive marker (Hiyama *et al.* **2003**).

In vitro reconstitution of human telomerase is possible in cell extracts with two partners, the template RNA component hTR and the catalytic protein subunit hTERT, but several other proteins are associated with hTERT or hTR and facilitate their folding or assembly (Fig. 1.3-1, Mergny *et al.* **2002**). A unique feature of telomerase is its ability to synthesize long stretches of DNA (often >100 nt) despite the minimal lengths of the templating RNA segment. This ability to synthesize DNA processively depends on two types of movement (Fig. 1.3-2): simultaneous translocation of the RNA–DNA duplex away from the active site following each nucleotide addition (type I) and translocation of the 3' end of the DNA substrate relative to the RNA template (type II). The latter translocation reaction enables telomerase to repeatedly utilize the same set of templating residues for DNA synthesis, thus generating long extension products. The propensity to carry out type I and type II translocation has been referred to as nucleotide addition and repeat addition processivity, respectively (Lue **2004**).

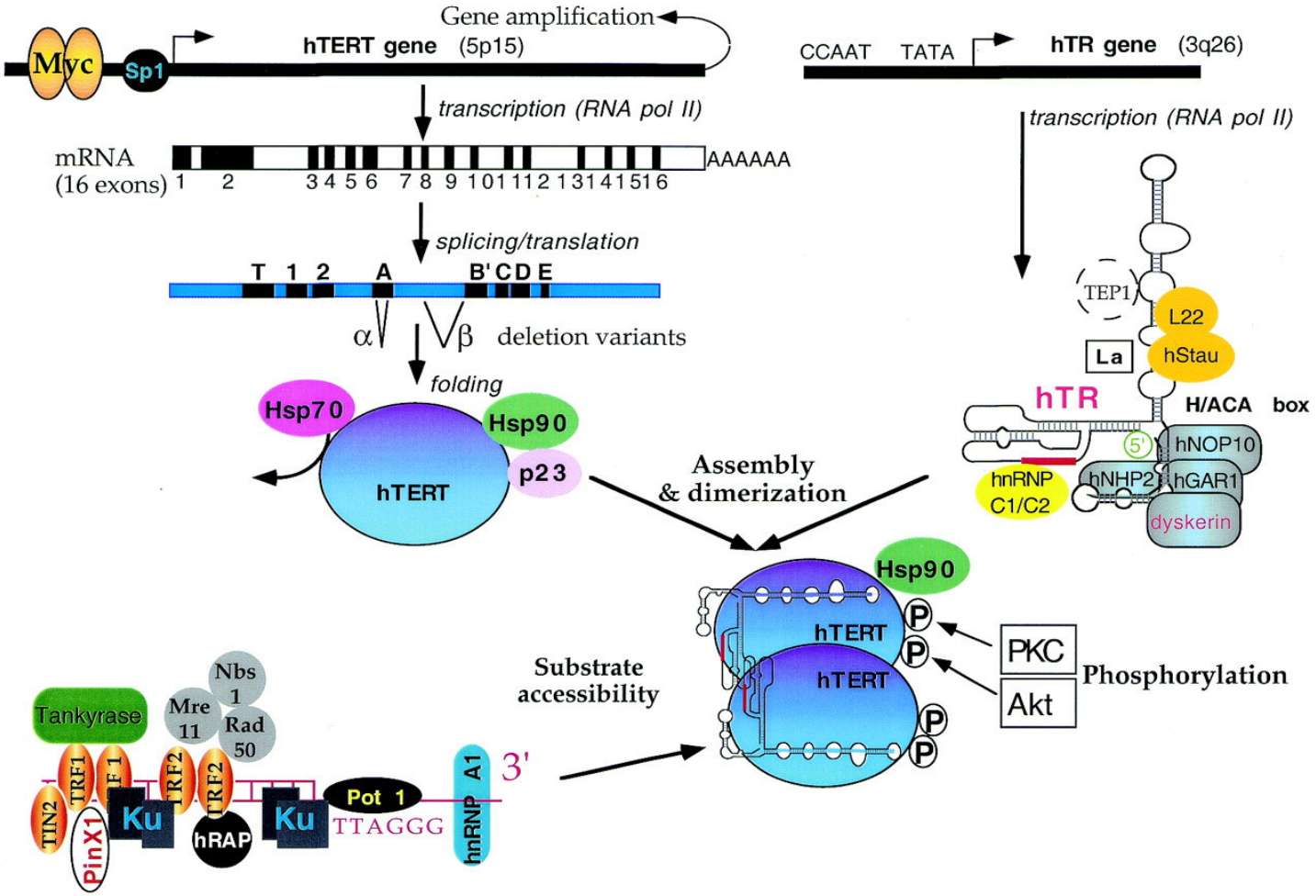

Fig. 1.3-1: Telomerase components. Telomerase is composed of two major components: the catalytic subunit (hTERT) and the template RNA (hTR). Several proteins are associated with hTERT or hTR and facilitate their folding or assembly. Many different proteins interact with telomeric DNA and participate in telomerase recruitment (Mergny *et al.* **2002**).

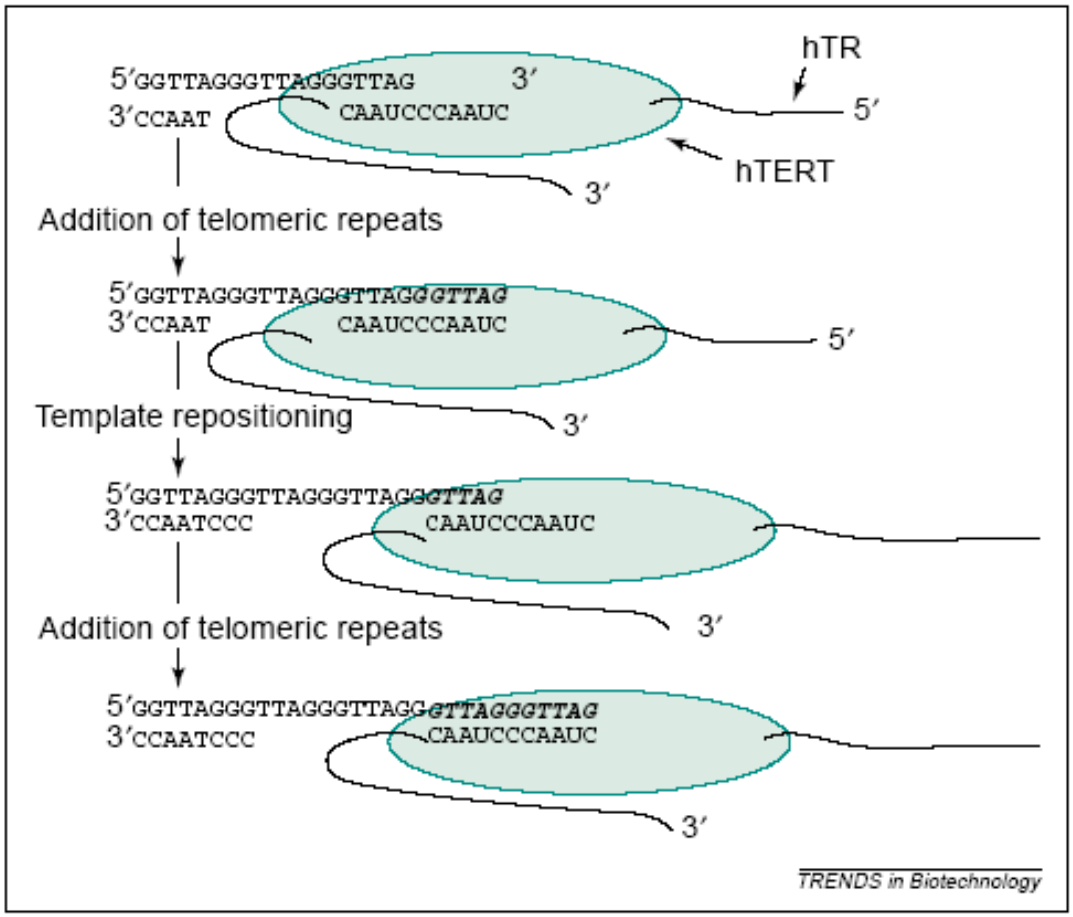

Fig. 1.3-2: The addition of telomeric repeats. Telomerase adds hexameric TTAGGG repeats by attaching to the end of the chromosome and then utilizing its internal template to specify the sequence of added nucleotides. As evidenced by telomerase repeat addition processivity, it then is able to reposition downstream and re-anchor its template for the addition of more telomeric repeats (White *et al.* **2001**).

1.4. Telomerase inhibitors

Telomerase properties described in the previous paragraph make this enzyme a target not only for cancer diagnosis but also for the development of novel therapeutic agents. The expected effects of telomerase inhibition on cancer cells as well as telomerase-positive normal cells are illustrated in Fig. 1.4-1 (White *et al.* **2001**). The classical model for inhibition of telomere maintenance and telomerase activity as a potential anticancer therapy suggests that the inhibition of telomerase in tumour cells will initially only result in telomere shortening at each successive round of replication. This will eventually drive telomerase-positive tumour cells to senescence prior to normal (and germ line) cells, as a consequence of the significantly shorter length of telomeric DNA in the former cells (Incles *et al.* **2003**).

There are some potential concerns that have been raised about telomerase as an anticancer target. First, with many (but not all) telomerase therapeutic approaches, one expects there will be a lag phase between the time telomerase is inhibited and the time telomeres of the cancer cells will have shortened sufficiently to produce detrimental effects on cellular proliferation. The exact number of nucleotides lost per round of replication in a typical tumour cell line is not generally known, but is likely to be around 50–200. So, for telomeres with an average length of 5 kb, about 50 rounds of replication will have to occur before the onset of senescence and subsequent apoptosis, assuming that telomeres must be completely eroded before observing an effect. This implies an extensive lag time before the positive effects of the drug can occur. For a tumour cell that has a 24-hour doubling time, there is the theoretical possibility that tumour growth will rapidly overtake telomere-shortening effects (Neidle *et al.* **2002**). If this is correct, it would suggest that telomerase inhibitors might be most effective in combinations with other conventional or experimental cancer treatments (Fig. 1.4-2). It is

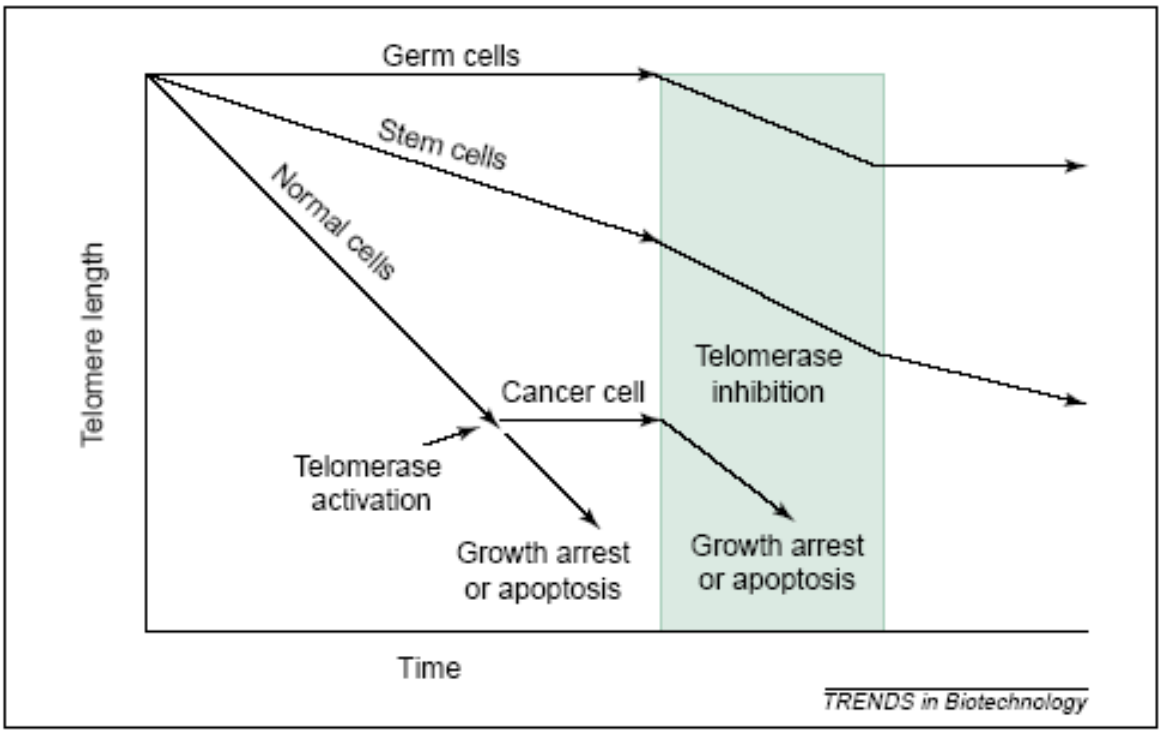

Fig. 1.4-1: Effects of telomerase inhibition on the telomere lengths and proliferative capacity of both cancer cells and telomerase positive normal human somatic cells and germ line cells. (White *et al.* **2001**).

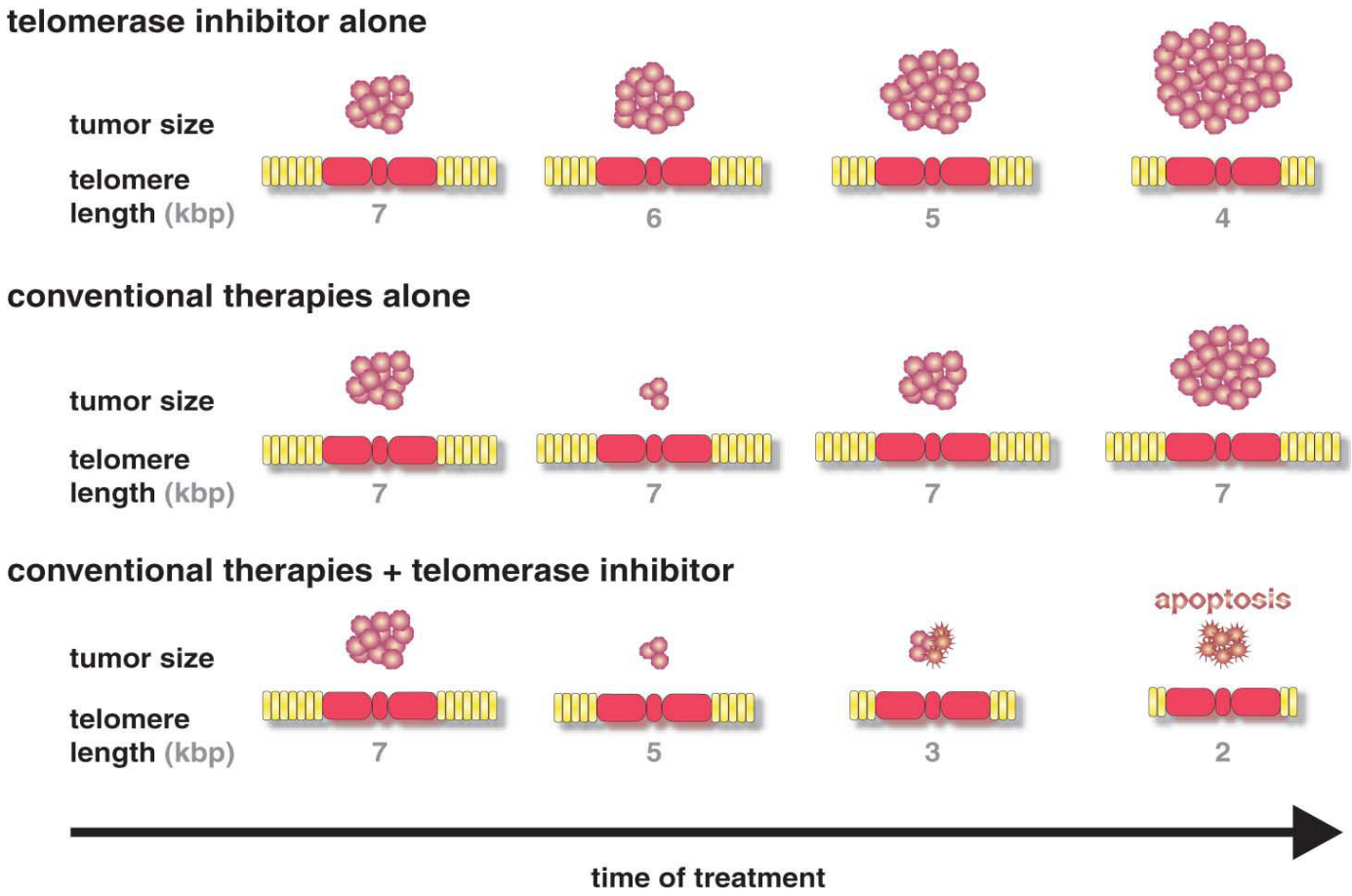

Fig. 1.4-2: Telomerase inhibitors and conventional therapies (Shay *et al.* **2002**). A telomerase inhibitor used as a single agent will progressively reduce telomere length, but there is an expected time delay until cell death. Conventional cytoxic therapies will initially reduce tumour burden but not affect telomere length. Combinations of conventional therapies with telomerase inhibitors would be predicted to both reduce tumour burden and shorten telomeres, potentially preventing or delaying tumour recurrences.

possible that in primary human tumours there will be some very short telomeres in most cells and that the lag phase before telomerase inhibitors produce proliferative deficiencies in vivo may be more rapid than that observed in tumour cell line preclinical models (Shay *et al.* **2002**).

Another issue that has been raised about telomerase inhibitors is that alternative mechanisms for telomere maintenance (referred to as ALT, alternative lengthening of telomeres) have been reported in other organisms, in experimentally derived human immortalized cell lines, and in some rare human cancers (Lundblad **2002**). Proposed ALT mechanisms involve telomeres recombination (Fig. 1.4-3, Wang *et al.* **1990**, Reddel *et al.* **1997**), but recent findings about t-loops (par. 1.1) could suggest analogous mechanisms inside one telomere terminus. Telomerase inhibitors might thus result in the emergence of drug-resistant telomerase-independent cancer cells. While this is certainly a possibility, there have been no published reports of telomerase-positive human tumour cells being experimentally converted to a telomerase-independent pathway using telomerase inhibitors (Shay *et al.* **2002**).

Telomerase is unusual among cancer molecular targets because a large body of outstanding basic science in telomere biology has preceded development of effective lead compounds, allowing potential problems to be anticipated before evidence of efficacy in model systems is in hand, exactly the opposite of the situation faced during most drug development. Even though telomerase does not cause cancer and its role in cancer is most probably permissive, cancer therapy directed at telomerase has advanced in some instances to clinical trials to validate safety and specificity (Shay *et al.* **2002**). The telomerase holoenzyme complex presents multiple potential sites for the development of inhibitors. These include the functional RNA or hTR, the catalytic reverse transcriptase subunit hTERT, the primer anchoring site, holoenzyme assembly and the factors involved in recruiting telomerase to the telomere (White *et al.* **2001**, Fig. 1.4-4).

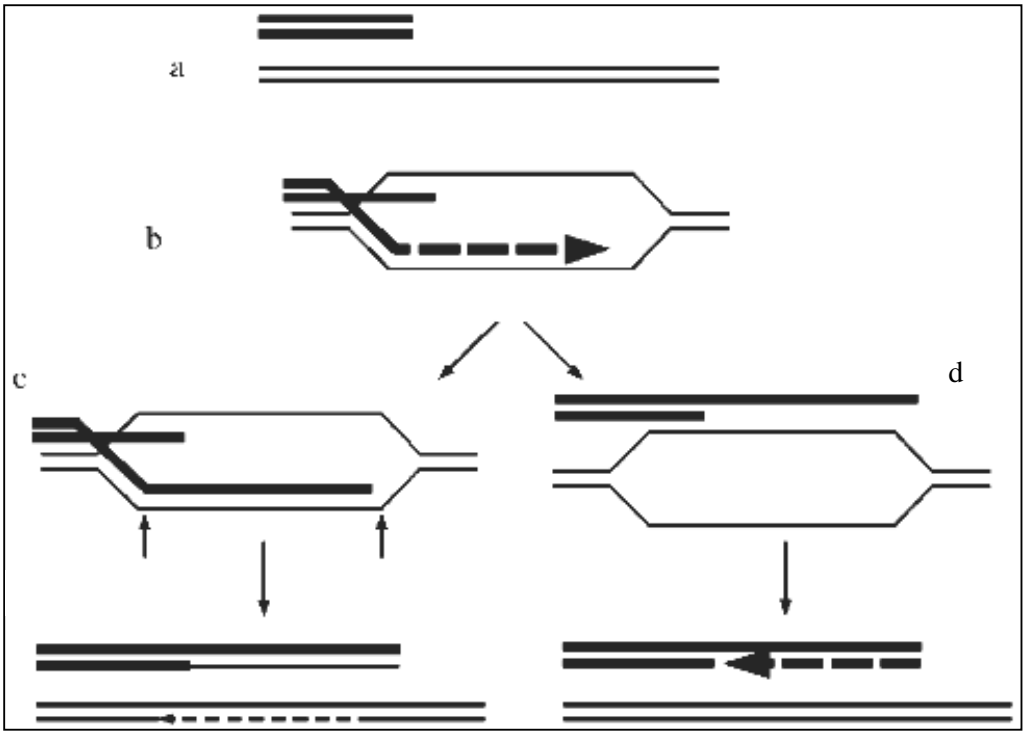

Fig. 1.4-3: A model for recombination-mediated lengthening of telomeres (Wang *et al.* **1990**). (a) When a telomere becomes critically short it may be interpreted by the cell as a double-strand break (DSB). (b) The DSB repair enzymes then mediate invasion by a single-stranded 3´ end of the short telomere between the strands of a longer telomere. DNA polymerase may then extend the short strand, using the long strand as the template. (c) The crossed-over strands may then be subject to cleavage by a nuclease (→) followed by ligation, resulting in recombinant DNA molecules. (d) Alternatively, the structure shown in (b) may be resolved by unwinding of the newly formed helix and rewinding, resulting in non-recombinant molecules. In either case, the staggered annealing of repeats in the short and long telomeres results in net telomere elongation (Reddel *et al.* **1997**).

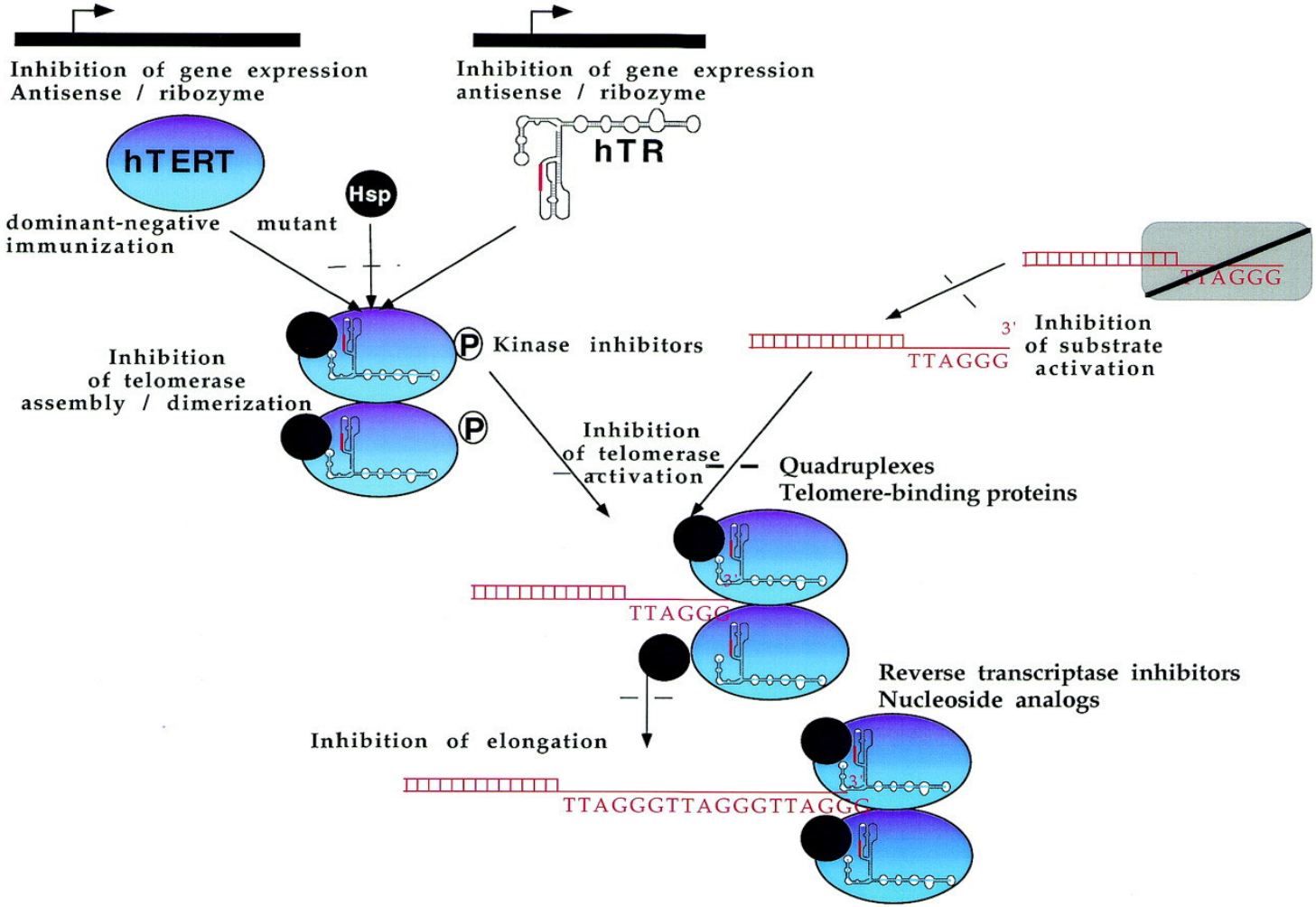

Fig. 1.4-4: Strategies for telomerase inhibition. Possible pathways of pharmacological inhibition of telomerase: targeting of the catalytic subunit; antisense or ribozyme strategies against hTR; targeting telomeric DNA (Mergny *et al.* **2002**).

Antisense oligodeoxynucleotides (ODN) are an area of heightened interest in the field of telomerase inhibition. These drugs consist of short stretches of DNA that are complementary to a target RNA. The mechanism of action for most applications is to hybridize to their complementary RNA by Watson–Crick base pairing and inhibit the translation of the RNA by a passive and/or active mechanism. The passive inhibition occurs simply by the competitive binding of the ODN to the mRNA, whereas the active mechanism recruits RNaseH to degrade the mRNA once the RNA–ODN hybridization occurs (Galderisi *et al.* **1999**). Telomerase presents itself as an intriguing target for these drugs because it possesses a functional RNA component as part of its structure. The template region of hTR must be exposed to add new telomeric repeats onto the chromosome, making this an accessible target for the ODN. Thus, rather than using ODNs to inhibit translation, ODNs directed against the hTR template are designed to directly inhibit telomerase activity. ODNs present several problems in drug development, mainly related to cellular delivery and degradation by a variety of exo- and endonucleases. Chemical modifications to the ODNs and transfecting agents have been implemented to reduce these problems. A variety of studies have been published on the inhibition of telomerase using antisense approaches directed both at the template and at non-template regions of hTR (White *et al.* **2001**). The first report was by Feng *et al.* (**1995**); since that first study there have been many reports on antisense ODN inhibitors of telomerase. Many of these have reported a reduction in telomerase activity in cancer cells treated in culture. Another class of oligonucleotides being studied are peptide nucleic acids (PNAs). PNAs are analogues of RNA and DNA, in which the pentose-phosphate backbone is replaced by an oligomer of N-(2-aminoethyl)glycine, making them resistant to degradation by endo- and exonucleases. Although the pharmacokinetics and uptake of these drugs in vivo is largely unknown, they present an exciting new class of oligonucleotide agents (White *et al.* **2001**). Hammerhead ribozymes are small RNA molecules that possess specific endoribonuclease

activity. They consist of a catalytic core flanked by anti-sense sequences that function in the recognition of the target site. This strategy for telomerase inhibition might prove to be a useful tool if investigators are able to demonstrate the expected effects on telomere biology with specific targeting of the telomerase RNA (White *et al.* **2001**).

Another approach to telomerase inhibition is based on dominant negative hTERT constructs (mutants that are catalytically inactive but still able to bind and sequester hTR). They effectively inhibit telomerase both *in vitro* and *in vivo*, as demonstrated by introducing cDNA that contains point mutations in the reverse transcriptase motifs of hTERT into human tumour cell lines (Zhang *et al.* **1999**). Because of its RNA-dependent DNA polymerase activity, telomerase could be in principle inhibited by classical reverse transcriptase inhibitors (RTIs), such as 3′-azido-3′-deoxythymidine (AZT). They were demonstrated to cause telomerase inhibition and slowed growth of cells in culture; however, they have not shown telomere erosion or eventual growth arrest of the cells after prolonged exposure (Strahl *et al.* **1996**). A plausible explanation might be that the RTIs have a toxic effect on the cells, perhaps by inhibiting mitochondrial DNA replication leading to the observed reduction in telomerase activity, which is dose dependent (White *et al.* **2001**).

Recently, there has been exciting work in the field of antigen-specific immune responses in tumour cells. Telomerase is present in the majority of human tumours and is, therefore, a good candidate as a universal tumour-associated antigen (White *et al.* **2001**).

1.5. Molecules able to induce and stabilize G-quadruplex structures as telomerase inhibitors

Inhibition of telomerase can be achieved by sequestration of the primer (the single-stranded telomeric end) required for the reverse transcriptase activity of this enzyme, by G-quadruplex formation (Fig. 1.5-1, Mergny *et al.* **1998**). This was first demonstrated by showing that K^+ inhibited telomere activity, presumably by facilitation of folding of the single-stranded telomeric DNA into a G-quadruplex structure (Fig. 1.5-2, Zahler *et al.* **1991**). Three approaches are being followed in this rapidly expanding field (Neidle *et al.* **2002**), and have been aided by the development of high-throughput G-quadruplex binding assays (FRET assays, par. 3.3.c). (i) Rational structure-based design: molecular models based on several quadruplex systems, in particular those derived from the NMR (Wang *et al.* **1993**) and X-ray (Parkinson *et al.* **2002**) models for the d[AGGG(TTAGGG)$_3$] intramolecular G-quadruplexes, have been used in structure-based design strategies (Fig. 1.5-3, Harrison *et al.* **1999**). (ii) Computational approaches: *in silico* screening for quadruplex-binding compounds has produced several successes, leading to the discoveries of several G-quadruplex interactive compounds, among which the perylene derivative PIPER (par. 1.6, Fedoroff *et al.* **1998**); this approach does require care in choosing a library of compounds that has some characteristics suitable for G-quadruplex high-affinity binding (Neidle *et al.* **2002**). (iii) Conventional screening: some success in identifying G-quadruplex ligands as telomerase inhibitors has been achieved by screening existing chemical libraries (Chen *et al.* **1996**) in combination with combinatorial approaches (Riou *et al.* **2002**); screening of the metabolites of the microorganism *Streptomyces anulatus* identified an exceptionally potent inhibitor, the eight-ring cyclic molecule telomestatin (Fig. 1.5-4, Shin-ya *et al.* **2002**).

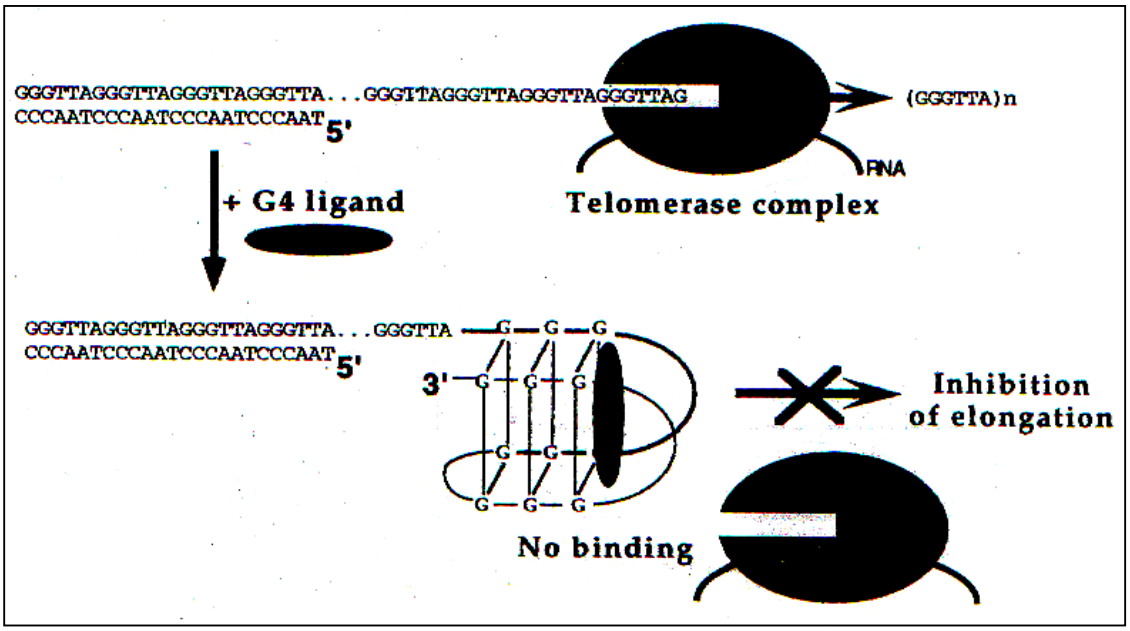

Fig. 1.5-1: Schematic of telomerase inhibition being produced by folding of the 3' end telomere primer strand into a G-quadruplex structure, which is stabilized by ligand stacking onto the G-quartet end. This folding then inhibits further hybridization of the primer with the hTR template from taking place during subsequent cycles of telomere extension. (Mergny *et al.* **1998**).

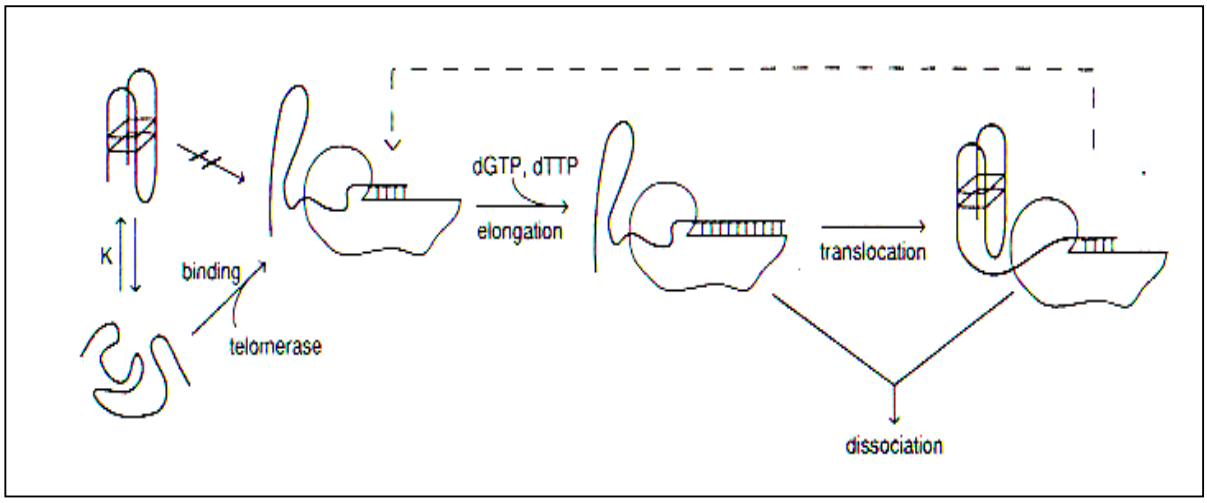

Fig. 1.5-2: Model for the effect of primer structure on telomerase action (Zahler *et al.* **1991**). The most stable folded form, represented as a G-quadruplex structure, is unable to bind to the RNA template of telomerase. The folded primer is in equilibrium with the unfolded form, which is able to bind the telomerase and is elongated by the addition of nucleotides. Once the end of the internal RNA template is reached, a translocation step must occur before the next repeat is synthesized.

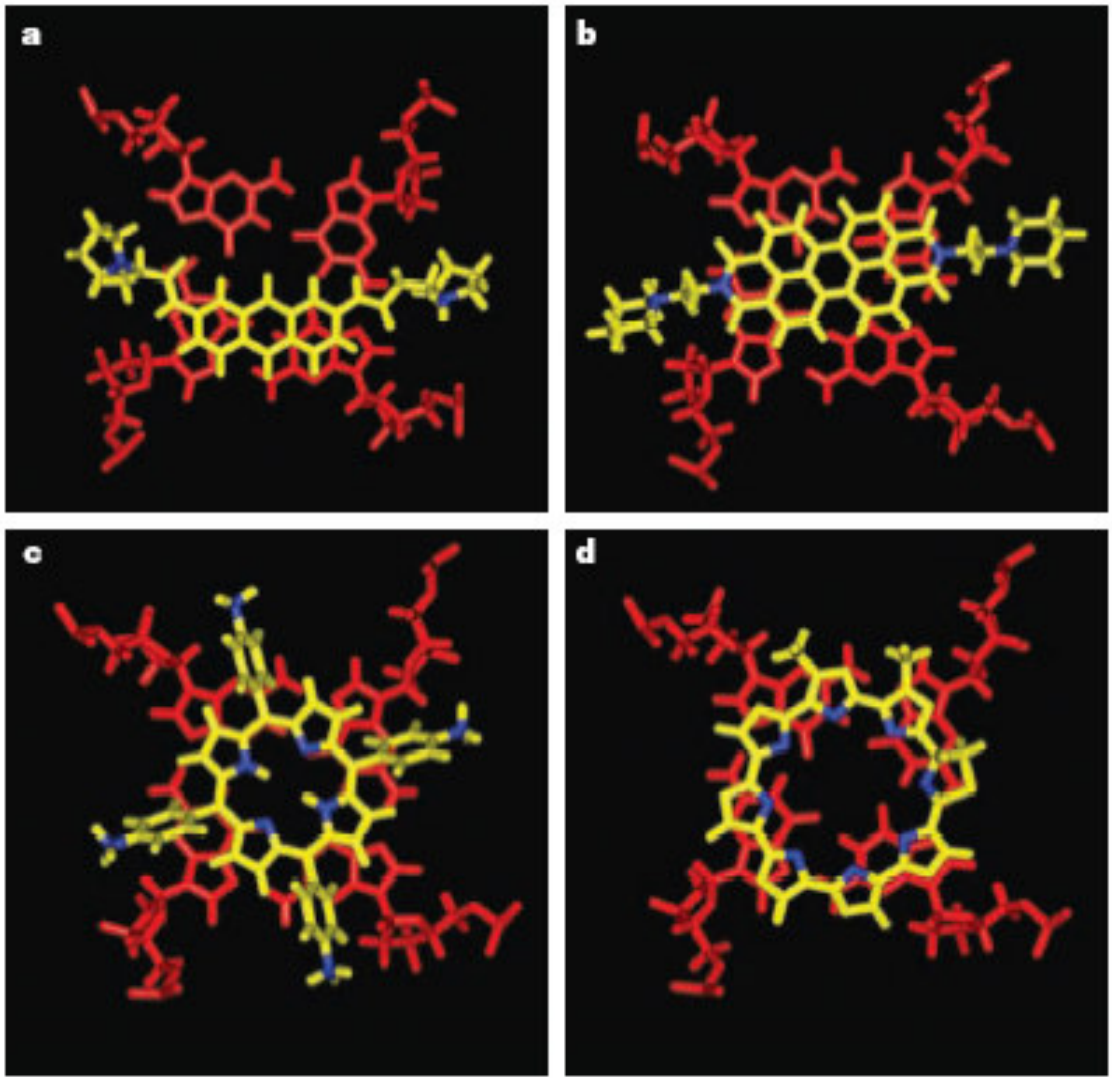

Fig. 1.5-3: Structure-based design of G-quadruplex ligands: views from molecular modeling of several inhibitors that interact with the G-quartet surface of a quadruplex. (a) A di-substituted anthraquinone, (b) the PIPER molecule, (c) a tetrapyridyl-porphyrin and (d) the telomestatin molecule. Differences in ligand–G-quartet overlap are clearly apparent (Neidle *et al.* **2002**).

All these different approaches led to a number of different classes of molecules that have been shown to be able to induce and/or stabilize G-quadruplex DNA structures and to inhibit human telomerase (Fig. 1.5-4). Almost all of the several hundred G-quadruplex ligands that have been discovered so far share the common structural feature of an extended planar aromatic chromophore, in common with conventional duplex DNA-intercalating drugs (Neidle *et al.* **2002**). An early proposal was that these compounds could similarly intercalate, but in between pairs of stacked G-quartets. However, molecular-modelling studies, together with interpretation of low-angle diffraction data from a crystal of a parallel-quadruplex complex, indicated an alternative model, in which the ligand is stacked onto the ends of the G-quartets (Read *et al.* **2000**). The unfavourable energetics and slow dissociation kinetics of G-quartet destacking also favour this structural model, which has a chromophore that is involved in π-π interactions with the terminus of the G-quartet system. This external model is supported by several NMR studies (Fedoroff *et al.* **1998**, Han *et al.* **2001**, Kim *et al.* **2002**), as well as by the stoichiometry found from solution binding studies (Read *et al.* **2001**). Molecular modelling indicates that ligand side chains could be positioned in the grooves of a quadruplex, stabilized by appropriate non-bonded interactions (Read *et al.* **1999**, Read *et al.* **2001**), and that these interactions can significantly contribute to overall stability and selectivity (Neidle *et al.* **2002**).

These design criteria are evident in the development of a number of promising compound series. For example, disubstituted amidoanthraquinones and amidoacridines (Fig. 1.5-4) inhibit telomerase in the low-micromolar range but exhibit equipotent cytotoxicity so that the IC_{50} (acute cellular toxicity) value is not much higher than the $^{tel}EC_{50}$ (telomerase inhibitory ability) value (Incles *et al.* **2003**). In contrast, trisubstituted anilino-acridines such as BRACO-19 (Cancer Research Technology, Fig. 1.5-4) demonstrate up to two orders of magnitude improvement in their $^{tel}EC_{50}$ values while exhibiting a parallel improvement in cytotoxicity.

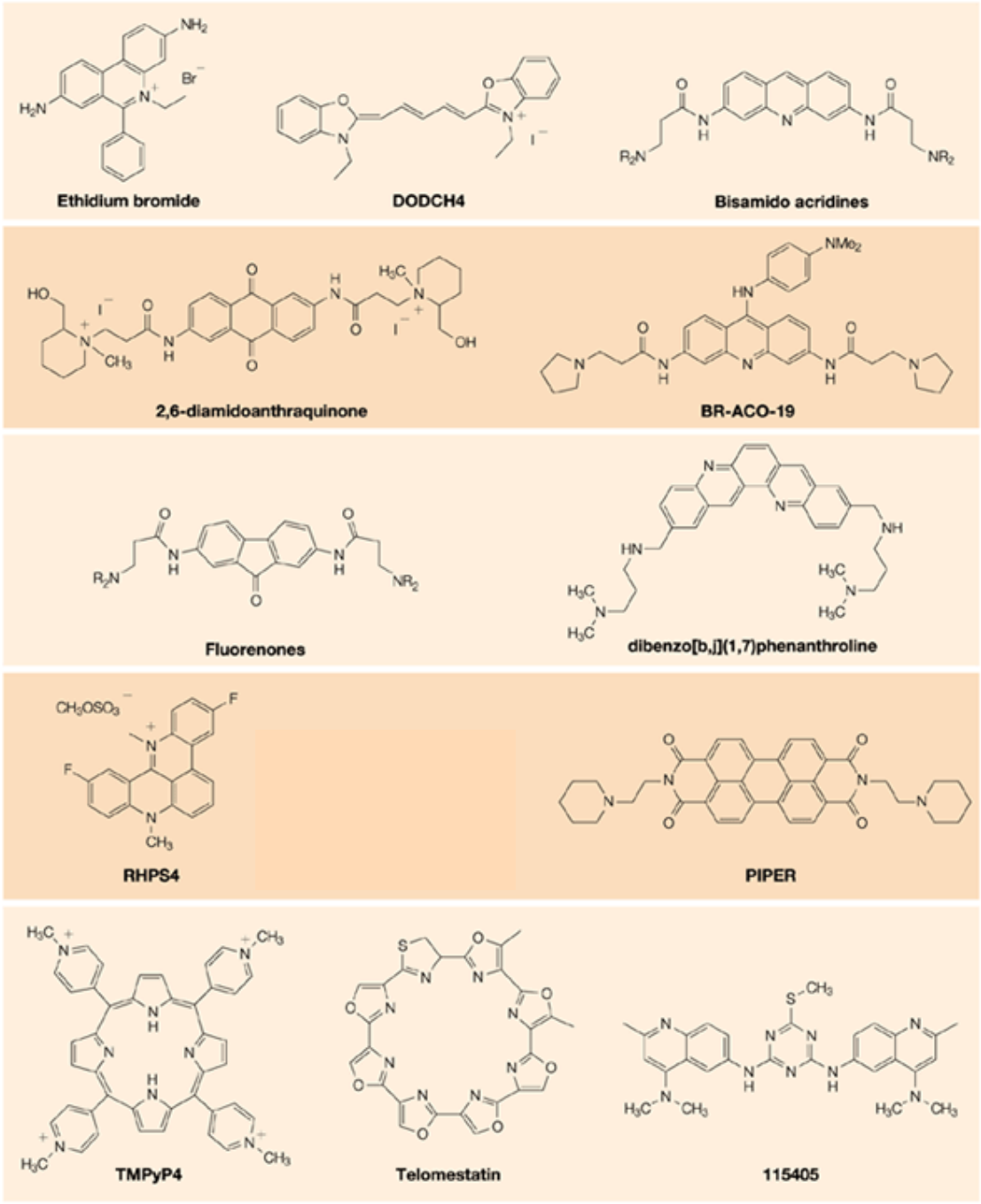

Fig. 1.5-4: Structures of representative G-quadruplex interactive compounds used as telomerase inhibitors (Neidle *et al.* **2002**).

Both these effects are believed to be due to the increased selectivity of the compounds for G-quadruplex over duplex DNA that results from the incorporation of the third side chain (Read *et al.* **2001**) and its recognition of the unique groove structural features of the human intramolecular quadruplex (Fig. 1.5-5). This is reflected in a 10-fold increase in G-quadruplex affinity compared to disubstituted acridines coupled with a reduction in duplex DNA affinity as a result of steric hindrance to duplex binding. Although the aromatic scaffold may drive the initial DNA recognition due to stacking, the interplay between peripheral moieties and other groups on the DNA (in particular, the negatively charged phosphates of the TTA loops and grooves) may be just as important and can lead to major variations in terms of both enzyme inhibition and selectivity (Incles *et al.* **2003**).

Extension of the acridine scaffold has led to the development of several potent compounds. As the surface presented for π-π stacking by the G-quartet is significantly larger than that in the case of a simple duplex base pair, these compounds are expected to demonstrate some preference for G-quartets. Good results have been achieved with dibenzophenanthrolines (Fig. 1.5-4, Read *et al.* **2001**). A different approach has also been reported for 2,7-disubstituted acridines, in which the joining of two such groups leads to a significant increase in the $^{tel}EC_{50}$ value of the resulting acridine dimer (Fig. 1.5-6), presumably due to the increased interactions of two acridine groups with the exposed guanines of the G-tetrad (Alberti *et al.* **2001**). Also dimerization of dibenzophenanthrolines (Fig. 1.5-6) led to large improvements in potency, with $^{tel}EC_{50}$ values of 0.13 μM, with improved telomerase inhibitory properties and G-quadruplex stabilization (Teulade-Fichou *et al.* **2003**).

Unlike other telomerase inhibitors, G-quadruplex-interactive compounds would be expected to affect cells that maintain telomeres by telomerase-dependent as well as telomerase-independent mechanisms because the latter involve recombination mechanisms quite possibly involving G-quadruplex structures (par. 1.4, Wang *et al.* **1990**, Reddel *et al.* **1997**). Moreover,

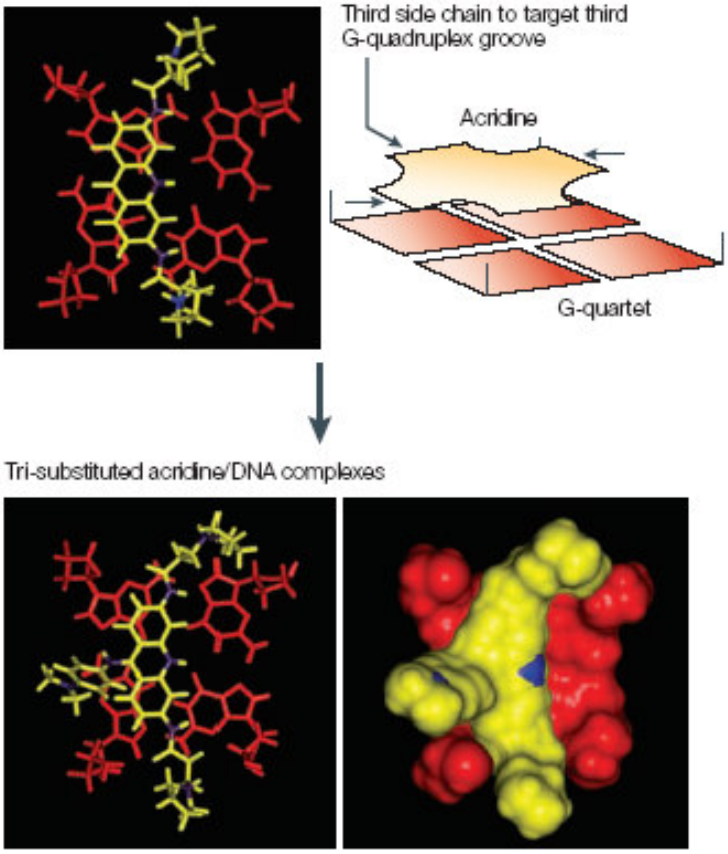

Fig. 1.5-5: The basis for the rational design of second-generation acridine inhibitors, showing how a third substituent on an acridine skeleton (yellow) can interact in a third groove of a quadruplex. Such a molecule has inherent selectivity over DNA-duplex-binding molecules, as the two grooves of B-form duplex DNA cannot readily accommodate tri-substitution. The views are down onto the plane of a G-quartet (Neidle *et al.* **2002**).

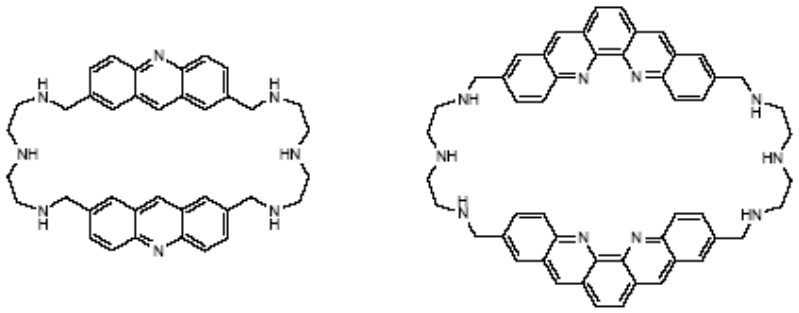

Fig. 1.5-6: Dimerization of G-quadruplex interactive compounds led to increased telomerase inhibition (Incles *et al.* **2003**).

an altered telomere state may be a more important consequence than critical telomere shortening (Karlseder *et al.* **2002**). Thus, sequestration of telomere ends by stabilization of G-quadruplex structures may lead to chromosome instability in presenescence cells. In particular, in cancer cells, where it is necessary to add telomeric sequences via a telomerase-dependent or telomerase-independent mechanism, the single-stranded DNA template becomes exposed in the uncapped state, and if either telomerase is deficient or G-quadruplex-interactive compounds are present, which facilitate folding of the G-quadruplex, irreversible uncapped telomeric ends and chromosome end-to-end fusion may result (Rezler *et al.* **2003**). This finding has important implications for the future clinical utility of G-quadruplex inhibitors, and clearly indicates that they might not require an extended time period before effects become significant (Fig. 1.5-7, Neidle *et al.* **2002**).

The formation of G-quadruplex structures in regions other than telomeres, for example in the promoter region of c-*myc*, may also lead to effects on telomerase because c-*myc* controls hTERT. Indeed, the G-quadruplex-interactive compound TMPyP4 (Fig. 1.5-4), is able to down-regulate c-*myc* and hTERT (Siddiqui-Jain *et al.* **2002**). The case of this porphyrin derivative is particularly interesting, since it was shown also to be able to promote the formation of the i-motif DNA structure in the cytosine-rich telomeric strand, complementary to the guanine-rich sequence (par. 1.2, Fedoroff *et al.* **2000**). This study raises the intriguing possibility that TMPyP4 can trigger the formation of unusual DNA structures in both strands of the telomeres, which may in turn explain the recently documented biological effects of TMPyP4 in cancer cells (Grand *et al.* **2002**).

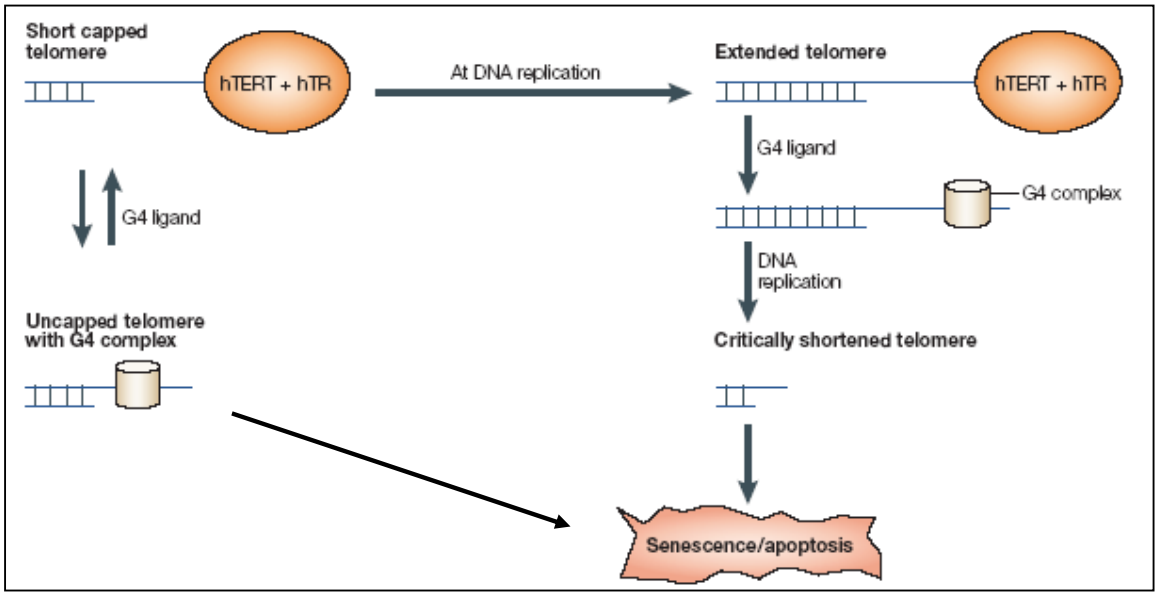

Fig. 1.5-7: Schematic of the sequence of events that can take place after quadruplex-induced telomerase inhibition, with two pathways to selective cell death being shown, dependent on telomere length (Neidle *et al.* **2002**).

1.6. Previous studies on perylene diimides and berberine

1.6.a. Perylene diimides

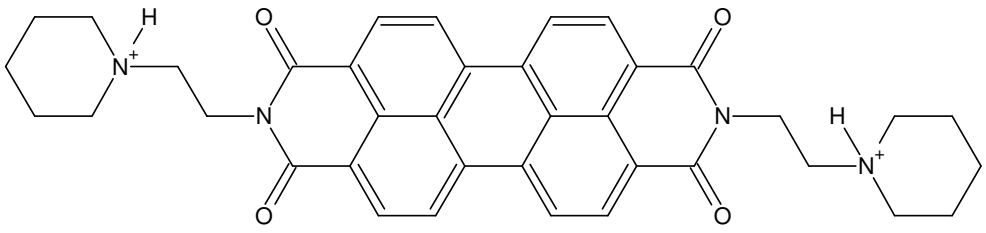

PIPER (N,N'-bis[2-(1-piperidino)ethyl]-3,4,9,10-perylenetetracarboxylic diimide) was reported to inhibit telomerase and bind to a G-quadruplex structure for the first time in 1998 in an NMR study by Hurley and coworkers (Fedoroff *et al.* **1998**). According to the NMR-based models, the ligand molecule does not intercalate within the G-quadruplex itself but rather stacks on the surface of the 3'-terminal G-tetrad (Fig. 1.6-1). This binding mode can be classified as a "threading intercalation", with a fast structural transition between the two orthogonal drug orientations (Fig. 1.6-2). The highly dynamic nature of the ligand-quadruplex complex makes the precise structural characterization extremely difficult (Fedoroff *et al.* **1998**). Successively, PIPER was reported as the first example of a small ligand behaving as a driver in the assembly of G-quadruplex structures (Han *et al.* **1999**). The authors of this paper demonstrate by means of gel-shift experiments that PIPER can dramatically accelerate the association of a DNA oligomer containing two tandem repeats of the human telomeric sequence (TTAGGG) into di- and tetrameric G-quadruplexes. In so doing, PIPER alters the oligomer dimerization kinetics from second to first order. The most likely pathways for the assembly of various dimeric and tetrameric G-quadruplex structures invoke both isomerization and association reactions (Fig. 1.6-3). Without external factors affecting

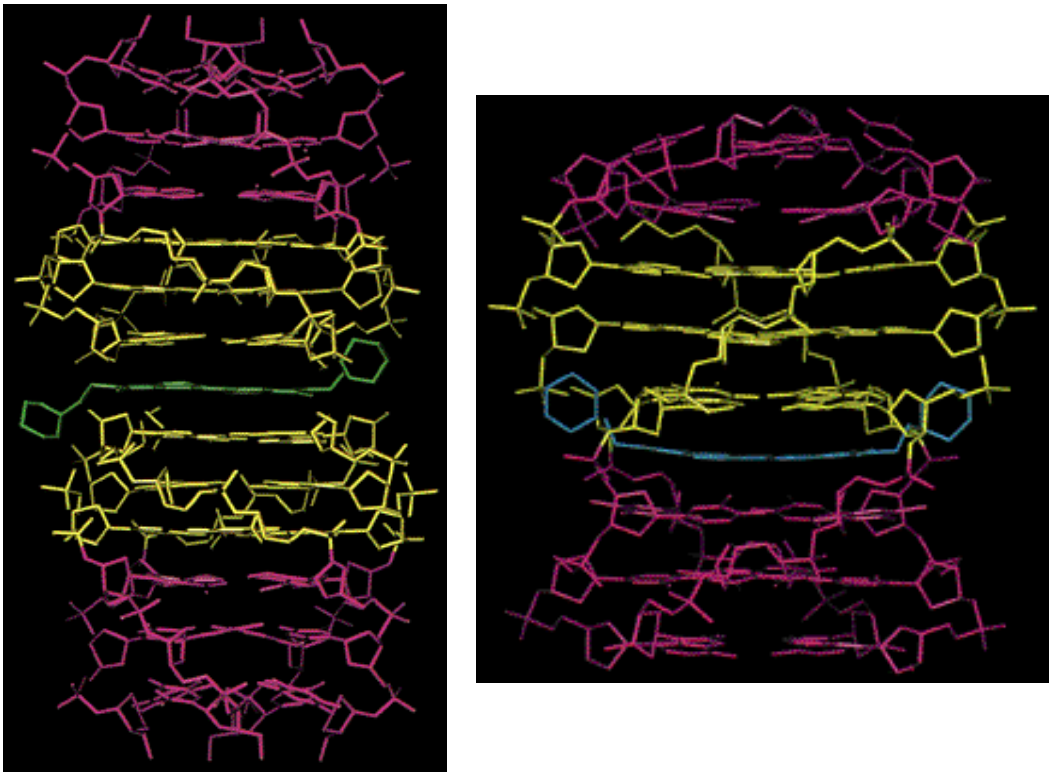

Fig. 1.6-1: NMR-based models of the 2:1 $[dTTAGGG]_4$-PIPER complex (left) and of the 1:1 $[dTAGGGTTA]_4$-PIPER complex (right). The ligand molecule is in green or blue, the DNA guanine residues are in yellow, and the adenine and thymine residues are in purple (Fedoroff *et al.* **1998**).

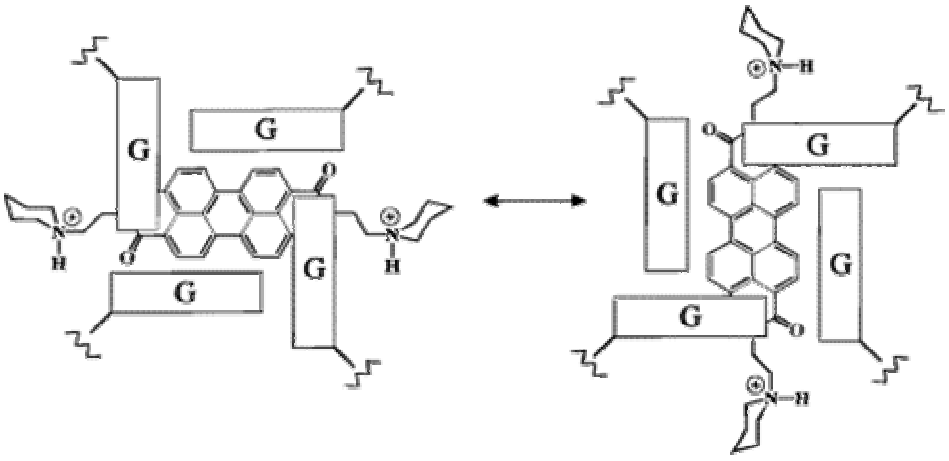

Fig. 1.6-2: NMR studies suggest a fast structural transition between the two possible orthogonal drug orientations (Fedoroff *et al.* **1998**).

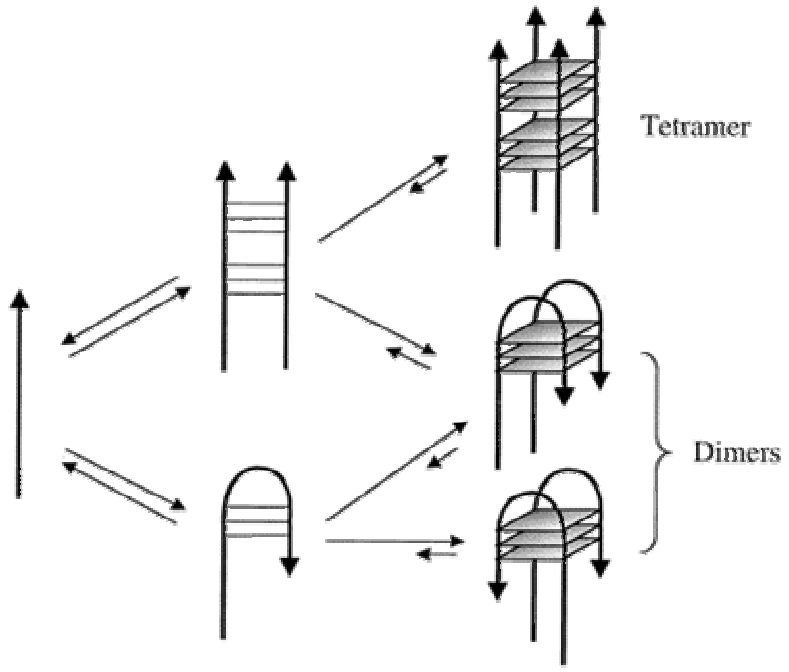

Fig. 1.6-3: Several dimeric G-quadruplex isomers can form via dimerization of guanine-guanine hairpins or folding of a guanine-guanine duplex (Han *et al.* **1999**).

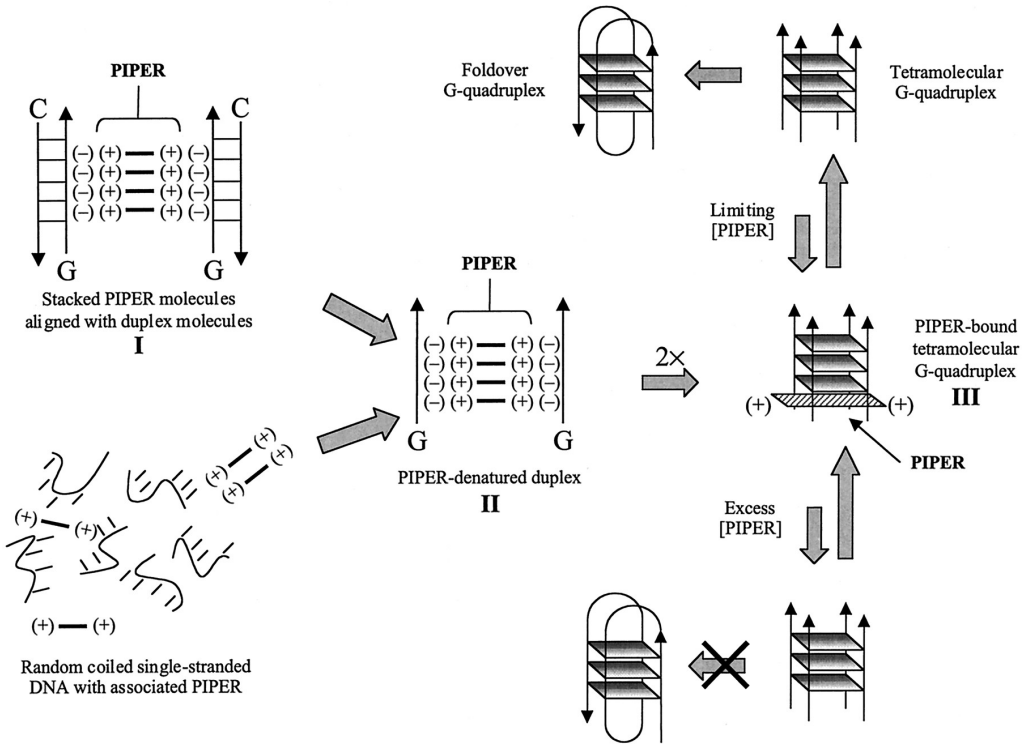

Fig. 1.6-4: Conversion of duplex and single-stranded G-rich oligonucleotides to G-quadruplex under conditions of limiting (*upper pathway*) and excess (*lower pathway*) PIPER (Rangan *et al.* **2001**).

oligonucleotide assembly, isomerization reactions probably proceed at much faster rates than association reactions. Thus, it is expected that in the absence of PIPER the rate-limiting step for formation of either dimeric or tetrameric G-quadruplexes involves a bimolecular collision of monomeric or dimeric intermediates, respectively. Although the precise mechanism by which PIPER acts has yet to be established, Hurley and coworkers propose that its behaviour as a polynucleotide driver is due to a propensity to accelerate the association of G-rich oligonucleotides. Consequently, isomerization reactions become the rate-limiting events in G-quadruplex assembly, and overall formation rates thereof are greatly enhanced (Han *et al.* **1999**).

More recently, PIPER has also been shown to prevent the unwinding of G-quadruplex structures by yeast Sgs1 helicase (Han *et al.* **2000**). PIPER specifically prevents the unwinding of G-quadruplex DNA but not duplex DNA by Sgs1. Competition experiments indicate that this inhibitory activity is due to the interaction of PIPER with G-quadruplex structures rather than the helicase itself (Han *et al.* **2000**). Furthermore, PIPER has been shown to promote the induction of duplex to G-quadruplex transition in the c-*myc* promoter region (Rangan *et al.* **2001**). As discussed in par. 1.2 and 1.5, these structurally altered DNA elements might serve as regulatory signals in gene expression or in telomere dynamics. In this paper, the authors suggest a more complex possible mechanism for the role of PIPER in inducing the formation of G-quadruplex structures, both from single-stranded and duplex DNA. In both cases PIPER self-aggregation play a fundamental role, since it is supposed to interact with DNA as an assembly of stacked molecules (Fig. 1.6-4). This aspect has been widely studied by Kerwin and coworkers (Kerwin *et al.* **2002**, Kern *et al.* **2002**). In a series of perylene diimides they observe that the ligands bind to both duplex and G-quadruplex DNA under low pH conditions, where the ligands are not aggregated. At higher pH, where the ligands are extensively aggregated, the apparent G-quadruplex DNA binding selectivity is

high. An explanation proposed by the authors is that the duplex DNA intercalation by these perylene diimides likely requires the ligand to be monomeric. In contrast, G-quadruplex DNA binding by perylene diimides occurs by end stacking interactions with G-tetrads. Because this stacking interaction requires only one free chromophore face, it is possible that G-quadruplex DNA binding may occur from either aggregated or monomeric ligand (Kerwin *et al.* **2002**).

1.6.b. Berberine and its analogues

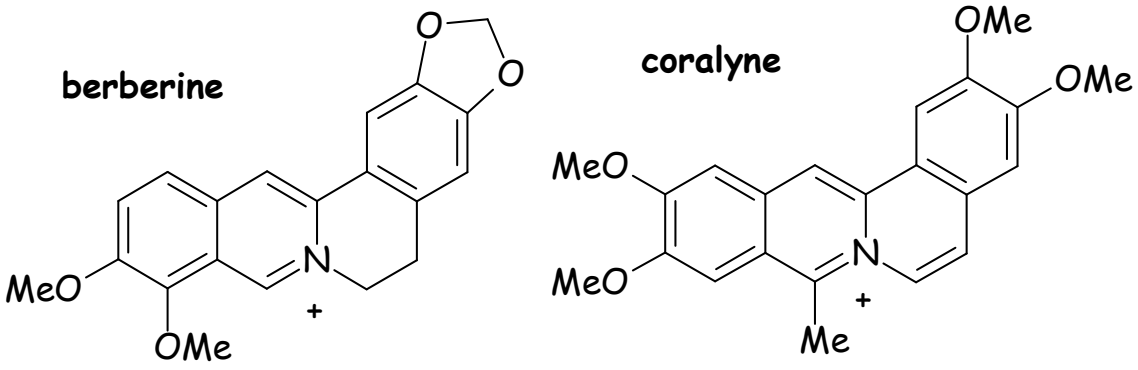

Berberine is an alkaloid originated from Chinese herbal medicine, where it is used as an antibiotic (Wu *et al.* **1999**); its anti-bacterial activity has been demonstrated against many species (Ghosh *et al.* **1985**). The drug was subsequently screened for anti-cancer activity following evidence of anti-neoplastic properties (Zhang **1990**). More recently, berberine was shown to be able to inhibit telomeres elongation (Naasani *et al.* **1999**) and to bind to G-quadruplex DNA (Ren *et. al.* **1999**). Coralyne is a synthetic analogue of berberine (Zee-Cheng *et al.* **1972**) and it is well known for its ability to bind to triplex DNA (Latimer *et al.* **1995**). Both these compounds show a great selectivity for triplex DNA, and to minor extent to quadruplex DNA, with respect to duplex DNA, according to competition dialysis experiments (Ren *et. al.* **1999**).

2. Aim of this thesis

The work described in this thesis has two main targets: the synthesis of G-quadruplex interactive compounds and the evaluation of their efficiency in inducing and stabilizing G-quadruplex structures and in inhibiting human telomerase. In particular, two classes of G-quadruplex interacting compounds have been considered: (i) perylene and coronene derivatives and (ii) berberine analogues and derivatives. The study of their ability to induce different G-quadruplex DNA structures has been aimed to understand the molecular mechanism of their action and the molecular features that are important in determining their selectivity towards different G-quadruplex topologies. Another very important aspect that has been considered is the selectivity of these compounds towards G-quadruplex DNA with respect to duplex DNA. To these aims, several experimental (PAGE, FRET, absorption spectroscopy) and theoretical (molecular modeling) techniques have been used. Finally, biological assays (TRAP) have been performed to evaluate the ability of the investigated compounds to inhibit human telomerase.

3. Materials and methods

3.1. Synthesis

3.1.a. Perylene diimides

Perylene diimides (Fig. 3.1.a-1), except PIPER7, were prepared from 3,4,9,10-perylenetetracarboxylic dianhydride (3g) and the appropriate primary amine (10% excess), in a refluxing mixture of N,N-dimethylacetamide (20ml) and 1,4-dioxane (20ml). The reaction products were precipitated adding water and separated by filtration. The resulting products (80-95% yield) were purified dissolving in 0.2M HCl and precipitating the respective hydrochlorides with acetone (75% yield). PIPER7 was prepared from PIPER2 (200mg) by reaction with methyl-trifluoromethanesulfonate (10 equiv) in refluxing 1,2-dichloroethane (10ml), with stirring for two days (Mitkin *et al.* **2001).** The reaction product was filtered, washed with chloroform and dried under vacuum. Then it was dissolved in 0.1M HCl and passed through a strong basic anion exchange resin Dowex1 (Fig. 3.1.a-2). PIPER7 was precipitated as hydrochloride with acetone in 12% total yield. Compounds were dried under vacuum and characterized by ^{1}H and ^{13}C-NMR spectroscopy (CF_3CO_2D, 300 MHz, 25°C) and elemental analysis or mass spectrometry. All perylene derivatives have been characterized and used as hydrochlorides (Rossetti *et al.* **2002**, Rossetti *et al.* **2004**).

PIPER (N,N'-bis[2-(1-piperidino)ethyl]-3,4,9,10-perylenetetracarboxylic diimide): ^{1}H NMR δ: 1.7-1.9 (2H), 2.0-2.4 (10H), 3.23 (4H), 3.83 (4H), 4.10 (4H), 4.93 (4H), 7.41 (2H),

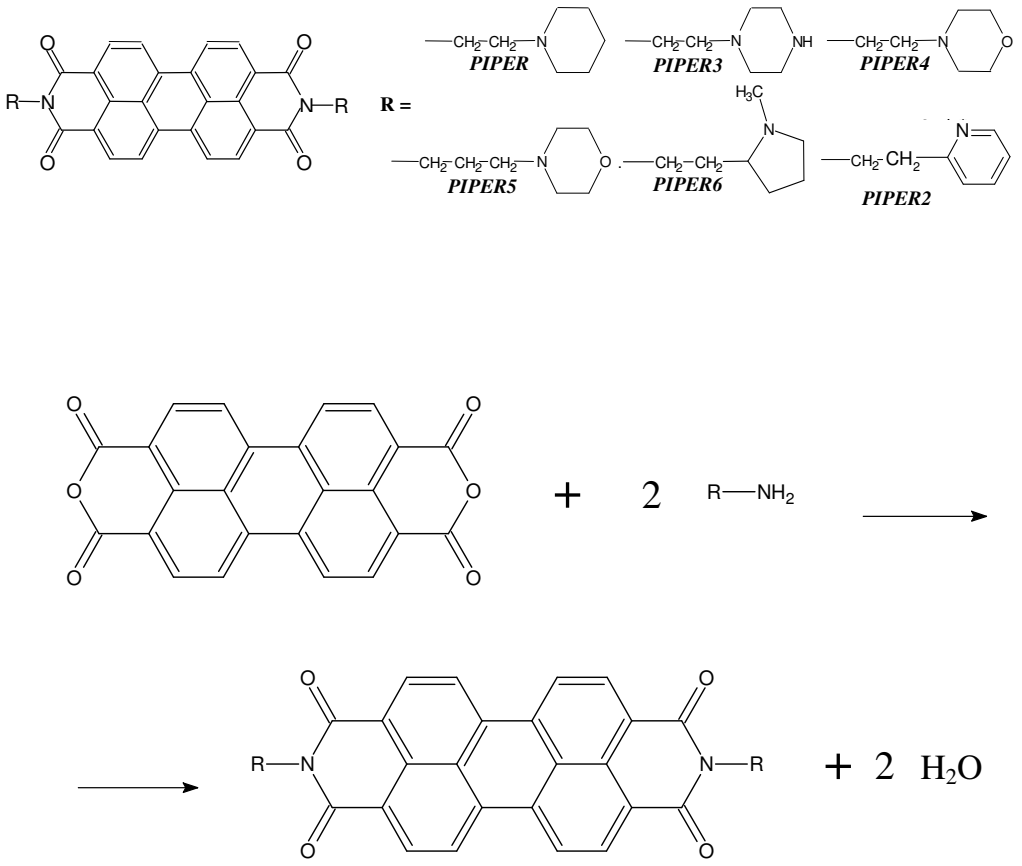

Fig. 3.1.a-1: Structures of the synthesized perylene diimides (top) and the scheme of their synthesis (bottom).

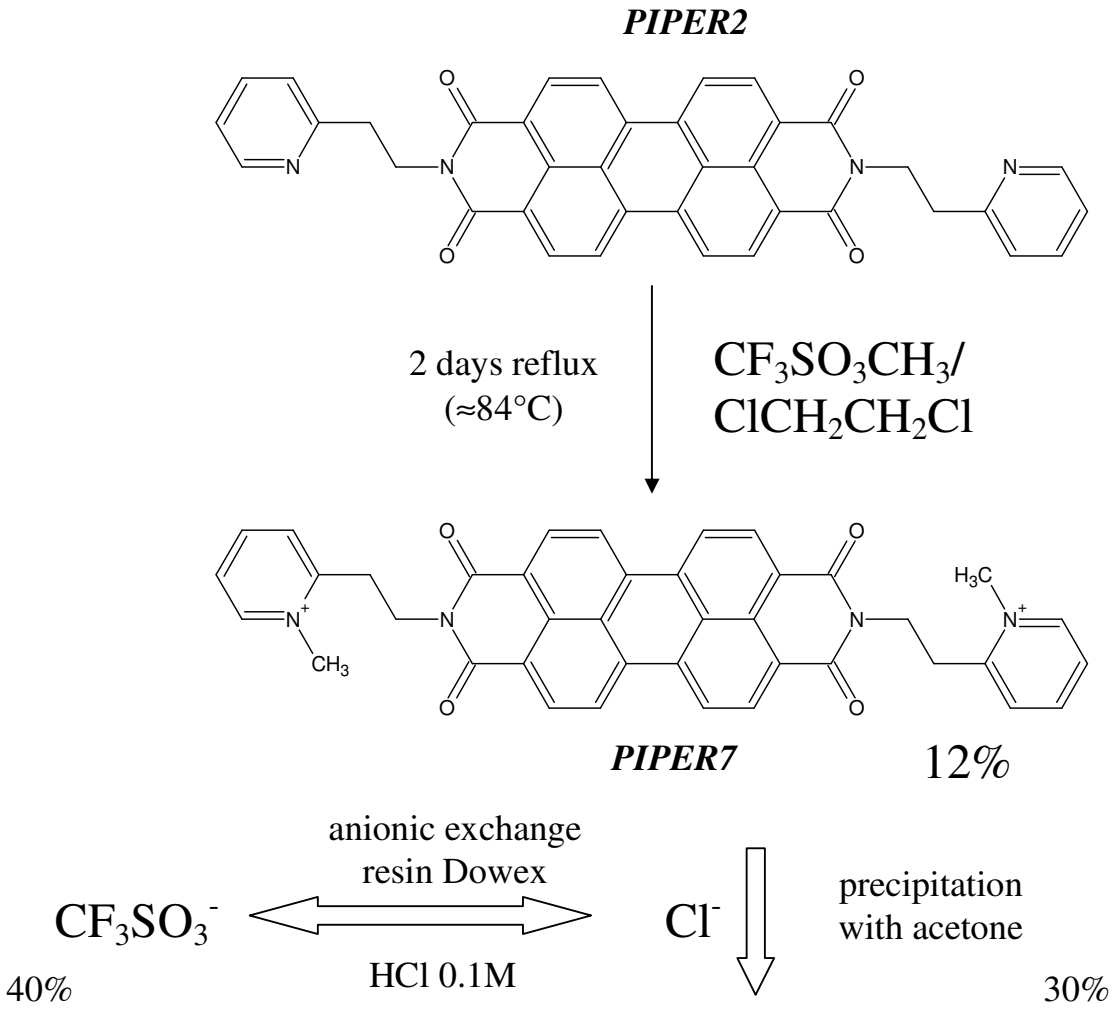

Fig. 3.1.a-2: Scheme of the preparation of PIPER7.

8.92 (8H); ^{13}C NMR δ: 11.6, 13.9, 26.7, 46.2, 47.5, 112.4, 115.4, 117.4, 120.3, 124.2, 127.4, 157.1; elemental analysis calculated ($C_{38}H_{38}N_4O_4Cl_2$): 66.6%C, 5.5%H, 8.2%N; found: 64.9%C, 5.9%H, 7.8%N. ESI *m/z*: 613 (MH^+).

PIPER2 (N,N'-bis[2-(2-pyridino)ethyl]-3,4,9,10-perylenetetracarboxylic diimide): ^{1}H NMR δ: 4.00 (4H), 5.09 (4H), 8.26 (2H), 8.45 (2H), 8.86 (2H), 9.00 (2H), 9.0–9.2 (8H); ^{13}C NMR δ: 26.0, 33.0, 115.0, 117.9, 119.2, 119.9, 121.9, 122.8, 126.6, 129.8, 134.5, 141.3, 147.5, 159.1; elemental analysis calculated (base, $C_{38}H_{24}N_4O_4$): 76.0%C, 4.0%H, 9.3%N; found: 75.3%C, 4.2%H, 9.25%N.

PIPER3 (*also known as Tel08,* Kerwin *et al.* **2002**, Kern *et al.* **2002**) **(N,N'-bis[2-(1-piperazino)ethyl]-3,4,9,10-perylenetetracarboxylic diimide):** ^{1}H NMR δ: 4.1-4.5 (16H), 4.78 (4H), 5.13 (4H), 9.0-9.2 (8H); ^{13}C NMR δ: 31.2, 37.8, 45.5, 52.8, 117.5, 120.4, 122.5, 125.4, 129.3, 132.5, 162.5; elemental analysis calculated ($C_{36}H_{38}N_6O_4Cl_2$): 56.8%C, 5.0%H, 11.1%N; found: 54.9%C, 5.7%H, 10.4%N.

PIPER4 (*also known as Tel10,* Kerwin *et al.* **2002**, Kern *et al.* **2002**) **(N,N'-bis[2-(4-morpholino)ethyl]-3,4,9,10-perylenetetracarboxylic diimide):** ^{1}H NMR δ: 3.66 (4H), 4.07 (4H), 4.3-4.5 (8H), 4.57 (4H), 5.04 (4H), 8.9-9.1 (8H); ^{13}C NMR δ: 31.5, 49.4, 53.3, 60.2, 117.6, 120.6, 122.6, 125.5, 129.4, 132.6, 162.3; elemental analysis calculated ($C_{36}H_{34}N_4O_6Cl_2$): 62.7%C, 4.9%H, 8.12%N; found: 60.8%C, 5.4%H, 7.5%N.

PIPER5 (*also known as Tel01,* Kerwin *et al.* **2002**, Kern *et al.* **2002**) **(N,N'-bis[3-(4-morpholino)propyl]-3,4,9,10-perylenetetracarboxylic diimide):** ^{1}H NMR δ: 2.73 (4H), 3.62 (4H), 3.77 (4H), 4.02 (4H), 4.38 (4H), 4.59 (4H), 4.72 (4H), 8.9-9.1 (8H); ^{13}C NMR δ: 18.5, 33.9, 48.6, 52.0, 60.1, 117.7, 120.3, 122.2, 125.2, 129.0, 132.1, 161.8; elemental analysis calculated ($C_{38}H_{38}N_4O_6Cl_2$): 63.6%C, 5.3%H, 7.8%N; found: 61.8%C, 5.8%H, 7.6%N.

PIPER6 (N,N'-bis[2-(2-(1-methyl)pyrrolidino)ethyl]-3,4,9,10-perylenetetracarboxylic diimide): ^{1}H NMR δ: 2.2-2.4 (8H), 2.83 (4H), 3.29 (6H), 3.47 (2H), 3.82 (2H), 4.13 (2H), 4.66 (4H), 7.79 (2H), 9.00 (8H); ^{13}C NMR δ: 17.4, 25.2, 25.4, 33.9, 36.6, 53.4, 65.2, 117.8, 120.4, 122.4, 125.3, 129.1, 132.2, 161.7; elemental analysis calculated ($C_{38}H_{38}N_4O_4Cl_2$): 66.7%C, 5.5%H, 8.2%N; found: 63.8%C, 6.1%H, 8.2%N.

PIPER7 (N,N'-bis[2-(2-(1-methyl)pyridino)ethyl]-3,4,9,10-perylenetetracarboxylic diimide): ^{1}H NMR δ: 4.23 (t, *J* = 7.3, 4H), 5.11 (s,6H), 5.28 (t, *J* = 7.3, 4H), 8.40 (t, *J* = 7.4, 2H), 8.57 (d, *J* = 7.4, 2H), 8.91 (t, *J* = 7.4, 2H), 9.21 (d, *J* = 7.4, 2H), 9.31 (d, *J* = 8.2, 4H), 9.37 (d, *J* = 8.2, 4H); ^{13}C NMR δ: 27.3, 34.5, 41.9, 117.8, 120.6, 122.6, 125.5, 125.8, 129.3, 132.6, 142.2, 142.5, 151.4, 161.8. ESI *m/z*: 629 [$(M-1)^+$], 315 [$(M/2)^{2+}$].

The commercially available DAPER (Liu *et al.* **1996**) was purchased by Sigma-Aldrich and used without further purification.

3.1.b. New perylene derivatives

In order to achieve more water-soluble perylene diimides, a synthetic strategy already applied in the synthesis of lipophilic perylene derivatives used as liquid crystalline dyes was applied (Fig. 3.1.b-1, Franceschin *et al.* **2004**). In particular, the same strategy described by Mullen and coworkers (bromination of the bay-area of 3,4,9,10-perylenetetracarboxylic dianhydride **1**) was considered (Rohr *et al.* **1998**, Rohr *et al.* **2001**), combined with the preparation of perylene diimides with hydrophilic side chains (Rossetti *et al.* **2002**), to obtain the brominated perylene diimide **3** PIPER-Br (Scheme 1), onto which two other hydrophilic substituents could be inserted. When bromine atoms on the perylene bay-area are substituted by piperidine or morpholine rings, new highly water-soluble perylene derivatives (**4**) are obtained (Scheme 2A).

The twofold bromination of the commercially available perylene-3,4:9,10-tetracarboxylic dianhydride (**1**) was easily carried out with elemental bromine in 96% sulphuric acid to give a mixture of the two isomers **2a** and **2b** in 98% yield (Scheme 1). The dianhydride **1** (9g) was initially dissolved in 96% sulphuric acid (150ml) and stirred for 4h at room temperature. Elemental iodine (200mg) was subsequently added and the mixture was heated. When a temperature of 80°C was reached, elemental bromine (3ml) was added drop wise, achieving a final excess of 20%. The reaction mixture was stirred at 80°C overnight. After cooling, it was added drop wise to ice and then filtered and washed with a 5% sodium metabisulfite solution to provide a red solid, that was dried and characterized. The two isomers (**2a** and **2b**) could not be separated and the isomeric mixture was used in the following step, in which the commercially available 1-(2-aminoethyl)piperidine was added to give a mixture of the two isomers **3a** and **3b** (Scheme 1). 6g of 2, obtained in the previous reaction, and 3.6ml of 1-(2-

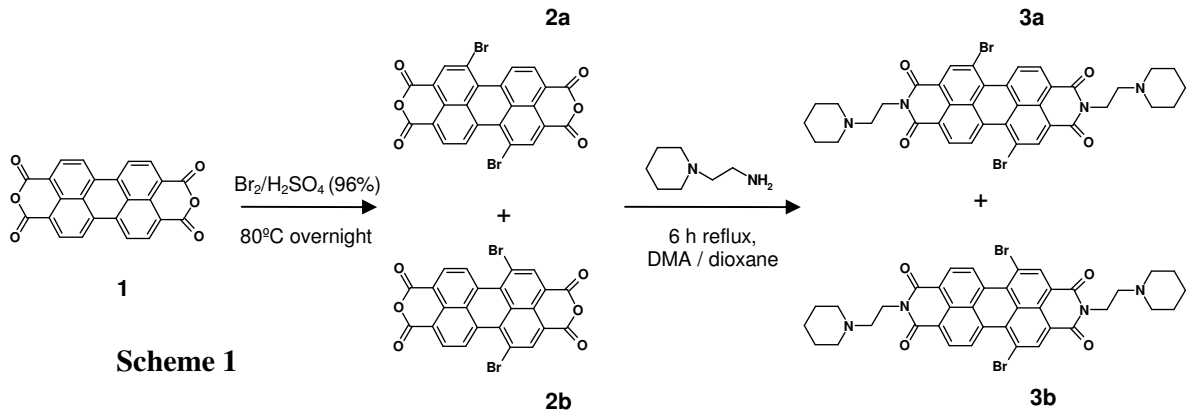

Scheme 1

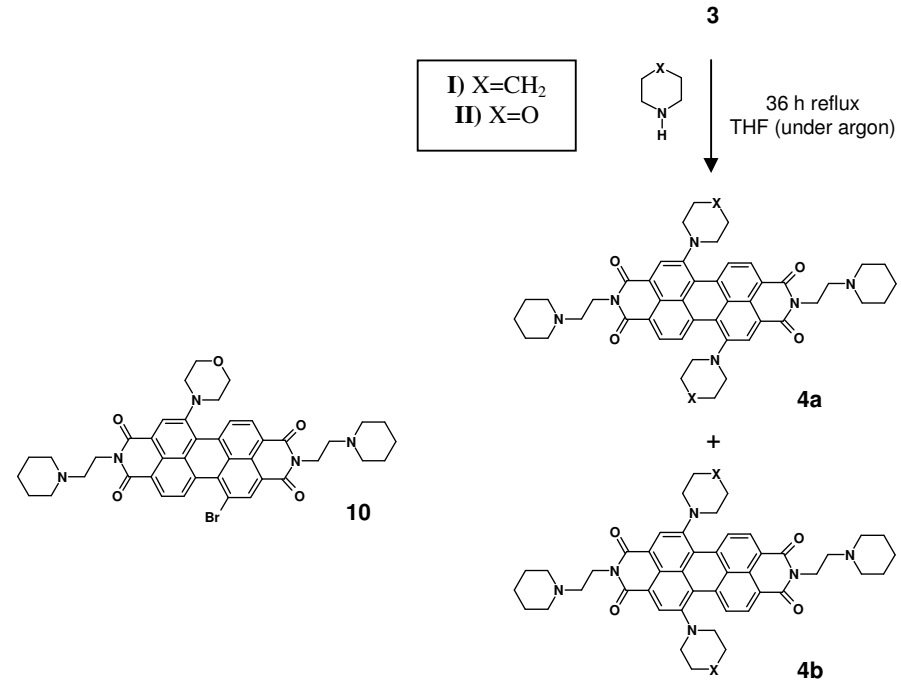

Scheme 2A

Fig. 3.1.b-1: Scheme for the synthesis of the new perylene derivatives (Franceschin *et al.* **2004**).

aminoethyl)piperidine were stirred in a refluxing mixture of N,N-dimethylacetamide (DMA, 60ml) and 1,4-dioxane (60ml) for 6h. After cooling, water was added and a red solid was separated by filtration (71% yield). This mixture of isomers (**3**) was used in the following steps (Schemes 2A and 2B).

When reacting **3** with piperidine (X=CH_2 in Scheme 2A) two isomers [**4a(I)** and **4b(I)**] were separated and characterized. 250mg of **3** were stirred under argon in a refluxing mixture of tetrahydrofuran (THF, 20ml) and piperidine (20ml) for 36h. After cooling, water was added and the crude product was extracted with ethyl acetate. The organic layer was extracted with water until the aqueous layer was neutral. The two isomers [**4a(I)** (30%) and **4b(I)** (5%), PIP-PIPER (1,7) and (1,6) respectively] were isolated by column chromatography on silica gel ($CHCl_3$). A standard commercial silica gel had been previously washed with 1N HCl, followed by water until the chlorine test was negative, activated at 120°C for 48h, and finally equilibrated with 10% water (Bianco *et al.* **2004**). In order to obtain the water soluble hydrochlorides, these compounds were dissolved in 0.2M HCl and, after filtration, the solution was concentrated under vacuum, adding repeatedly an equal volume of chloroform until water had been eliminated completely. When repeating the same experimental conditions using morpholine (X=O in Scheme 2A) only the isomer **4b(II)** [MORPHO-PIPER(1,6)] has been isolated from the chromatographic column (5% yield). With reaction times under 12h, monosubstituted derivatives can be obtained. In particular, it was possible to purify and characterize the compound **10** (30% yield, Fig. 3.1.b-1).

1,7-dibromoperylene-3,4:9,10-tetracarboxylic dianhydride (2a) ^{1}H NMR (200 MHz, D_2SO_4): δ 10.42 (d, J = 8Hz, 2H, aromatic H), 9.75 (s, 2H, aromatic H), 9.53 (d, J = 8Hz, 2H, aromatic H). The signals of the minor (1,6) isomer (**2b**) are mainly superimposed with those reported for **2a**, a part from the doublet centred at 10.34 ppm, that is sufficiently separated

from the other signals to be integrated, giving a ratio between **2a** and **2b** of 6:1. $C_{24}H_6O_6Br_2$: calcd. C 52.4, H 1.1%; found C 51.6, H 1.1%.

***N,N'*-bis[2-(1-piperidino)-ethyl]-1,7-dibromoperylene-3,4:9,10-tetracarboxylic diimide (PIPER-Br, 3a)** ^{1}H NMR (300 MHz, $CDCl_3$): δ 9.44 (d, J = 8Hz, 2H, aromatic H), 8.89 (s, 2H, aromatic H), 8.67 (d, J = 8Hz, 2H, aromatic H), 4.41 (t, J = 7Hz, 4H, N_{imidic}-CH), 2.8-2.6 (broad, 12H, $N_{piperidine}$-CH), 1.8-1.4 (broad, 12H, $CH_{piperidine}$); ^{13}C NMR APT (200 MHz, $CDCl_3$): δ 162.14 (C=O), 161.64 (C=O), 137.31 (CH ar.), 132.17 (C ar), 132.02 (C ar.), 129.29 (CH ar.), 128.50 (C ar.), 127.78 (CH ar.), 126.28 (C ar.), 122.55 (C ar.), 122.12 (C ar.), 120.18 (C ar.), 55.74, 54.24, 37.41, 25.48, 23.81. MS (ESI) *m/z*: 771.10 [$(M+1)^+$] (calcd. for $C_{38}H_{34}N_4O_4Br_2$ M = 770.09). In this case, all ^{1}H NMR signals of the two isomers are superimposed and it is not possible to obtain the isomeric ratio.

***N,N'*-bis[2-(1-piperidino)-ethyl]-1,7-bis(1-piperidinyl)perylene-3,4:9,10-tetracarboxylic diimide [PIP-PIPER(1,7), 4a(I)]:** ^{1}H NMR (200 MHz, $CDCl_3$): δ 9.46 (d, J = 8Hz, 2H, aromatic H), 8.33 (s, 2H, aromatic H), 8.30 (d, J = 8Hz, 2H, aromatic H), 4.32 (t, J = 7Hz, 4H, N_{imidic}-CH), 3.38 (m, 4H, C_{ar}-$N_{piperidine}$-CH), 2.81 (m, 4H, C_{ar}-$N_{piperidine}$-CH), 2.7-2.4 (broad, 12H, $N_{piperidine}$-CH), 1.8-1.5 (broad, 24H, $CH_{piperidine}$); ^{13}C NMR APT (200 MHz, $CDCl_3$): δ 163.05 (C=O), 162.91 (C=O), 150.20 (C ar.), 134.90 (C ar.), 129.36 (C ar.), 127.50 (CH ar.), 123.70 (C ar.), 123.17 (CH ar.), 122.64 (CH ar.), 122.34 (C ar.), 121.85 (C ar.), 120.30 (C ar.), 55.87, 54.21, 52.27, 37.15, 25.50, 25.21, 23.88, 23.27. MS (ESI) *m/z*: 779.41 [$(M+1)^+$] (calcd. for $C_{48}H_{54}N_6O_4$ M = 778.42).

***N,N'*-bis[2-(1-piperidino)-ethyl]-1,6-bis(1-piperidinyl)perylene-3,4:9,10-tetracarboxylic diimide [PIP-PIPER(1,6), 4b(I)]:** ^{1}H NMR (200 MHz, $CDCl_3$): δ 9.63 (d, J = 8Hz, 2H, aromatic H), 8.53 (d, J = 8Hz, 2H, aromatic H), 8.31 (s, 2H, aromatic H), 4.30 (m, 4H, N_{imidic}-CH), 3.29 (m, 4H, C_{ar}-$N_{piperidine}$-CH), 2.79 (m, 4H, C_{ar}-$N_{piperidine}$-CH), 2.7-2.4 (broad, 12H, $N_{piperidine}$-CH), 1.9-1.5 (broad, 24H, $CH_{piperidine}$); ^{13}C NMR (200 MHz, $CDCl_3$): δ 163.23

(C=O), 163.10, (C=O), 152.76 (ar.), 135.60 (ar.), 131.24 (ar.), 130.21 (ar.), 128.34 (ar.), 127.51 (ar.), 123.26 (ar.), 122.69 (ar.), 122.61 (ar.), 121.85 (ar.), 120.20 (ar.), 119.68 (ar.), 55.91, 54.22, 52.63, 37.24, 37.06, 25.51, 25.28, 23.84, 23.27. MS (ESI) *m/z*: 779.43 [$(M+1)^+$] (calcd. for $C_{48}H_{54}N_6O_4$ M = 778.42).

***N,N'*-bis[2-(1-piperidino)-ethyl]-1,6-bis(4-morpholinyl)perylene-3,4:9,10-tetracarboxylic diimide [MORPHO-PIPER(1,6), 4b(II)]:** ^{1}H NMR (200 MHz, $CDCl_3$): δ 9.80 (d, J = 8Hz, 2H, aromatic H), 8.55 (d, J = 8Hz, 2H, aromatic H), 8.32 (s, 2H, aromatic H), 4.31 (m, 4H, N_{imidic}-CH), 3.87 (m, 8H, $CH_{morpholine}$), 3.19 (m, 4H, $CH_{morpholine}$), 3.03 (m, 4H, $CH_{morpholine}$), 2.6-2.4 (broad, 12H, $N_{piperidine}$-CH), 1.6-1.3 (broad, 12H, $CH_{piperidine}$); ^{13}C NMR (200 MHz, $CDCl_3$): δ 162.45 (C=O), 162.41 (C=O), 151.07 (ar.), 134.44 (ar.), 130.81 (ar.), 129.68 (ar.), 127.84 (ar.), 127.29 (ar.), 123.35 (ar.), 122.70 (ar.), 122.57 (ar.), 120.98 (ar.), 120.54 (ar.), 119.93 (ar.), 65.52, 55.29, 53.70, 50.79, 36.80, 36.57, 24.92, 23.31. MS (ESI) *m/z*: 783.39 [$(M+1)^+$] (calcd for $C_{46}H_{50}N_6O_6$ M = 782.38).

***N,N'*-bis[2-(1-piperidino)-ethyl]-1-bromo-7-(4-morpholinyl)perylene-3,4:9,10-tetracarboxylic diimide (10):** ^{1}H NMR (200 MHz, $CDCl_3$): δ 9.61 (d, J = 8Hz, 1H, aromatic H), 9.30 (d, J = 8Hz, 1H, aromatic H), 8.73 (s, 1H, aromatic H), 8.51 (d, J = 8Hz, 1H, aromatic H), 8.44 (d, J = 8Hz, 1H, aromatic H), 8.39 (s, 1H, aromatic H), 4.31 (m, 4H, N_{imidic}-CH), 3.86 (m, 4H, $CH_{morpholine}$), 3.28 (m, 2H, $CH_{morpholine}$), 3.10 (m, 2H, $CH_{morpholine}$), 2.7-2.4 (broad, 12H, $N_{piperidine}$-CH), 1.6-1.3 (broad, 12 H, $CH_{piperidine}$). MS (ESI) *m/z*: 776.31 [$(M+1)^+$] (calcd for $C_{42}H_{42}N_5O_5Br$ M = 775.24).

3.1.c. CORON: a new hydrosoluble coronene derivative

When bromine atoms on the perylene bay-area of PIPER-Br are substituted by the piperidine containing 1-alkyne **7** a two steps cyclization can occur, leading to the new hydrophilic coronene derivative **6** CORON (Fig. 3.1.c-1, Franceschin *et al.* **2004**). **3** was reacted with the previously prepared **7** to give the intermediate **5**, using the conditions previously described by Sonogashira *et al.* (**1975**); **5** was found to be already partially closed to coronene and provided **6** in the following cyclization step (Scheme 2B). In this case, the minor isomer due to the initial presence of 1,6-dibromoperylene diimide **3b** cannot be separated from the major isomer, which is the only one reported in Scheme 2B. **7** was prepared from the commercially available 3-butyn-1-ol by a mesylate conversion: 3-butyn-1-ol was converted into its mesylate (Crossland *et al.* **1970**), 1g of which, without purification, was stirred with piperidine (1.35ml) in refluxing absolute ethanol overnight under nitrogen. After cooling, solvent was evaporated under vacuum, then dichloromethane was added and the organic layer was repeatedly washed with saturated NaCl solution. Finally the organic layer was dried under vacuum to give 390mg of liquid **7** (42% yield). 2g of **3** were dissolved in anhydrous THF (80ml) and triethylamine (80ml), then CuI (50mg) and $Pd(PPh_3)_4$ (240mg) were added. After adding 1.45g of **7**, argon was bubbled into the reaction mixture that was then refluxed with stirring under argon for 24h. After cooling, 150ml of diluted HCl ($HCl:H_2O$ 1:3) were added and the product was extracted with dichloromethane, after neutralization with NaOH 2M. The organic layer was extracted with water until the aqueous layer was neutral. The crude product was purified by column chromatography on a silica gel ($CHCl_3$:MeOH 100:0, 98:2, 95:5, 90:10) to give 510 mg (22% yield) of intermediate **5**, together with a small amount of **6**. Separation and better characterization were not possible at this stage, and the entire mixture

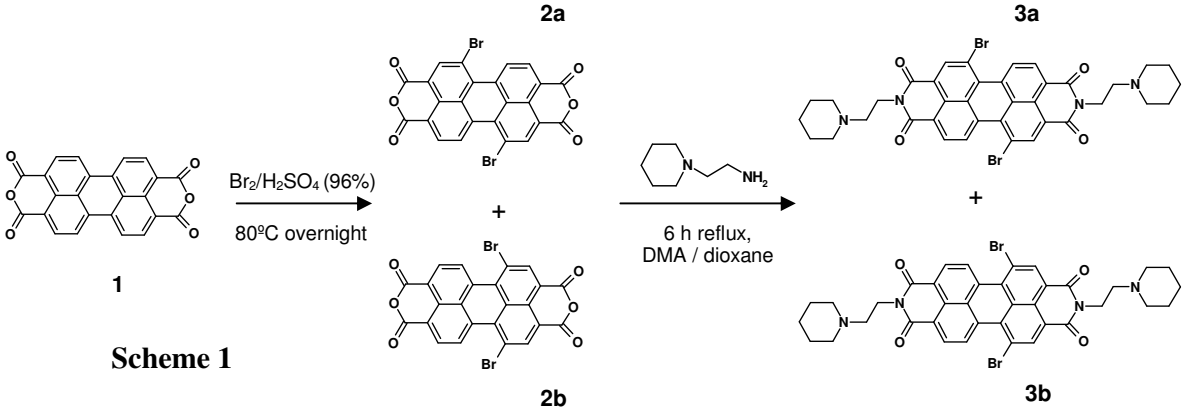

Scheme 1

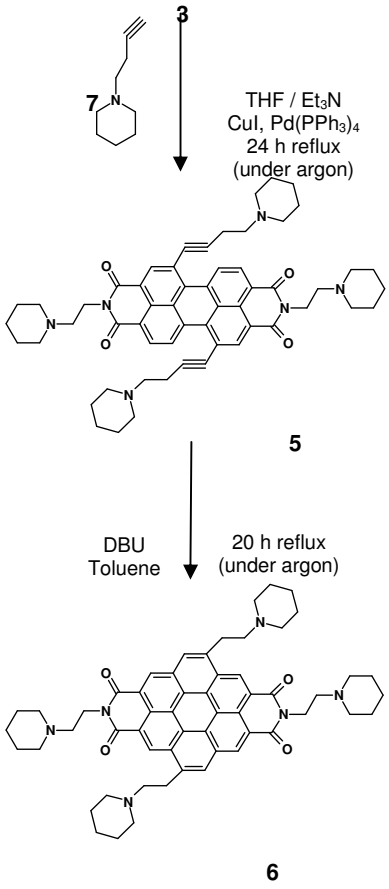

Scheme 2B

Fig. 3.1.c-1: Scheme for the synthesis of the coronene derivative (**6**). In Scheme 2B only the major isomers are reported (Franceschin *et al.* **2004**).

was used in the following cyclization step. The mixture was poured into 50ml of toluene and 0.17ml of 1,8-diazabicyclo[5.4.0]undec-7-ene (DBU) were added. The reaction mixture was refluxed with stirring under argon for 20h. After cooling, water was added and the crude product was extracted with dichloromethane. The organic layer was extracted with water until the aqueous layer was neutral. The crude product was purified by column chromatography on a silica gel ($CHCl_3$:MeOH 100:0, 98:2, 95:5, 90:10, 80:20) to give 160 mg (31% yield) of compound **6**. It was then purified dissolving in 0.2M HCl and precipitating the respective hydrochloride with acetone (64% yield).

1-(3-butynyl)-piperidine (7): ^{1}H NMR (200 MHz, $CDCl_3$): δ 2.49 (m, 2H, ≡C-CH), 2.4-2.2 (broad, 6H, N-CH), 1.90 (t, J = 3 Hz, 1H, C≡C-H), 1.53 (m, 4H, $CH_{piperidine}$), 1.37 (m, 2H, $CH_{piperidine}$); ^{13}C NMR (200 MHz, $CDCl_3$): δ 82.50 (≡C), 68.30 (≡CH), 57.29, 53.64, 25.36, 23.74, 16.10.

***N,N'*-bis[2-(1-piperidino)-ethyl]-5,11-bis[2-(1-piperidino)-ethyl]-coronene-2,3:8,9-tetracarboxylic diimide (CORON, 6):** ^{1}H NMR (300 MHz, $CDCl_3$): δ 9.22 (s, 2H, aromatic H), 9.02 (s, 2H, aromatic H), 8.25 (s, 2H, aromatic H), 4.61 (t, J = 7Hz, 4H, N_{imidic}-CH), 3.66 (m, 4H, C_{ar}-CH), 3.1-2.5 (broad, 24H, $N_{piperidine}$-CH), 1.9-1.4 (broad, 24H, $CH_{piperidine}$). ^{13}C NMR (300 MHz, $CDCl_3$): δ 163.66 (C=O), 163.50 (C=O), 138.63 (ar.), 130.77 (ar.), 128.70 (ar.), 127.98 (ar.), 127.72 (ar.), 127.40 (ar.), 124.75 (ar.), 121.26 (ar.), 120.80 (ar.), 120.35 (ar.), 120.12 (ar.), 118.62 (ar.), 60.23, 56.55, 54.92, 54.81, 38.20, 30.86, 26.24, 24.57. Aromatic ^{1}H NMR singlets due to the minor (5,10) isomer can be detected at 9.28 and 8.92 ppm. Integration of the signals shows that the ratio of the two isomers is about 5:1. It is worth noting that the strong ring-current effect of the coronene system leads to unusually high deschielding of about 1-2 ppm, in comparison with a benzenic system, both of the aromatic and benzilic-like protons. ^{1}H NMR (300 MHz, CF_3COOD, hydrochloride): δ 10.74 (s, 2H,

aromatic H), 10.51 (s, 2H, aromatic H), 9.64 (s, 2H, aromatic H), 5.38 (m, 2H, N_{imidic}-CH), 4.88 (m, 2H, N_{imidic}-CH), 4.5-4.1 (broad, 16H, $N_{piperidine}$-CH + C_{ar}-CH), 3.7-3.4 (broad, 12H, $N_{piperidine}$-CH), 2.6-1.9 (broad, 24H, $CH_{piperidine}$); ^{13}C NMR (300 MHz, CF_3COOD, hydrochloride): δ 163.51 (C=O), 163.07 (C=O), 131.35 (ar.), 128.94 (ar.), 127.27 (ar.), 126.84 (ar.), 125.55 (ar.), 123.87 (ar.), 121.48 (ar.), 120.39 (ar.), 119.42 (ar.), 118.03 (ar.), 116.95 (ar.), 116.71 (ar.), 54.53, 52.73, 51.47, 51.21, 32.35, 24.37, 19.35, 19.22, 17.14. MS (ESI) *m/z*: 883.49 [$(M+1)^+$] (calcd for $C_{56}H_{62}N_6O_4$ M = 882.48).

3.1.d. Berberine analogues and derivatives

Since the natural compound berberine shows a very interesting N^+-containing aromatic moiety and was previously shown to be able to inhibit telomeres elongation (Naasani *et al.* **1999**) and to bind to G-quadruplex DNA (Ren *et al.* **1999**, par. 1.6.b), it has been interesting to add a side chain analogue to that of PIPER on this molecular moiety, which shows G-quadruplex induction and stabilization, even without any side chain (par. 4.3 and 4.6). The synthetic strategy, reported in Fig. 3.1.d-1, uses a previously described acetonyl-berberine intermediate **A** (Kim *et al.* **1999**), that can be transformed in the second intermediate **B**. Iodine on **B** can be easily replaced by piperidine to obtain the desired side chain of **C**. Using different secondary amines, a series of different side chains can be easily obtained, similarly to the series of perylene diimides.

3g of berberine chloride were dissolved in 18ml of water and 4.5ml of NaOH 50% solution were added. While stirring, 3.0ml of acetone were added drop wise. After stirring for 30 minutes at room temperature, the reaction mixture was filtered and washed with 80% methanol to give 2.65g of **A** (83.5% yield). It was dissolved in 75ml of CH_3CN and 7.4ml of 1,3-diiodopropane were added. The reaction mixture was stirred at 80°C for 6h. After cooling, it was filtered and washed repeatedly with acetonitrile. The crude product was purified by column chromatography on a silica gel ($CHCl_3$:MeOH 9:1 and then 8:2) to give 370mg (8.7% yield) of **B**. They were reacted for 4 hours with 0.86ml of piperidine in 36ml of refluxing ethanol. After cooling, the reaction mixture was dried under vacuum and the crude product was purified by column chromatography on a silica gel equilibrated with 10% of water ($CHCl_3$) to give 265mg (77% yield) of **C**. In order to obtain the respective hydrochloride, it was then dissolved in 0.1M HCl and passed through a strong basic anion exchange resin

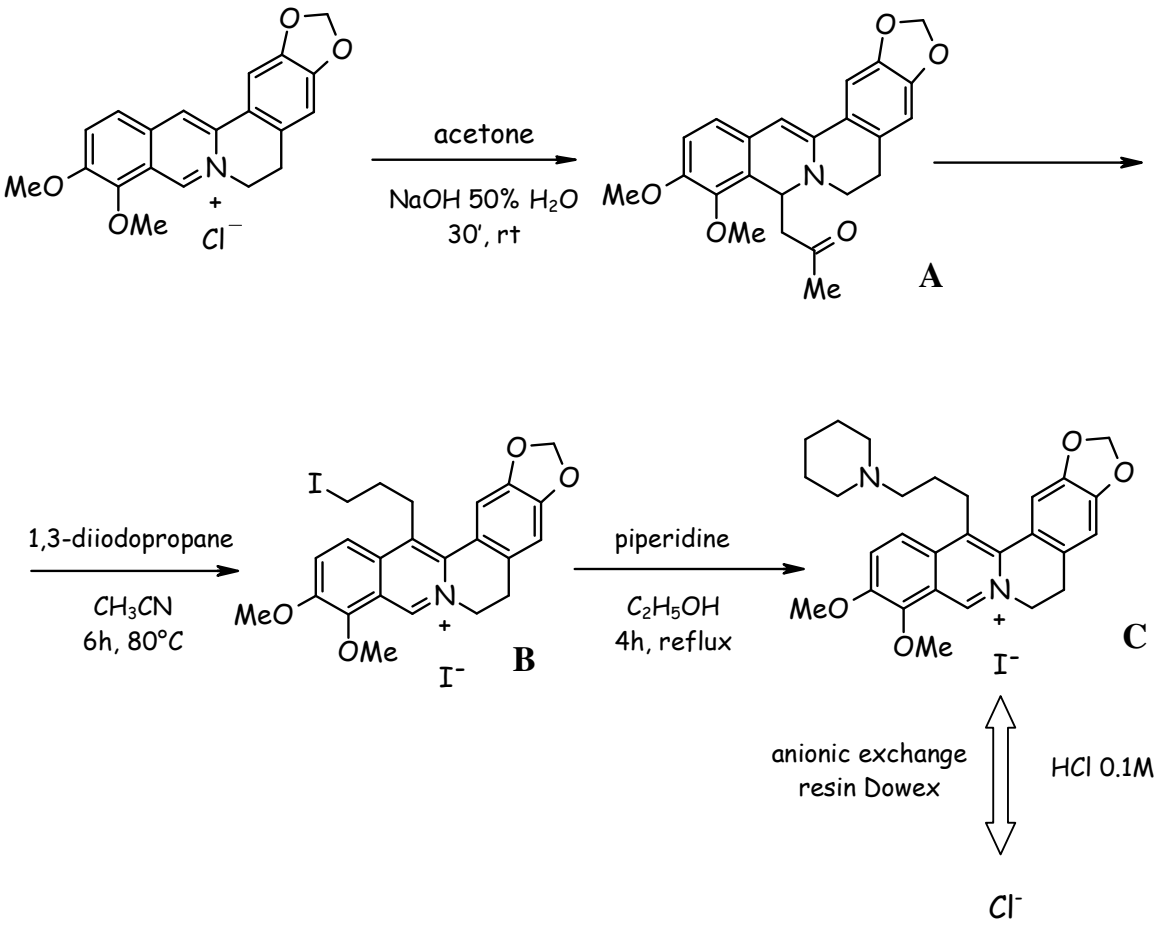

Fig. 3.1.d-1: Scheme of the synthesis of the new berberine derivative **C**.

Dowex1. The acid solution was concentrated under vacuum, adding repeatedly an equal volume of chloroform, until a powder was obtained, that was then dried under vacuum.

8-acetonyldihydroberberine (A): ^{1}H NMR (300 MHz, $CDCl_3$): δ 7.13 (s, 1H, aromatic H), 6.77 (d, J = 8 Hz, 1H, aromatic H), 6.75 (d, J = 8 Hz, 1H, aromatic H), 6.57 (s, 1H, aromatic H), 5.94 (m, 2H, O-CH_2-O), 5.89 (s, 1H, aromatic H), 5.32 (dd, X part of ABX system, 1H, J_{AX}=7Hz, J_{BX}=4Hz, CH-N)**,** 3.89 (s, 3H, CH_3-O), 3.84 (s, 3H, CH_3-O), 3.34 (m, 2H, CH_2-N), 3.07 (dd, A part of ABX system, 1H, J_{AX}=7Hz, J_{AB}=15Hz, N-CH-CO)**,** 2.79 (m, 2H, CH_2-Ar), 2.41 (dd, B part of ABX system, 1H, J_{BX}=4Hz, J_{AB}=15Hz, N-CH-CO)**,** 2.05 (s, 3H, CH_3-CO).

13-(3-iodopropyl)berberine iodide (B): ^{1}H NMR (300 MHz, $CDCl_3$): δ 10.26 (s, 1H, aromatic H), 8.00 (d, J = 9 Hz, 1H, aromatic H), 7.89 (d, J = 9 Hz, 1H, aromatic H), 7.09 (s, 1H, aromatic H), 6.89 (s, 1H, aromatic H), 6.10 (s, 2H, O-CH_2-O), 5.08 (bs, 2H, CH_2-N^+), 4.37 (s, 3H, CH_3-O), 4.07 (s, 3H, CH_3-O), 3.51 (t, J = 8Hz, 2H, CH_2-Ar), 3.32 (t, J = 6Hz, 2H, CH_2-Ar), 3.23 (t, J = 5Hz, 2H, CH_2-I), 2.30 (m, 2H, $CH_{2(propyl)}$).

13-[3-(1-piperidino)propyl]berberine iodide (C): ^{1}H NMR (300 MHz, $CDCl_3$): δ 9.69 (s, 1H, aromatic H), 8.20 (d, J = 9 Hz, 1H, aromatic H), 7.93 (d, J = 9 Hz, 1H, aromatic H), 7.10 (s, 1H, aromatic H), 6.88 (s, 1H, aromatic H), 6.15 (s, 2H, O-CH_2-O), 4.78 (bs, 2H, CH_2-N^+), 4.31 (s, 3H, CH_3-O), 4.09 (s, 3H, CH_3-O), 3.63 (t, J = 7Hz, 2H, CH_2-Ar), 3.43 (m, 2H, CH_2-Ar), 3.11 (bs, 4H, CH_2-$N_{piperidine}$), 2.98 (t, J = 8Hz, 2H, CH_2-$N_{piperidine}$), 2.35 (bs, 2H, $CH_{2(propyl)}$), 1.87 (bs, 4H, CH_2-$\beta_{piperidine}$), 1.60 (bs, 2H, CH_2-$\gamma_{piperidine}$). ^{13}C NMR (300 MHz, $CDCl_3$): δ 150.55 (ar.), 150.31 (ar.), 147.68 (ar.), 145.22 (ar.), 144.80 (ar.), 136.51 (ar.), 133.02 (ar.), 132.68 (ar.), 125.62 (ar.), 122.16 (ar.), 121.01 (ar.), 119.86 (ar.), 109.74 (ar.), 108.36 (ar.), 102.32 (ar.), 68.16, 62.43, 57.84, 56.88, 55.65, 52.77, 28.25, 26.88, 25.27, 23.13, 21.75. MS (ESI) *m/z*: 461.0 [M^+] (calcd for $C_{28}H_{33}N_2O_4$ M =461.2).

13-[3-(1-piperidino)propyl]berberine hydrochloride (piperidin-berberine): ^{1}H NMR (300 MHz, D_2O, HDO suppressed): δ 9.57 (s, 1H, aromatic H), 8.03 (d, J = 9 Hz, 1H, aromatic H), 7.97 (d, J = 9 Hz, 1H, aromatic H), 7.13 (s, 1H, aromatic H), 6.94 (s, 1H, aromatic H), 5.99 (s, 2H, O-CH_2-O), 4.75 (m, 2H, CH_2-N^+), 3.98 (s, 6H, CH_3-O), 3.42 (t, J = 7Hz, 2H, CH_2-Ar), 3.25 (m, 2H, CH_2-Ar), 2.98 (bs, 4H, CH_2-$N_{piperidine}$), 2.72 (t, J = 9Hz, 2H, CH_2-$N_{piperidine}$), 1.98 (m, 2H, $CH_{2(propyl)}$), 1.74 (m, 4H, CH_2-$\beta_{piperidine}$), 1.55 (m, 2H, CH_2-$\gamma_{piperidine}$). Elemental analysis calculated for $C_{28}H_{34}N_2O_4Cl_2$•$CHCl_3$: 53.3%C, 5.4%H, 4.3%N; found: 54.1%C, 6.1%H, 4.4%N.

The berberine analogue coralyne has been purchased from Sigma-Aldrich and used without further purification (par. 4.1).

3.2. Instruments for the characterization of the synthesized compounds

Nuclear Magnetic Resonance (NMR): ^{1}H and ^{13}C-NMR spectra were performed on Varian Gemini 200 and Varian Mercury 300 MHz instruments.

Elemental analysis: The elemental analysis of the synthesized compounds was performed at the "Servizio di Microanalisi" of the Department of Chemistry using an EA1110 CHNS-O (CE) instrument.

UV/Vis absorption spectra: New perylene and coronene derivatives spectra were performed at 300K using a JASCO V-530 spectrophotometer. As for perylene diimides without substitution on the bay-area, 1mM DMSO stocks were diluted to the final desired concentration in the selected buffer. In this last case a Varian "Cary 50" spectrophotometer was used.

Mass spectrometry: ESI spectra were performed on high resolution Micromass MS/MS Q-TOF MICRO instrument.

3.3. Biophysical and biological assays

3.3.a. Gel shift assays by PAGE (PolyAcrylamide Gel Electrophoresis)

The ability of the studied compounds to induce the formation of inter- and intramolecular G-quadruplex structures was investigated by PAGE (PolyAcrylamide Gel Electrophoresis). In fact, G-quadruplex DNA structures involving a different number of oligonucleotides and with different shapes, have a different electrophoretic mobility, which depends on the molecular weight and conformation of macromolecules (Cantor *et al.* **1980**, p. 676). If a macromolecule has a net charge q, then application of an electric field **E** will result in an applied force $\mathbf{F}=q\mathbf{E}$. This force will cause acceleration of the particle in a fluid until a steady-state velocity **v** is reached. At this velocity, frictional forces are equal and opposite to the applied force, so

$$\mathbf{v} = q\mathbf{E}/f$$

If the electrical field originates from parallel plates or the equivalent, the molecule travels in a straight line; the electrophoretic mobility u can be defined as the velocity per unit field:

$$u = \mathrm{v}/\mathbf{E} = q/f$$

This means that the electrophoretic mobility does not depend on the applied electrical field, but only on the macromolecule charge (q) and its translational frictional coefficient (f), that in turn depends on the shape and dimensions of the macromolecule. This relationship allows to use electrophoresis to obtain information about relative charge (for molecules of the same size and shape) or about relative size (for molecules of the same charge).

In aqueous solution, the presence of counterions and diffusion phenomena make difficult to elaborate a quantitative theory that allows to obtain structural data. Despite all these complications, electrophoresis is a powerful and practical tool in the analysis and separation

of proteins and nucleic acids. In fact, these problems can be minimized in zonal electrophoresis, using a solid support permeated with buffer. In particular, polyacrylamide and agarose gels retard the motion of certain molecules relative to one another, so that macromolecules can be discriminated by shape and molecular weight. The use of a solid support makes a quantitative analysis of mobility nearly impossible, but useful information can be obtained if suitable standards and references are provided.

Oligonucleotides: The DNA oligomers 2HTR (5'-AATCCGTCGAGCAGAGTTAGGGTTAGGGTTAG-3') and TSG4 (5'-GGGATTGGGATTGGGATTGGGATT-3') used in the experiments reported in this thesis were purchased from MWG. They were labelled at the 5' end by reaction of T4 polynucleotide kinase (2.5U/μg of DNA) for 30 minutes at 37°C in 50μL of buffer containing 50mM Tris-HCl pH 7.5, 10mM $MgCl_2$, 10mM 2-mercaptoethanol and 30μCi of [γ-^{32}P] ATP. The reaction was quenched heating the mixture at 65°C for 10 minutes. The reaction mixture was then purified through phenol/chloroform and chloroform extractions. After precipitation with ammonium acetate and ethanol and washing with 80% ethanol, the DNA was dried and then dissolved in the desired amount of water. The radioactivity was quantified by Beckman LS 5000 TD Scintillation System.

Drugs stocks preparation: Drugs samples were prepared dissolving the desired amount of drug in DMSO, so that to obtain 1mM stocks; further dilutions were carried out in the buffer used for each experiment.

Gel shift assays: Oligonucleotides (8 or 12μM) were heated at 95°C for 10 minutes and quickly cooled in ice to disrupt any possible preformed structure. Then they were incubated

for 2h at 30 °C in the presence of different drugs concentrations, in MES-KCl buffer (10mM MES*, pH 6.5, 50mM KCl) or TRAP-derived buffers (par. 3.3.d). In particular, TRAP buffer (20mM Tris*-HCl (pH 7.5), 68mM KCl, 15mM $MgCl_2$, 10mM EDTA, 0.5% Tween20) was used for 2HTR, while in the case of TSG4 a lower KCl concentration was used ([KCl]=5 mM), because at higher potassium concentrations the G-quadruplex monomeric structure is formed also in the absence of drugs. Complexes and structures formed after incubation were studied by native PAGE (15% polyacrylamide gel, TBE* 0.5X, KCl 20mM, run overnight at 4°C) (Rossetti *et al.* **2002**, Rossetti *et al.* **2004**, Han *et al.* **1999**).

* MES = 2-[N-morpholino]ethanesulfonic acid, Tris = Tris(hydroxymethyl)aminomethane [2-amino-2-(hydroxymethyl)-1,3-propanediol], TBE (1X) = Tris 90 mM, boric acid 90 mM, EDTA 2.5 mM

DMS footprinting: To verify the attribution of electrophoretic bands to G-quadruplex structures, dimethylsulfate (DMS) methylation protection experiments were performed. The N7 of guanine is directly involved in the Hoogsteen hydrogen bond of G–G base pair, so the formation of G-quadruplex structures should protect guanine residues from methylation by DMS, while guanines not involved in quadruplex structures remain susceptible (Rossetti *et al.* **2002**, Fig. 3.3.a-1). Oligonucleotides (free or after incubation with the drugs) were treated with DMS at a final concentration of 1% (v/v), for 10 minutes at room temperature. Immediately thereafter, the products were gel-purified by native 16% PAGE: the bands corresponding to single stranded and G-quadruplex DNA were separated and successively treated with piperidine to induce strand cleavages at methylated bases. Finally, the reaction products were loaded on a denaturing gel 20% polyacrylamide gel (Negri *et al.* **1996**). In Fig. 3.3.a-2 the results obtained for PIPER and PIPER3, that induce tetrameric and dimeric G-

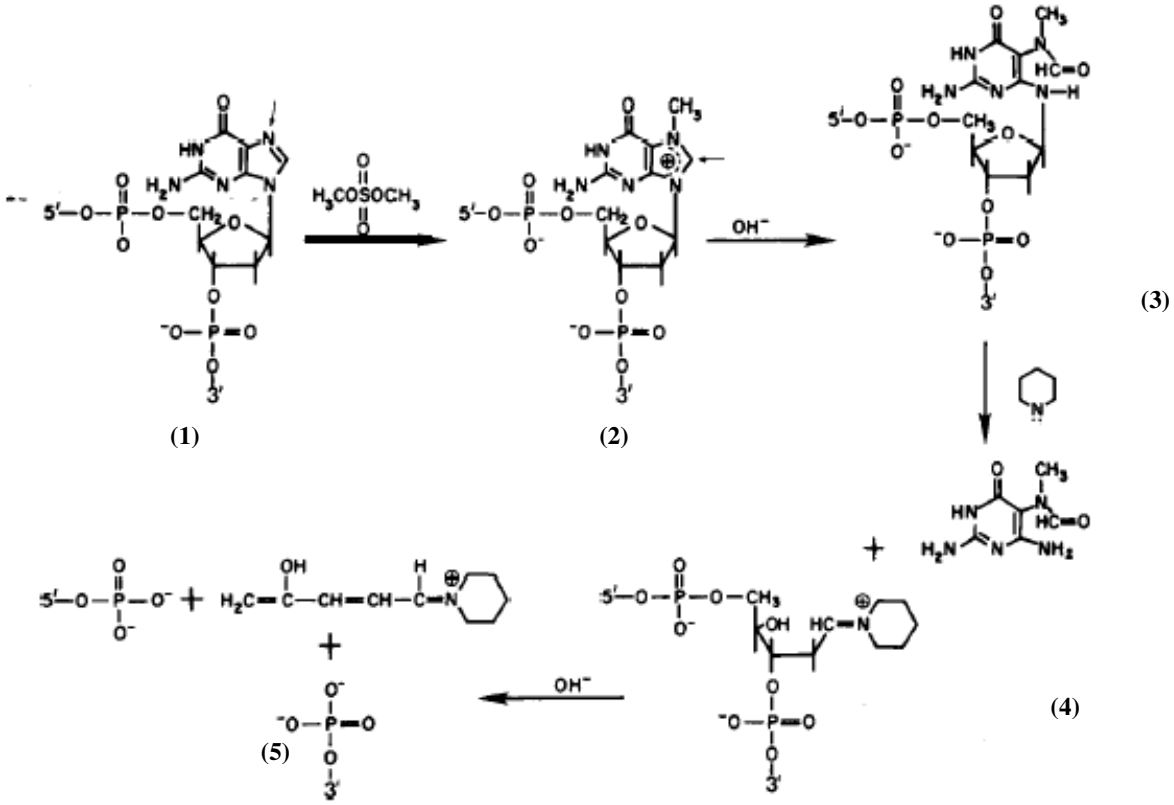

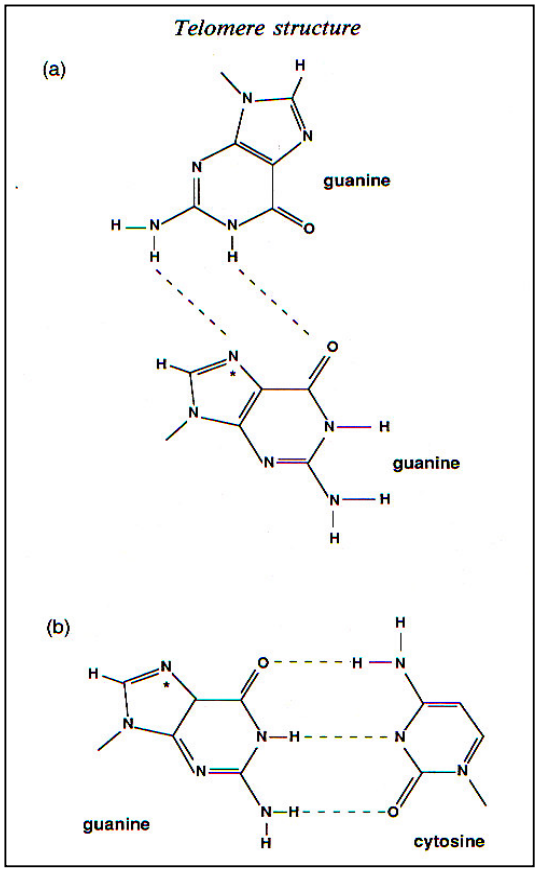

Fig. 3.3.a-1: Comparison (left) between Hoogsteen H-bonds of two guanines involved in a G-quartet structure (a) and classical Watson-Crick GC base paring (b). The nitrogen atom labelled with * is the guanine N7 atom involved in the Hoogsteen paring, while it is free in the GC paring (Kipling **1995**). In the last case, as well as in single stranded DNA, it can be methylated by DMS (above). The intermediate (2) is easily hydrolysed in basic environment, and the so formed (3) reacts with piperidine leading to the cleavage of the oligonucleotide (4 and 5). Guanines protected by Hoogsteen H-bonds are not susceptible to this treatment.

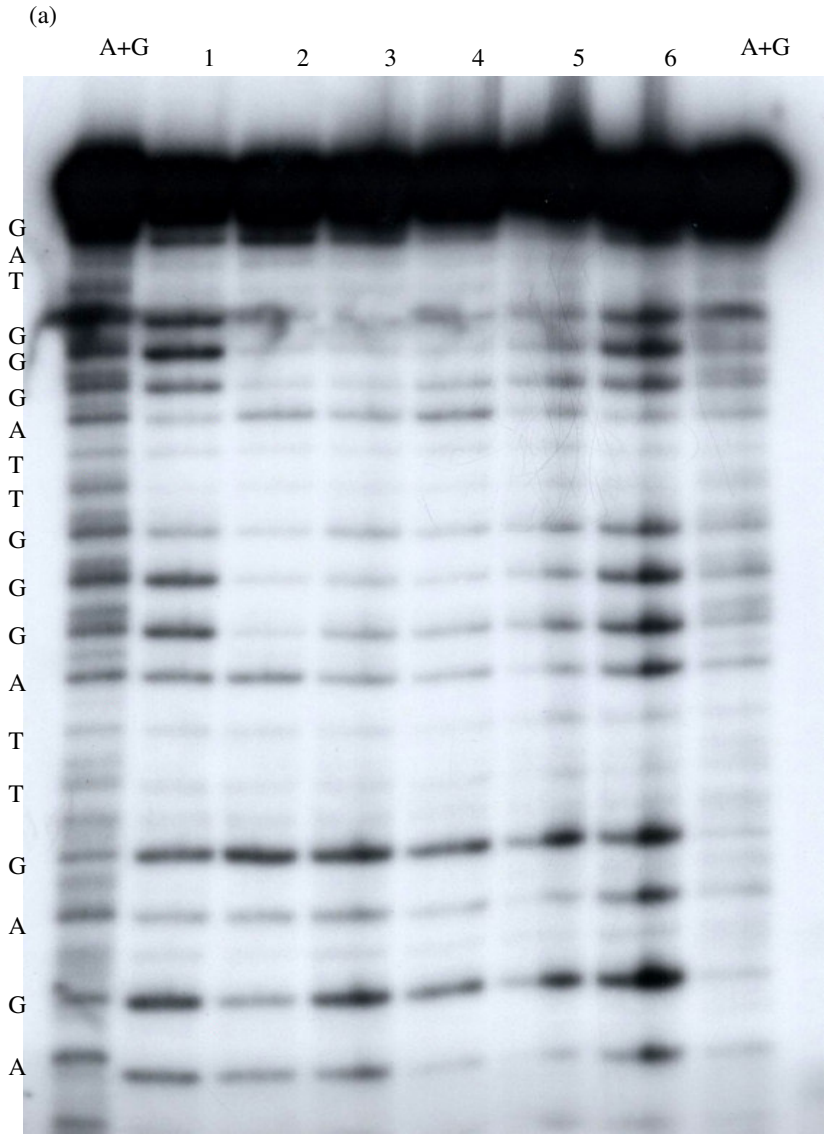

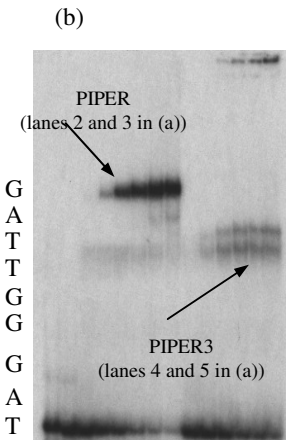

Fig. 3.3.a-2: Dimethyl sulfate (DMS) footprinting. (a) 2HTR (free (1 and 6) and incubated with PIPER (2-3) and PIPER3 (4-5) at 20 and 50 μM respectively) was treated as described in the text; the products (tetramer, dimer and free oligomer) were gel-purified by native PAGE (b): after reaction with piperidine to induce strand cleavages, the reaction products were loaded on the denaturing polyacrylamide gel reported in (a). A+G: Maxam and Gilbert reaction for purins. (c) Densitometric profiles of the corresponding lanes.

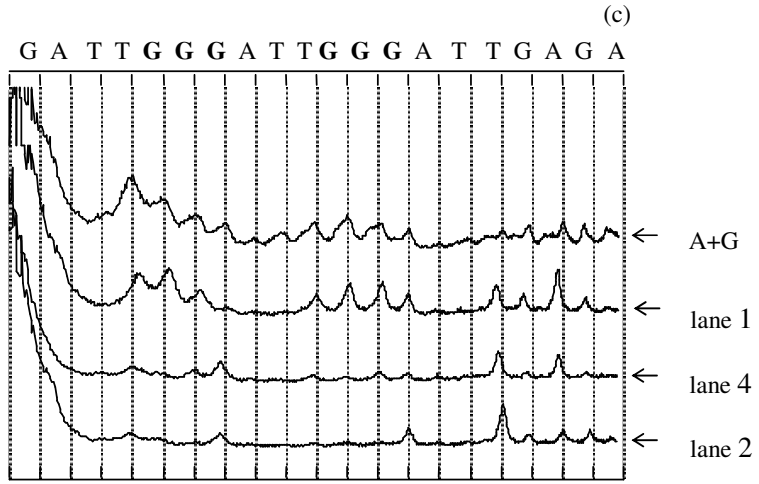

quadruplex structures on 2HTR respectively, are reported. The free oligomer 2HTR (lanes 1 and 6) was uniformly methylated by DMS at every guanine residue. On the contrary, in the case of the tetrameric (lanes 2 and 3) and dimeric (lanes 4 and 5) G-quadruplex complexes, induced, respectively, by PIPER and PIPER3, the guanines that were within the two human telomeric repeats resulted protected, while the guanine residues in the tail remained always sensitive. All these data confirm that the bands with different electrophoretic mobility with respect to single stranded DNA induced by PIPER and PIPER3 correspond to G-quadruplex structures stabilized by the association of four guanines in a cyclic Hoogsteen hydrogen-bonding arrangement. Analogues experiments have been performed with the other drugs and the TSG4 oligomer, to confirm G-quadruplex formation.

3.3.b. Absorption and circular dichroism spectroscopy

UV/Vis absorption spectra of perylene diimides in the presence of different concentrations of duplex and quadruplex DNA were performed using a spectrophotometer Varian "Cary 50". Circular dichroism spectra were performed on Jasco "J-7000".

Absorption spectra were registered between 350 and 650 nm in polystyrene cuvettes, in order to minimize adsorption phenomena of perylene derivatives, which can occur using glass cuvettes. 1mM drug stocks were diluted in MES buffer (10mM, pH 6.5) to 10μM. Oligonucleotides representing models for G-quadruplex structures were purchased from MWG and dissolved in buffer containing MES 10mM pH 6.5, KCl 100mM, EDTA 0.01mM. Then, they were annealed heating the sample at 95°C for 2 minutes and cooling slowly to room temperature. Circular dichroism spectra were registered and compared to those reported in the literature, to be sure of the correct G-quadruplex folding. In particular, in Fig. 3.3.b-1 circular dichroism spectra of $(T_4G_4)_2$ before and after annealing are reported. As duplex model, calf thymus DNA was considered. Since its average length is 13kb, it was treated with ultrasound (Soniprep 150 sonicator) for 8 minutes to obtain an average length of 500bp (according to gel electrophoresis analysis with Mass Ruler DNA ladder mix - low range). The concentrations of the various DNA were determined by measurement of absorbance at 260nm. Initial DNA concentration was 800μM; adding increasing volumes of 10μM drug stock the DNA/drug ratio was decreased until a final DNA concentration of 20μM, while taking constant drug concentration.

Preliminary experiments of circular dichroism were performed, using solutions prepared separately at the desired drug/DNA ratio.

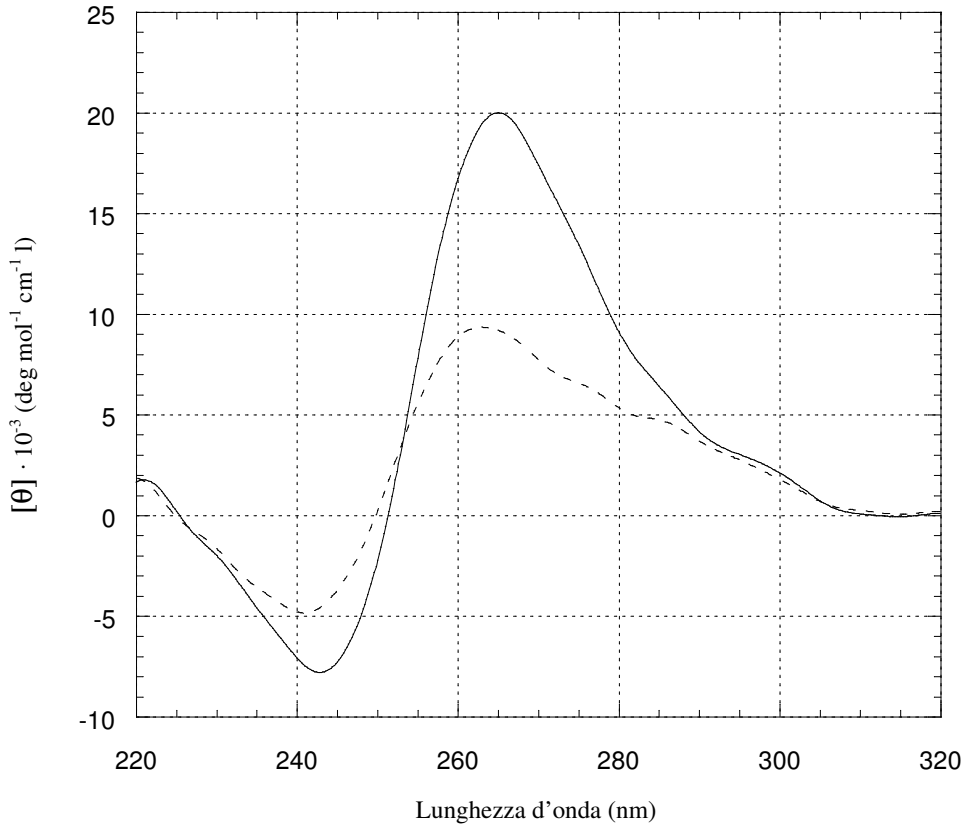

Fig. 3.3.b-1: Circular dichroism spectra of $(T_4G_4)_2$ in MES/KCl buffer (MES 10 mM pH 6.5, KCl 100 mM) before (————) and after (- - - - -) the annealing at 95 °C.

3.3.c. Fluorescence Resonance Energy Transfer (FRET) assays

Fluorescence resonance energy transfer (FRET) is a distance-dependent interaction between the electronic excited states of two dye molecules in which excitation is transferred from a donor molecule to an acceptor molecule without emission of a photon. Primary conditions for FRET are: 1) donor and acceptor molecules must be in close proximity (typically 10–100 Å); 2) the absorption spectrum of the acceptor must overlap the fluorescence emission spectrum of the donor (Fig. 3.3.c-1(a)); 3) donor and acceptor transition dipole orientations must be approximately parallel (Cantor *et al.* **1980**, p. 448).

The efficiency of FRET is dependent on the inverse sixth power of the intermolecular separation (Fig. 3.3.c-1(b)), making it useful over distances comparable with the dimensions of biological macromolecules. In most applications, the donor and acceptor dyes are different, in which case FRET can be detected by the appearance of sensitized fluorescence of the acceptor or by quenching of donor fluorescence.

FRET can be used to probe the secondary structure of oligodeoxynucleotides mimicking repeats of the G-rich strand of vertebrate telomeres, provided a fluorescein (donor) molecule and a tetramethylrhodamine (acceptor) derivative are attached to the 5'- and 3'-ends of the oligonucleotide, respectively (Koeppel *et al.* **2001**). In the unfolded form, little transfer is expected, as the average distance of the two chromophores is larger than the Förster critical distance (calculated to be ≈5.0 nm, Fig. 3.3.c-1). Intramolecular folding into a G-quadruplex should bring the two chromophores in close enough proximity to observe energy transfer. Therefore, FRET should be a convenient method to monitor the 3'- to 5'-end distance (Koeppel *et al.* **2001**).

(a)

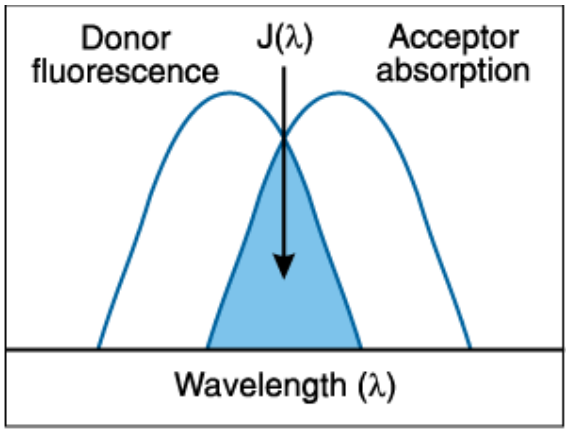

(b)

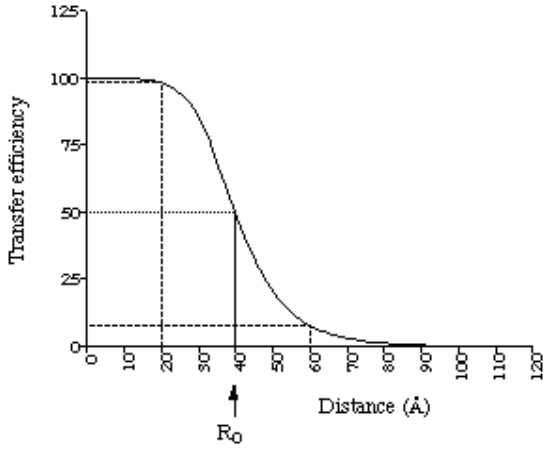

$$E = \frac{R_o^6}{R_o^6 + R^6}$$

Fig. 3.3.c-1: (a) Schematic representation of the superimposing of the absorption spectrum of the acceptor and the fluorescence emission spectrum of the donor. (b) Relationship between the efficiency of the fluorescence resonance energy transfer and the distance separating the two probes (R); R_o is the Förster distance, that is, the distance between the donor and acceptor probe at which the energy transfer is (on average) 50% efficient.

Fig. 3.3.c-2: ***(next page)*** Molecular structures and absorption/fluorescence spectra in aqueous buffer of the fluorescein derivative (6-carboxyfluorescein - FAM) used as donor and of the tetramethylrhodamine derivative (5-carboxytetramethylrhodamine - TAMRA) used as acceptor in the FRET experiments reported in this thesis.

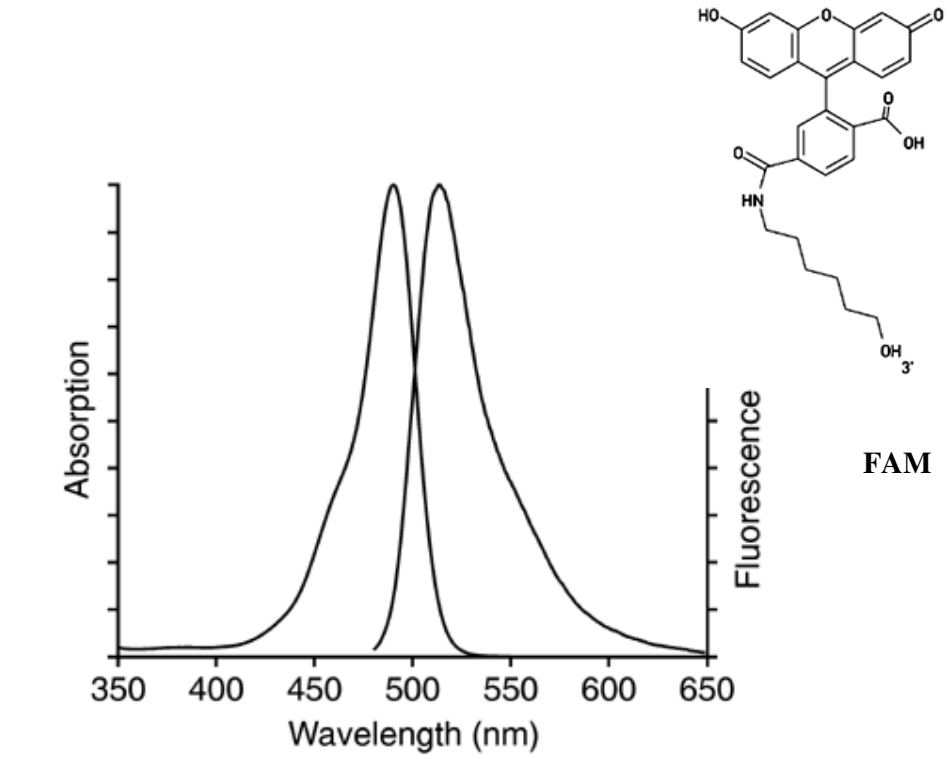

FAM

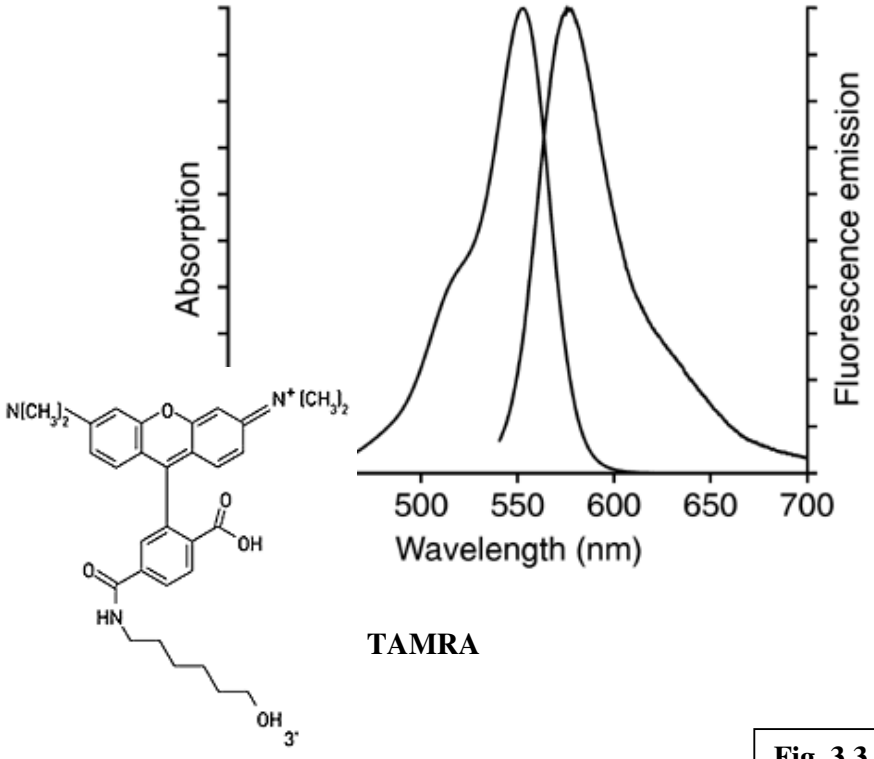

TAMRA

Fig. 3.3.c-2

The donor-acceptor pair used in the FRET experiments reported in this thesis is composed by a fluorescein derivative (6-carboxyfluorescein - FAM) as donor and a tetramethylrhodamine derivative (5-carboxytetramethylrhodamine - TAMRA) as acceptor (Mergny *et al.* **2001**). Their structures and absorption/fluorescence spectra in aqueous buffer are reported in Fig. 3.3.c-2.

The two probes are linked (by mean of a C-6 linker) to the ends of the used oligonucleotides and detection is made on quenching of donor fluorescence, so that during DNA melting an increase of fluorescence is observed, due to the increasing of the distance between the two probes, that are instead close enough to give efficient FRET when DNA is annealed.

Oligonucleotides: Two different fluorescent conjugated oligonucleotides were used as models for intramolecular G-quadruplex and duplex DNA respectively. Both of them were purchased from Oswel (Southampton, UK). G-quadruplex forming sequence was 5'-FAM-dGGG(TTAGGG)$_3$-TAMRA-3' (F21T), while duplex model was 5'-FAM-dTATAGCTATA-(CH$_2$-CH$_2$-O)$_6$-dTATAGCTATA-TAMRA-3' (F10D). DNA was initially dissolved as a stock 20μM solution in 10mM TE (Tris, EDTA) buffer (pH 8.0); further dilutions were carried out in 50mM potassium cacodylate buffer (pH 7.4).

Drugs stocks preparation: Drugs were dissolved in bidistilled water, so that to obtain 1mM stocks; further dilutions were carried out in 50mM potassium cacodylate buffer (pH 7.4). Stocks were used within 72 hours from their preparation. They were kept at +4°C, avoiding light exposure.

FRET stabilisation assay: The ability of the compounds to stabilize intramolecular G-quadruplex and duplex DNA was investigated using a FRET assay modified to be used in a

96-well format. Oligonucleotides were diluted in the relevant buffer to the 2x concentration (400nM) and then annealed by heating to 85°C for 5 minutes, followed by cooling to room temperature in the heating block.

96-well plates (MJ Research, Waltham, MA) were prepared by aliquoting 50µL of the annealed DNA to each well, followed by 50µL of the compound solutions. Samples were left equilibrating for half an hour before starting the experiment. Measurements were made on a DNA Engine Opticon (MJ Research) with excitation at 450-495nm and detection at 515-545nm. Fluorescence readings were taken at intervals of 0.5°C over the range 30-100°C, with a constant temperature being maintained for 30 seconds prior to each reading to ensure a stable value. Final analysis of the data was carried out using a script written in the program Origin 7.0 (OriginLab Corp., Northampton, MA).

Drug concentrations were chosen so that to have the final drug/DNA ratios (R) as reported in the following table.

conc.(µM)		0.02	0.04	0.06	0.10	0.15	0.20	0.40	0.60	1.00	1.50	2.00
R		**0.10**	**0.20**	**0.30**	**0.50**	**0.75**	**1.00**	**2.00**	**3.00**	**5.00**	**7.50**	**10.00**

All the experiments were carried out in triplicate. Maximum drug concentrations were proven not to have enough fluorescence on their own to disturb fluorescence of the probes. Where necessary DMSO stocks were used, with a final DMSO concentration less than 0,5% not affecting DNA stability. The poor fluorescence of berberine and piperidin-berberine allowed to reach drug concentrations of 5 and 10µM (R=25 and 50 respectively) for these compounds.

3.3.d. Telomeric Repeat Amplification Protocol (TRAP) assays

In order to study the ability of the considered compounds to inhibit telomerase, two different telomeric repeat amplification protocol (TRAP) assays were considered. Its schematic principles are reported in Fig. 3.3.d-1. First, the standard not telomeric TS oligonucleotide (5'-AATCCGTCGAGCAGAGTT-3') was used as telomerase substrate (Kim *et al.* **1994**): because of the specific feature of this sequence, TRAP only allows the detection of G-quadruplex-induced telomerase inhibition after the synthesis of at least two or four telomeric repeats. TRAP assays were repeated using TSG4 oligonucleotide (par. 3.3.a) as telomerase substrate (Gomez *et al.* **2002**): it is able to form intramolecular G-quadruplex also before the telomerase synthesis. In fact, the KCl concentration used in the TRAP assay (68mM) allows the formation of G-quadruplex by TSG4. Nevertheless, a similar structure is not so stable and in the absence of a G-quadruplex stabilizing molecule, it may be efficiently unfolded and extended by telomerase (Rossetti *et al.* **2004**).

In all cases, drugs were added at different concentrations to the reaction mixture (50µL), that contains 50µM dNTPs, 0.5µM TS primer, 1µL of cell extract (prepared from 10^9 cultured HeLa cells, as previously described (Kim *et al.* **1994**)) in TRAP buffer (20mM Tris-HCl (pH 7.5), 68mM KCl, 15mM $MgCl_2$, 10mM EDTA, 0.5% Tween20). Samples were incubated for 2 hours at 30°C, before the addition of the cell extract. After 30 minutes of incubation at 30°C, the samples were purified by phenol/chloroform extraction. ^{32}P radiolabeled TS (or TSG4), 0.5µM ACT (or CX_{ext} respectively, Gomez *et al.* **2002**) primer (Kim *et al.* **1997**) and 2U Taq DNA polymerase (Eppendorf) were added and 27 PCR (Polymerase Chain Reaction) cycles were performed (94°C 30", 50°C 30", 72°C 1'30"). This technique allows obtaining large amounts of DNA copies starting from small amounts of an initial sequence, which is

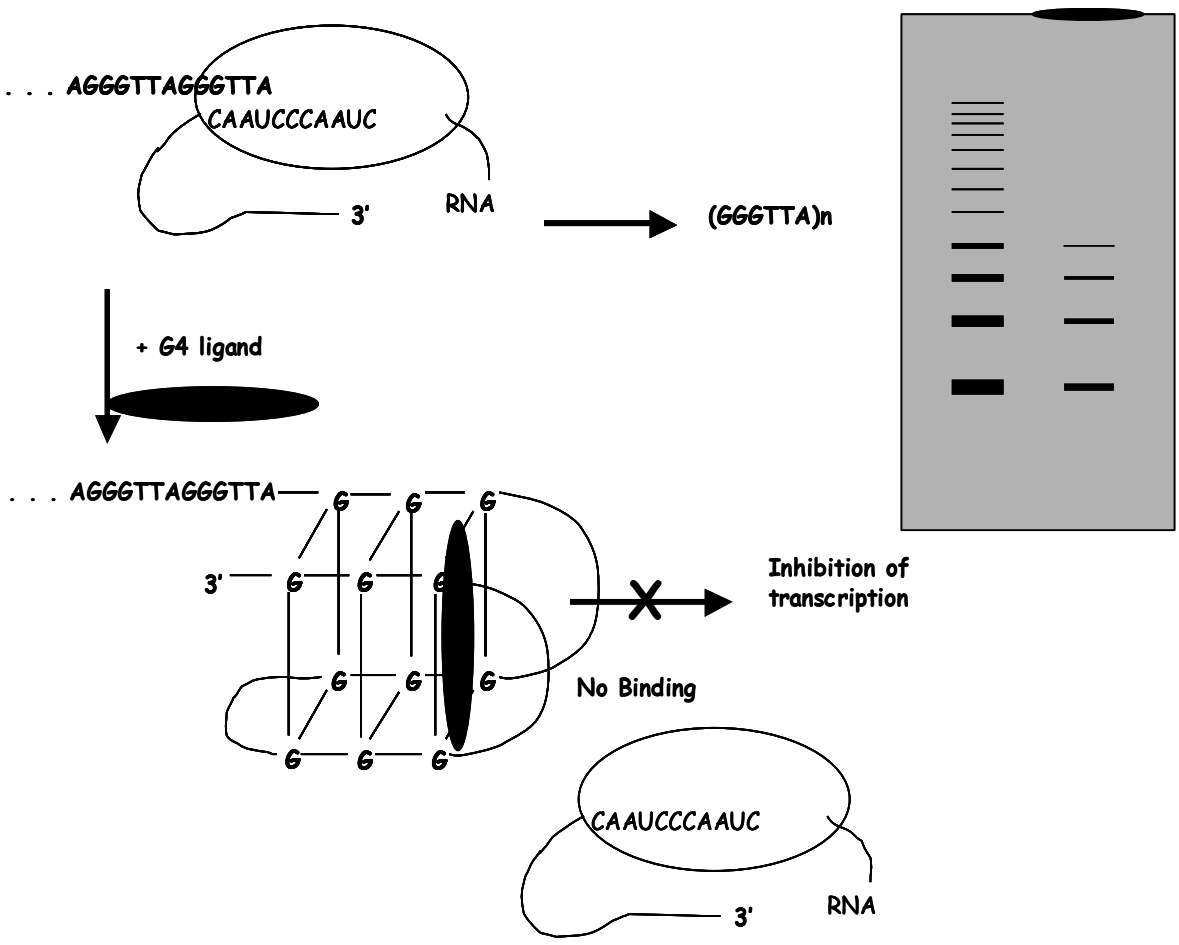

Fig. 3.3.d-1: Telomeric Repeat Amplification Protocol (TRAP) assays. Telomerase can add sequences of six nucleotides, starting from a suitable substrate, so that to give a ladder when the products of elongation are loaded on polyacrylamide gel (left lane). In the presence of a molecule able to induce and/or stabilize G-quadruplex structures in telomeric sequences, telomerase cannot bind to its substrate and the result is a weaker and shorter ladder (right lane).

amplified by DNA polymerase, if suitable complementary primers are provided. Finally, the samples were loaded on non-denaturing 12% polyacrylamide gel. As references, a sample in which no drug was added, one where cell extract was not added and one in which heat inactivation was performed by heating 10µL extract at 75°C for 10 minutes, prior to assaying 1µL by TRAP analysis, were considered. A 130bp "internal standard" (IS) was used to control the PCR amplification efficiency (Gan *et al.* **2001**).

3.4. Molecular modeling

All the experiments were performed using the InsightII package on an SGI workstation. This software is widely used for the modeling of protein-ligand complexes, and more rarely for DNA-ligand complexes (Osiadacz *et al.* **2000**).

The G-quadruplex structure used in all the simulations is the X-ray derived monomeric structure of the 22-mer human telomeric DNA sequence $AGGG(TTAGGG)_3$, 1KF1 code in the PDB (Fig. 1.2-5, Parkinson *et al.* **2002**). The PDB coordinates file was imported into the InsightII modeling package; the potassium ions in the central channel between the planes of each G-quartet were preserved, while all water molecules were deleted. Hydrogen atoms were added to the structure and potentials and partial charges were assigned according to the CVFF force-field, considering a pH of 7.0. A +1 partial charge was assigned to each potassium ion.

Ligand molecules were built using the Builder module in InsightII. Nitrogen atoms in the side chains were protonated assigning a +1 formal charge (except for PIPER2, no charge, and PIPER3, par. 4.5) and CVFF force-field atom and bond types were assigned to all the structures (except for PIPER7, for which CFF parameters were necessary). All the structures were energy-minimized (2000 steps, Polak-Ribiere conjugate gradient) using the Discover_3 module.

Docking was performed in two phases with the Affinity Docking module of InsightII. The binding pocket was defined as all and only H atoms on the guanine bases of the external G-quartet planes (one of the two possible external planes at a time, par. 4.5). In the first phase 200 ligand orientations were randomly centred on the G-quadruplex structure. In this phase charges were not considered, non-bonded cut-offs were set to 8Å and Van der Waals radii to 10% of the full value. The complexes were minimized for 500 steps using Polak-Ribiere

conjugate gradient method; energy tolerance and energy range were set respectively to 10000 and 40kcal/mol. In the second phase, the 75 lowest energy structures were used to perform simulated annealing. During this phase Van der Waals radii were adjusted to their full values and a distance-dependent dielectric constant of 4.0 was used. Each system was again minimized for 500 steps of conjugate gradient and then molecular dynamics was performed, starting at a temperature of 800K and cooling the system to 200K over a period of 10ps. The resulting structures were minimized for 2000 steps of conjugate gradient and the 25 structures with the lowest total energies were evaluated with the Analysis module of InsightII. The Docking module was used to calculate the intermolecular (binding) energy, obtained as a sum of electrostatic and Van der Waals contributions, between drug and DNA, setting cut-offs to 100Å.

4. Results

4.1. Investigated compounds and their physico-chemical properties

4.1.a. Perylene and coronene derivatives

All perylene and coronene derivatives studied in this thesis are reported in Fig. 4.1.a-1, their synthesis is described in chapter 3.1, or otherwise their commercial source is indicated.

Simple perylene diimides have been widely studied (Fedoroff *et al.* **1998**, Han *et al.* **1999**, Rossetti *et al.* **2002**, Kerwin *et al.* **2002**, Kern *et al.* **2002**, Rossetti *et al.* **2004**), since PIPER has been known for several years for its ability in inducing G-quadruplex structures and in inhibiting telomerase (par. 1.6.a). In this series of compounds, maintaining unchanged the stacking interactions due to the perylene aromatic core, it is possible to compare the effect of different side chains linked to the same aromatic moiety. In particular, PIPER side chains are characterized by a nitrogen atom in a piperidine ring ($pK_a \approx 11$), so that it can be considered totally charged, in the adopted experimental conditions (pH 6.5 and 7.5). In the case of PIPER2, instead, the nitrogen atom in the aromatic pyridine ring ($pK_a \approx 5.5$) is positively charged only in a small fraction of the molecules, in the same conditions. The piperazine ring of PIPER3 has two nitrogen atoms, whose first dissociation constant is comparable to that of PIPER, while the second one is comparable to that of PIPER2, so that a small fraction of molecules will be doubly charged in the experimental conditions around neutrality, while in the molecules with a single charge, it can be positioned alternatively on one of the two

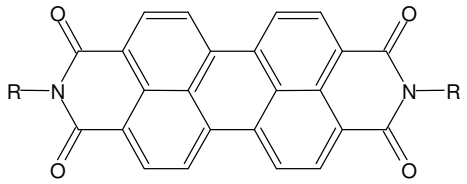

R =

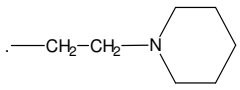

PIPER

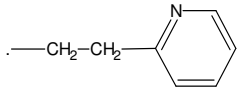

PIPER2

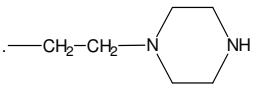

PIPER3

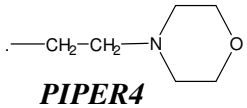

PIPER4

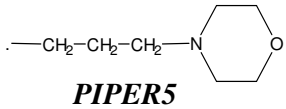

PIPER5

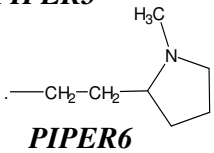

PIPER6

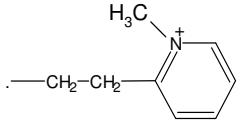

PIPER7

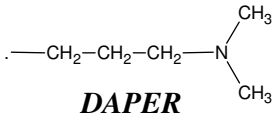

DAPER

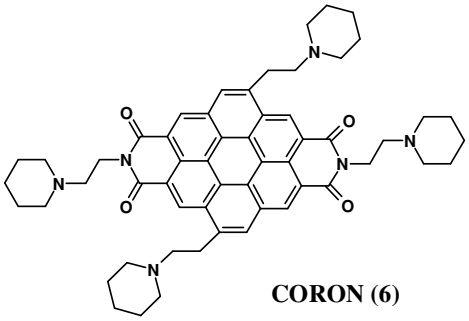

CORON (6)

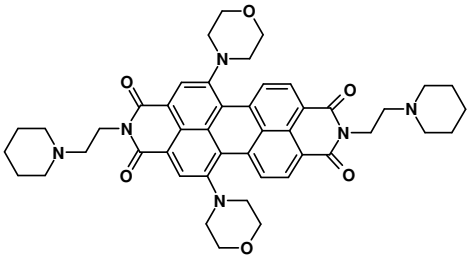

MORPHO–PIPER (1,6) [4b(II)]

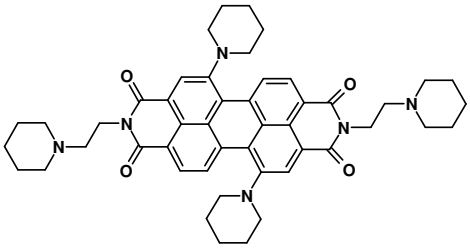

PIP–PIPER (1,7) [4a(I)]

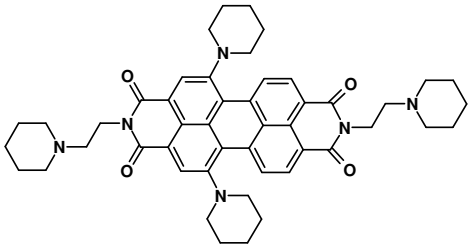

PIP–PIPER (1,6) [4b(I)]

Fig. 4.1.a-1: Complete schematic representation of all studied perylene and coronene derivatives.

nitrogen atoms; furthermore, the possibility exists to make different hydrogen bonds with DNA phosphates than PIPER. Two compounds have a morpholine ring in the side chains: PIPER4 and PIPER5; the expected pK_a for these compounds is about 8. They have ethyl and propyl linkers respectively to connect the morpholine N atom to the aromatic moiety; the oxygen atom on the morpholine ring leads to a greater polar chain than all the other considered compounds, except PIPER3. PIPER6 and PIPER7 have not the charged nitrogen atom directly linked to the side chain; both of them have an ethyl linker and the expected pK_a for PIPER6 is about 10. This means that the distance of the nitrogen atom from the aromatic core is roughly the same as in the case of PIPER5, that is characterized by a propyl linker. This is also the case of DAPER, whose nitrogen atom in the side chains even having pK_a comparable to that of PIPER, is not inside a cycle, so that its charge has a different stereochemistry.

The "self-aggregation" process of the perylene diimides, due to the stacking interactions between drug molecules, deeply influences both their interactions with the G-quadruplex (even though the mechanism has not been fully understood) and their water solubility (Rossetti *et al.* **2004**, Kerwin *et al.* **2002**, Kern *et al.* **2002)**. In Fig. 4.1.a-2 (top) the UV/Vis absorption spectra of PIPER in organic solvent (DMSO) and water are reported. A strong hypochromic effect can be observed in aqueous solution, suggesting a "self-association" process, which is confirmed by the poor resolution of the respective aromatic NMR signals. The other perylene diimides present identical UV/Vis spectra in DMSO, with peaks at 462, 493 and 529nm, whose intensities are equal for all the different compounds (Fig. 4.1.a-2 (bottom)), while the spectra in aqueous solution show a strong hypochromic effect, but to a different extent, depending on the different side chains (Fig. 4.1.a-3). This clearly indicates that the "self-aggregation" process depends on the different side chains, and it is probably mainly related to their different basicity. In Fig. 4.1.a-3, representative PIPER (A) and

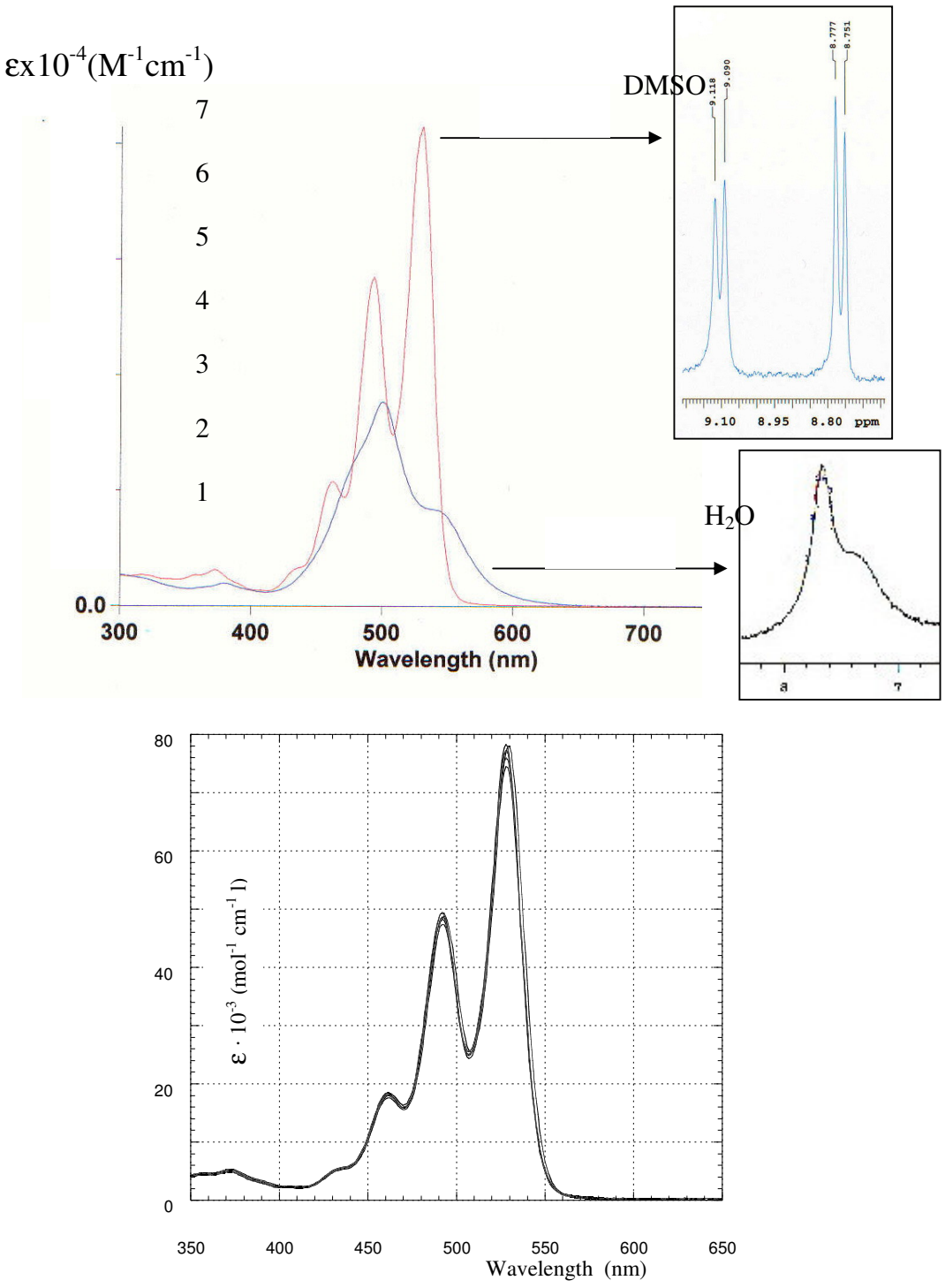

Fig. 4.1.a-2: UV/Vis absorption spectra of PIPER in DMSO (red) and water (blue) and the respective aromatic protons signals by NMR (top). Perylene derivatives UV/Vis absorption spectra in DMSO (bottom).

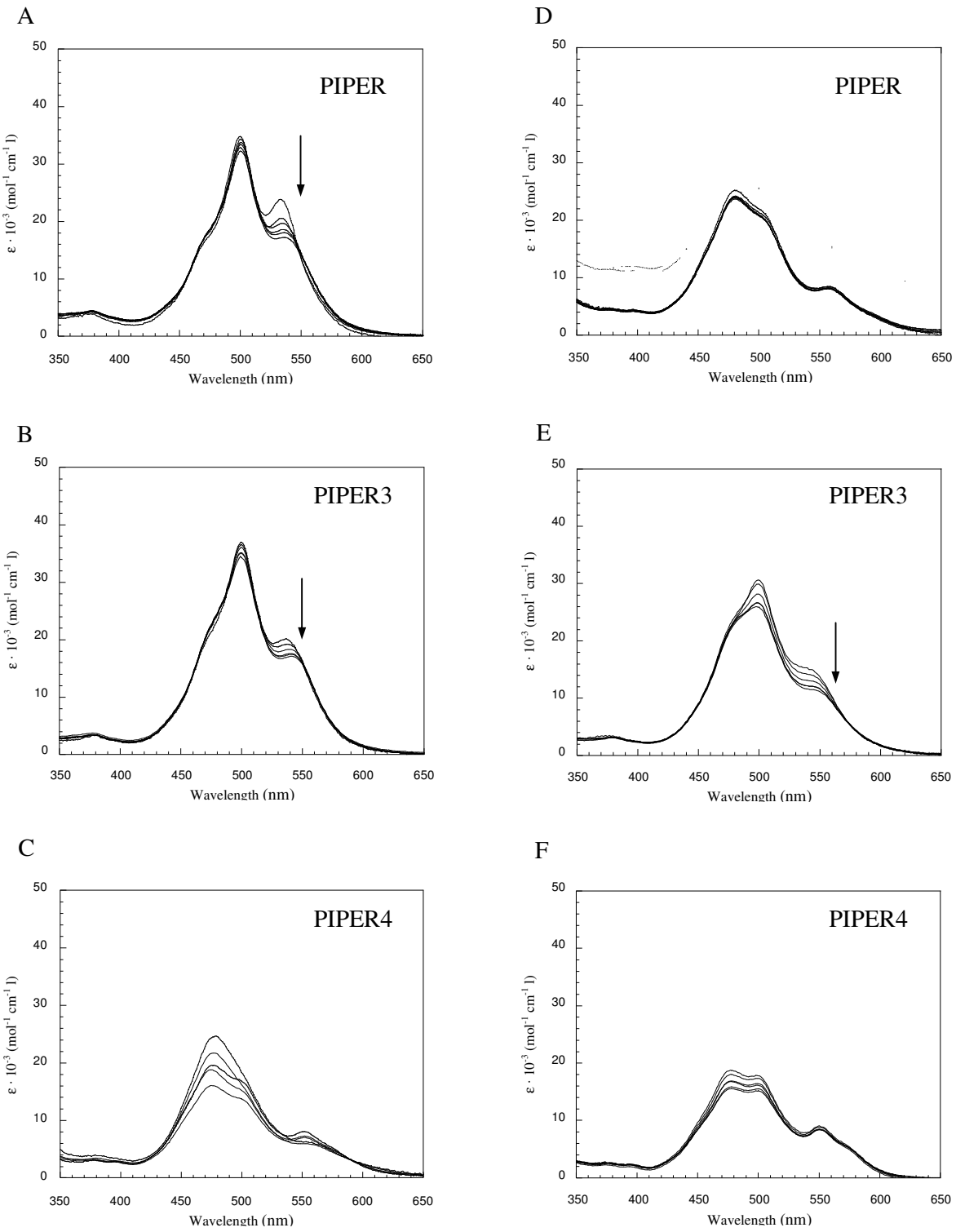

Fig. 4.1.a-3: Visible absorption spectra of serial dilutions of three perylene derivatives, PIPER, PIPER3 and PIPER4 in 10 mM MES buffer pH 6.5 (respectively **A**, **B** and **C**) and in TRAP buffer pH 7.5 (respectively **D**, **E** and **F**). The concentrations of the drugs solutions are in the range of 5-50 μM, the higher extinction coefficients corresponding to the more dilute solutions. The arrow indicates the isobestic point.

PIPER3 (B) spectra in MES buffer (pH 6.5, par. 3.3.a) are reported. The spectra have a maximum at 500nm with a shoulder at 540nm and an isobestic point at 550nm; the presence of one isobestic point suggests that there is an equilibrium between a monomeric and a multimeric drug form (Rossetti *et al.* **2004**). PIPER4 and PIPER5 spectra are different considering three main features: (i) the isobestic point is absent, (ii) the hypochromic effect is larger than in the case of the other four derivatives and (iii) the peak at 500nm is substituted by a broad band centred at about 470nm (representative PIPER4 spectrum is reported in Fig. 4.1.a-3(C)). All these features seem consistent with the formation of more than one type of multimeric aggregates. All these absorption spectra were measured also in TRAP buffer at pH 7.5 (par. 3.3.a). In these experimental conditions the absorption spectrum of PIPER (Fig. 4.1.a-3(D)) becomes very similar to those of PIPER4 and PIPER5, while the absorption spectra of the other perylene derivatives are basically unchanged (in Fig. 4.1.a-3 representative PIPER3 (E) and PIPER4 (F) spectra are reported). In all cases an increasing of the molar extinction coefficient when decreasing drug concentration can be observed, suggesting a decreasing of the self-association process due to dilution (Rossetti *et al.* **2004**).

In order to obtain more water-soluble perylene derivatives, as well as to study the effect of changing the aromatic conjugation in this class of molecules, the synthesis of the new perylene derivatives PIP-PIPER and MORPHO-PIPER (in their different isomeric forms) was carried out (Fig. 4.1.a-1, par. 3.1.b). These new compounds show a very high water solubility, as expected, so that it was even difficult to precipitate the corresponding hydrochloride salts with the simple adding of acetone, as for previous perylene derivatives, and another efficient method was used (par. 3.1.b). The effect of the conjugation of the new nitrogen atoms inserted on the perylene bay-area is evident by comparing their absorption spectra with those of perylene derivatives that have not this conjugation. In fact, the absorption spectra of compounds **4a(I)**, **4b(I)** and **4b(II)**, performed in chloroform and reported in Fig. 4.1.a-4(A),

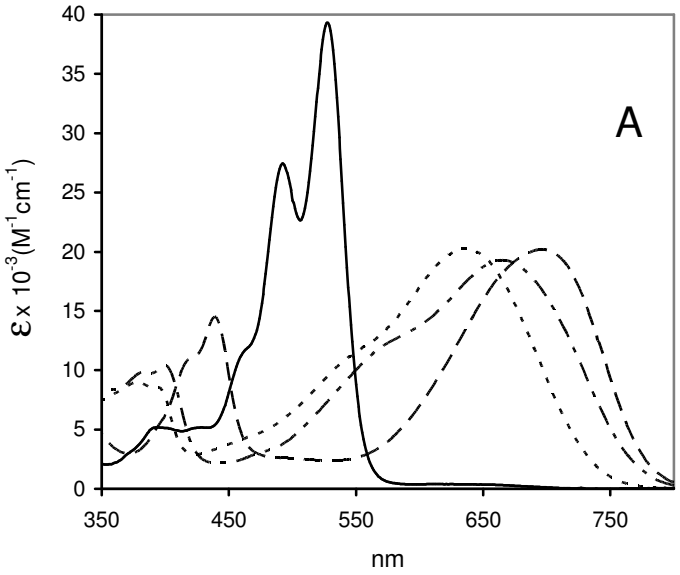

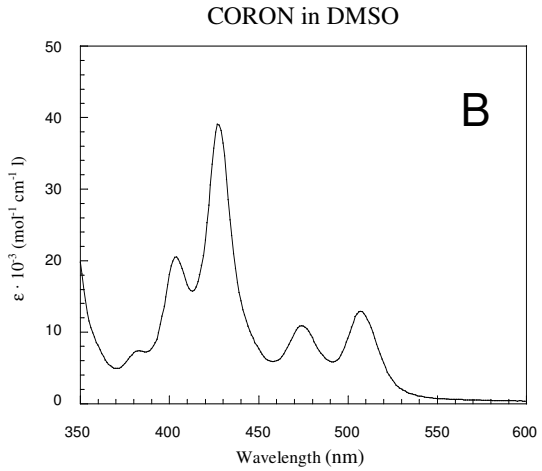

Fig. 4.1.a-4: UV/Vis absorption spectra in $CHCl_3$ of PIPER-Br (**3**) (———), MORPHO-PIPER(1,6) [**4b(II)**] (- - - - -), PIP-PIPER(1,6) [**4b(I)**] (– · – · –) and PIP-PIPER(1,7) [**4a(I)**] (– – – –) (A). UV/Vis absorption spectra in DMSO of CORON (**6**) (B).

show a broad band between 500 and 800nm, that is not present in the spectrum of PIPER-Br (**3**). This is due to the conjugation of the N atom of the piperidine or morpholine ring and the aromatic core of perylene, to which it is directly linked. This leads to an interesting chromatic change from the typical red colour of PIPER-Br (**3**) (analogous to that of 3,4,9,10-perylenetetracarboxylic dianhydride and previously derived perylene diimides) to the green colour of **4a(I)** and the blue of **4b(I)** and **4b(II)**. It is also interesting to note that the colour of each compound depends on the relative positions of the two nitrogen atoms directly linked to the aromatic core: the (1,7) isomer is green, while the (1,6) isomers are blue, regardless of the different kind of cyclic ammine (Franceschin *et al.* **2004**).

Structural studies on the perylene diimides and many other G-quadruplex interactive compounds, both by NMR and molecular modeling, are based on the model of "threading intercalation". According to this model (par. 1.6), proposed in particular by Hurley and coworkers (Fedoroff *et al.* **1998**) for PIPER, it is possible to suppose that a wider aromatic core and four positively charged side chains should improve the interactions between these ligands and the G-quadruplex, leading to higher binding constants and consequently to increased telomerase inhibition. In order to obtain a new molecule with these two molecular features, the synthesis of the new hydrosoluble coronene derivative CORON (**6**) was carried out (par. 3.1.c). The UV/Vis spectrum of CORON (**6**) in DMSO shows the characteristic five bands between 350 and 550nm of coronene (Fig. 4.1.a-4(B), Rohr *et al.* **1998**, Rohr *et al.* **2001**). The visible absorption spectra of serial dilutions of CORON hydrochloride in MES buffer (pH 6.5) and in TRAP buffer (pH 7.5), in the range of 5-50 μM (Fig. 4.1.a-5), show a minor resolution of the bands and a strong hypochromic effect with respect to the DMSO spectrum, similarly to what has been observed in the case of perylene derivatives. In particular, in this case no isobestic point can be observed, suggesting the formation of more than one type of multimeric aggregates.

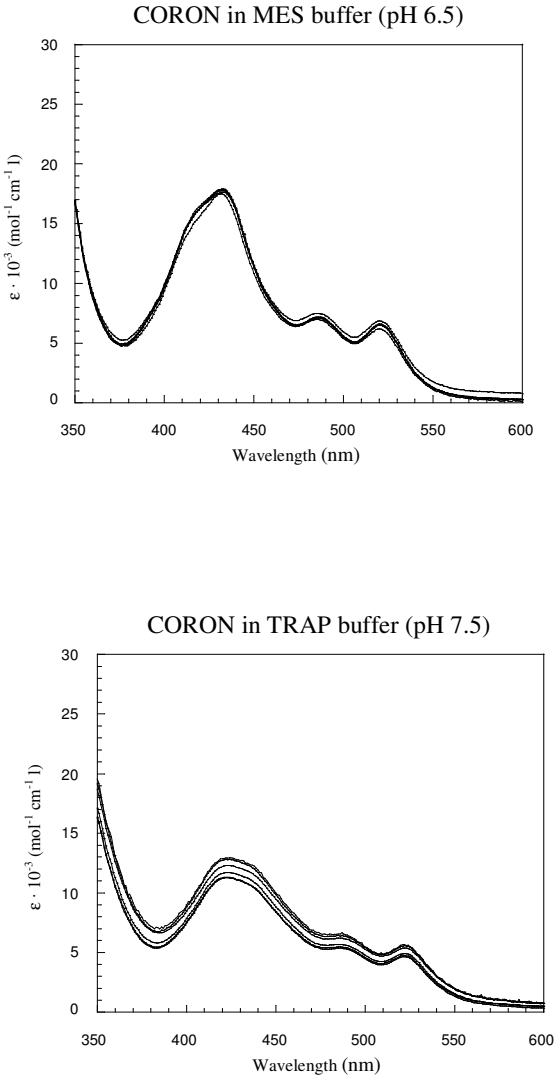

Fig. 4.1.a-5: Visible absorption spectra of serial dilutions of CORON hydrochloride in MES buffer (pH 6.5, top) and in TRAP buffer (pH 7.5, bottom). Drug concentrations are in the range of 5-50 µM.

4.1.b. Berberine analogues and derivatives

Berberine is an alkaloid that has been recently shown to be able to inhibit telomeres elongation (Naasani *et al.* **1999**) and to bind to G-quadruplex DNA (Ren *et. al.* **1999**, par. 1.6.b).

After considering perylene and coronene synthetic derivatives, it was interesting to examine the activity of this natural compound, whose aromatic moiety is suitable for stacking interaction with the G-tetrad and, probably due to the presence of a positive charged nitrogen atom, is able to induce and bind to G-quadruplex DNA, even without side chains. Also its commercially available analogue coralyne was shown to bind to quadruplex and tetraplex DNA (Ren *et. al.* **1999**). So, on these bases, the new piperidin-berberine derivative was synthesized (Fig. 4.1.b-1, par. 3.1.d). This compound represents a sort of molecular chimera, in which a side chain analogue to that of PIPER has been attached to the aromatic moiety of berberine. These molecules represent a new class of G-quadruplex interacting compounds and telomerase inhibitors, structurally related to natural products.

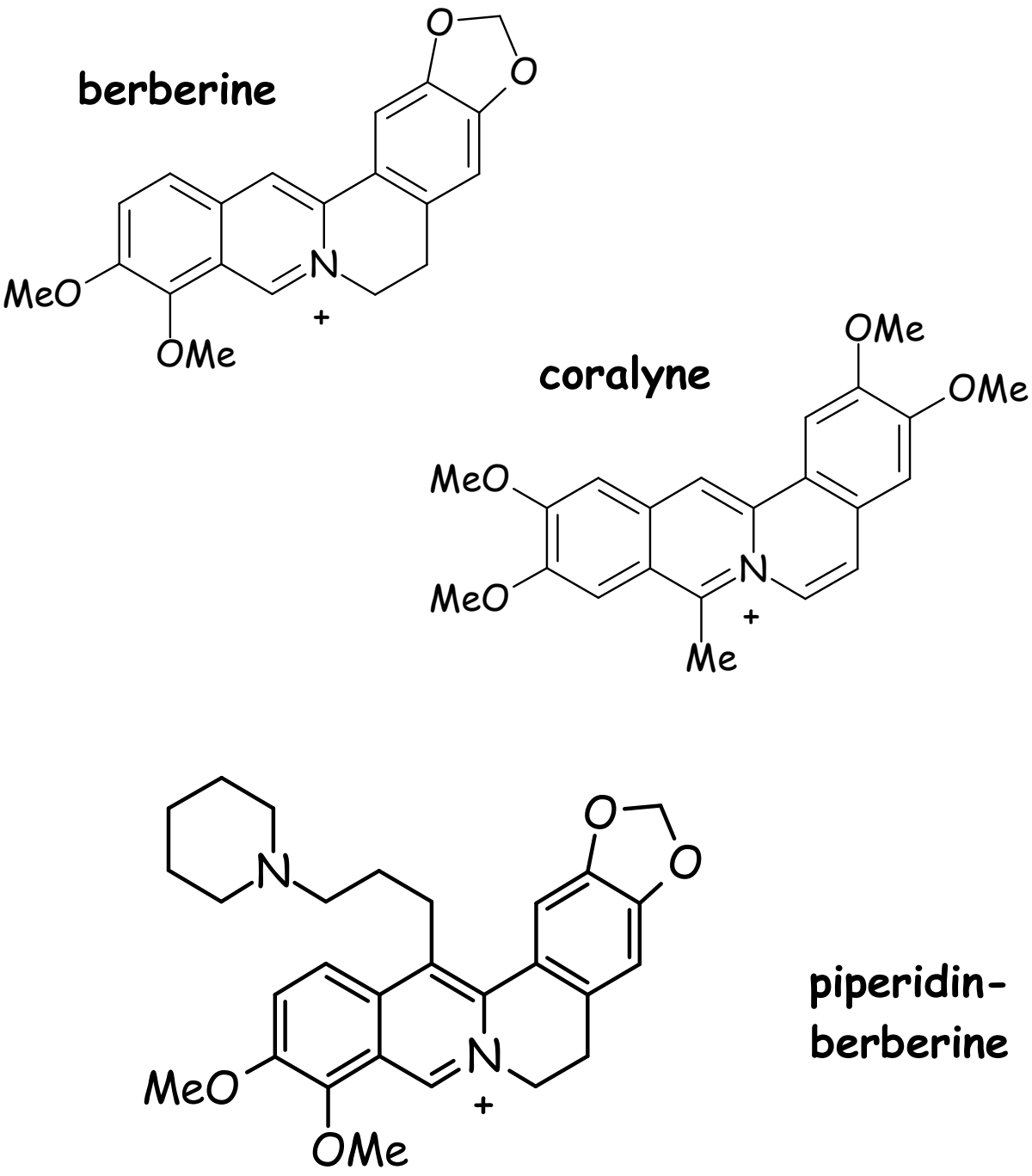

Fig. 4.1.b-1: Berberine analogues and derivatives studied in this thesis.

4.2. Induction of G-quadruplex structures in telomeric sequences: perylene diimides with different side chains are selective in inducing different G-quadruplex DNA structures

The role of the different side chains of perylene derivatives in the formation of inter- and intramolecular G-quadruplex structures was investigated by PAGE (PolyAcrylamide Gel Electrophoresis), according to the experimental procedure described in par. 3.3.a. The DNA oligonucleotides 2HTR and TSG4 were used in these experiments (Rossetti *et al.* **2002**, Rossetti *et al.* **2004**): 2HTR (5'-AATCCGTCGAGCAGAGTTAGGGTTAGGGTTAG-3') is formed by the TS sequence (that is the usual primer for telomerase elongation, par. 3.3.d) followed by two human telomeric repeats, it is able to form only dimeric and/or tetrameric intermolecular G-quadruplex structures; TSG4 (5'-GGGATTGGGATTGGGATTGGGTT-3') forms preferentially intramolecular G-quadruplex structures and can act as a substrate for telomerase elongation in a modified TRAP assay (Gomez *et al.* **2002**, Rossetti *et al.* **2004**, par. 4.4). They were incubated with all perylene derivatives at increasing concentration and the formation of G-quadruplex structures was investigated by PAGE analysis (Fig. 4.2-1/4). Considering previous gel shift data obtained in similar experimental conditions (Han *et al.* **1999**) and the mobility standard obtained by G-quadruplex dimeric forms induced by the potassium ions (Fang *et al.* **1993**), major electrophoretic bands are identified as single stranded DNA (ss), dimeric (D), tetrameric (T) and monomeric (M) G-quadruplex structures. Intramolecular structure (M) corresponds to the highest mobility band: in fact, its particular structure favours the running in the gel grid also with respect to single stranded DNA (Henderson *et al.* **1987**, Williamson *et al.* **1989**). To better compare the different behaviour of the different molecules, the percentage of the induced G-quadruplex structures has been reported as a function of drugs concentration (Fig. 4.2-1/4).

The most striking aspect that emerges from the results obtained using 2HTR oligomer and reported in Fig. 4.2-1 is that, although PIPER2 should be able to establish stacking interactions with the G-tetrads, the strong decrease of electrostatic interactions with the DNA grooves due to the weak basicity of pyridine nitrogen atoms does not allow the formation of G-quadruplex structures. On the other hand, through the quaternization of the nitrogen atom on the pyridine ring (par. 3.1.a), PIPER7 achieves a fully charged nitrogen atom and shows an activity comparable to the best perylene derivatives. In fact, the obtained results reported in Fig. 4.2-2, using 2HTR oligomer in MES buffer pH 6.5, KCl 50mM, show that all the other perylene derivatives are almost equally able to induce intermolecular G-quadruplex structures, except PIPER4, that is definitively less efficient. Furthermore, PIPER is the only perylene derivative able to induce a G-quadruplex structure that involves four strands, while it is barely efficient in inducing dimers (Fig. 4.2-1/2). To study the effect of the different perylene derivatives in the formation of intramolecular G-quadruplex, TSG4 oligonucleotide was used. In this case, incubating the samples in the presence of KCl 5mM (in this experimental conditions no G-quadruplex structure is formed in drug absence), all perylene derivatives are able to induce intramolecular G-quadruplex, corresponding to a high mobility electrophoretic band (Fig. 4.2-2(B,D)). It is worth noting that PIPER4 induces intramolecular G-quadruplex structures only at a drug concentration higher than those considered (data not shown), since the intermediate bands, evidenced at lower concentrations, can not be considered as canonical intramolecular G-quadruplex. Performing the same experiment in the presence of KCl 50mM, the monomeric G-quadruplex structure is formed also in absence of any drug. In these conditions, all perylene derivatives bind to the preformed intramolecular G-quadruplex structure, slightly varying its mobility (Fig. 4.2-3).

To take into account the different basicity of drugs side chains, which is surely important for the interactions with G-quadruplex structures, electrophoretic mobility shift assays were

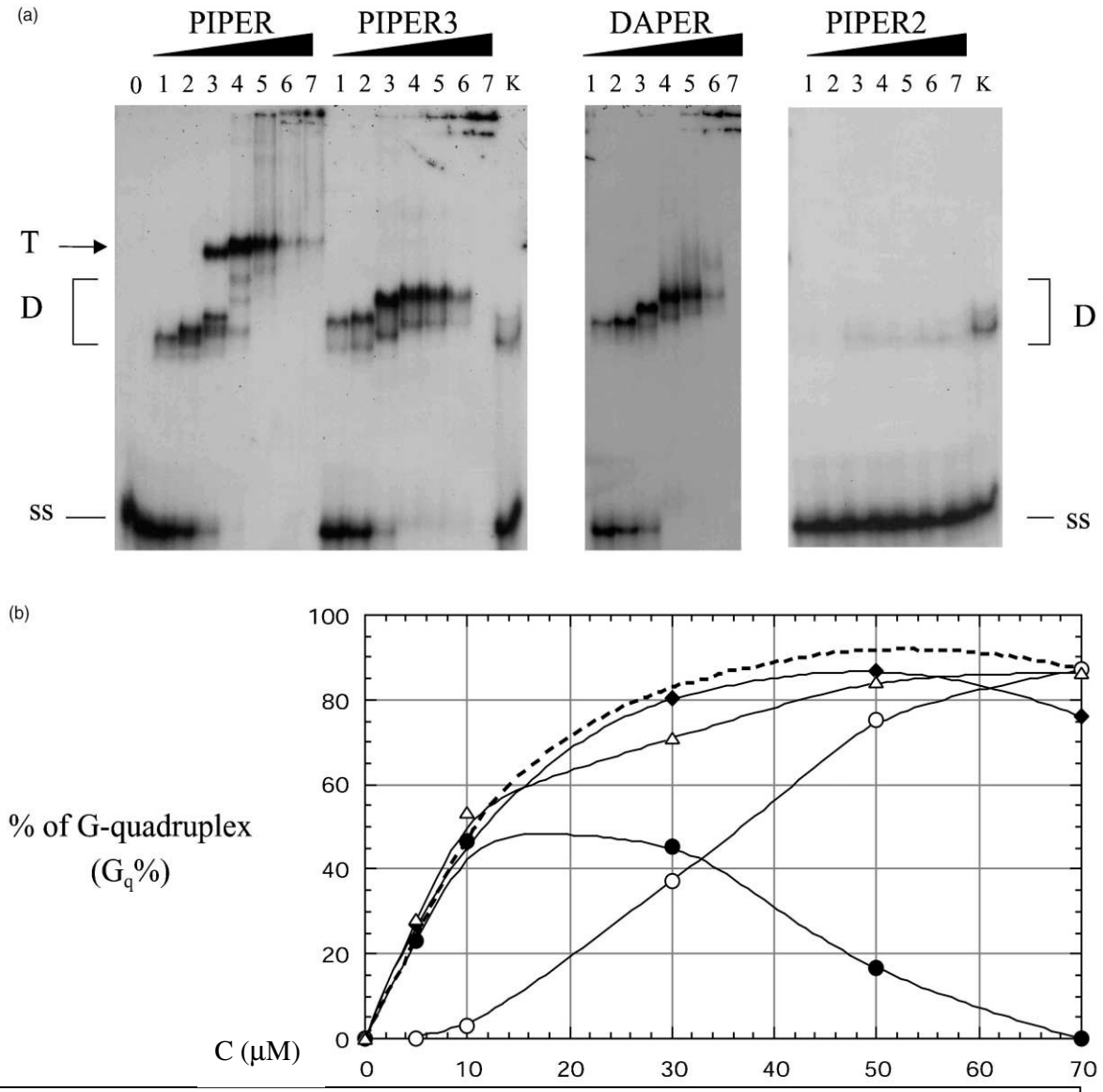

Fig. 4.2-1: G-quadruplex structures formation induced by PIPER, PIPER2, PIPER3 and DAPER (Fig. 4.1.a-1), studied by native PAGE (PolyAcrylamide Gel Electrophoresis) according to the experimental procedure described in par. 3.3.a. (a) 8 μM 2HTR was incubated in MES-KCl buffer (pH 6.5) in the presence of different drugs concentrations: 5 μM (lane 1), 10 μM (2), 30 μM (3), 50 μM (4), 70 μM (5), 100 μM (6), 130 μM (7) and with no drug (lane 0). In lane K, 2HTR was incubated with KCl 1 M. Major bands are identified as single stranded DNA (ss), dimeric (D) and tetrameric (T) G-quadruplex structures. (b) Percentage of G-quadruplex structures formed (G_q%) versus drug concentration (C) of PIPER, PIPER3 (♦) and DAPER (Δ). In the case of PIPER, dimeric (●) and tetrameric (○) structures can be distinguished (the dashed line being their sum). In this plot, the values corresponding to concentrations higher than 70 μM have not been considered because of the increasing amount of higher-order structures. G_q% represents the ratio between the intensity of the relative band on the electrophoresis gel and the total amount of DNA, obtained by Instant Imager (Rossetti *et al.* **2002**).

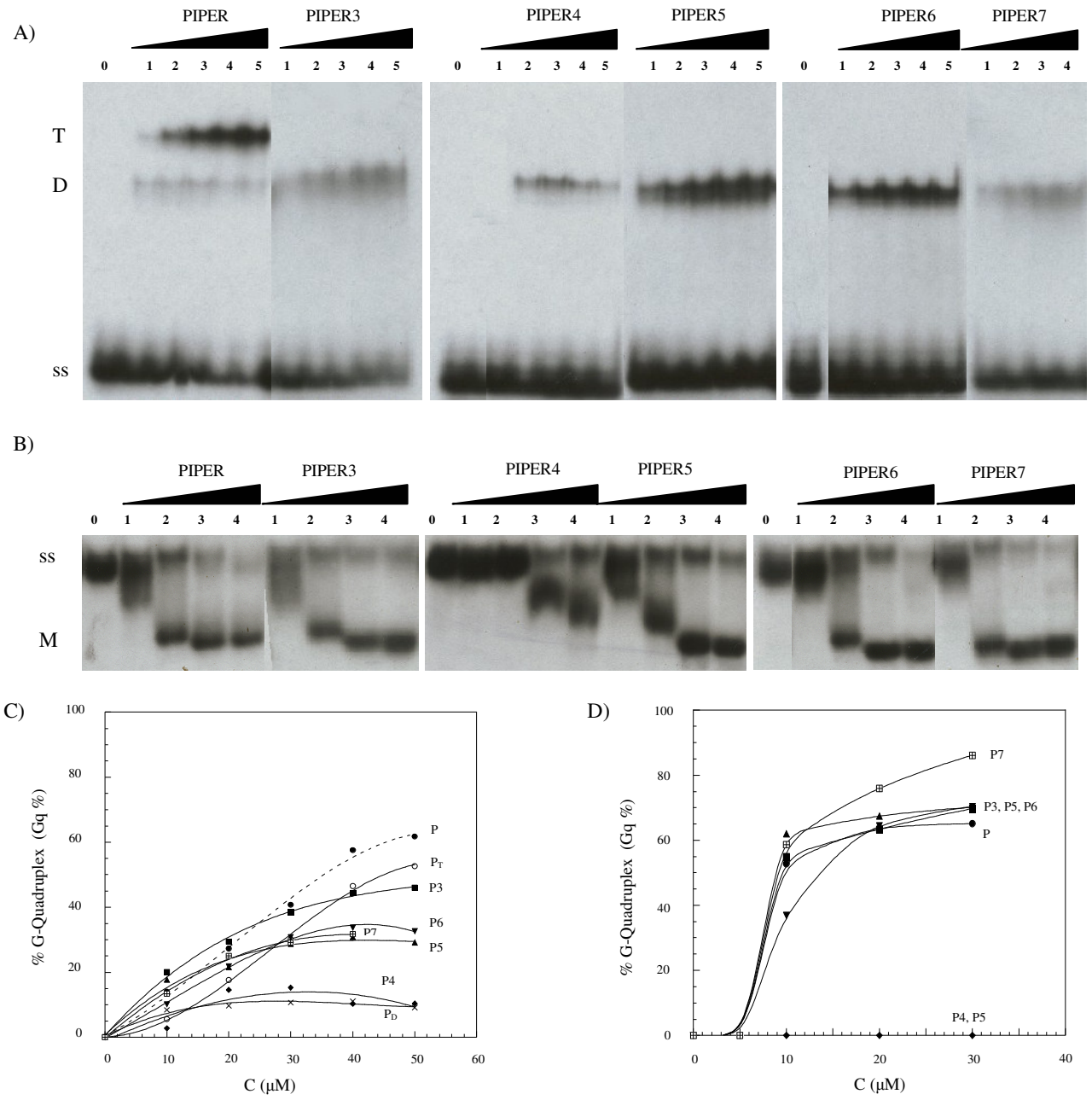

Fig. 4.2-2: G-quadruplex structures formation induced by the six perylene derivatives indicated, whose structures are reported in Fig. 4.1.a-1, studied by native PAGE (PolyAcrylamide Gel Electrophoresis) according to the experimental procedure described in par. 3.3.a. **A)** 2HTR (12 μM) was incubated in MES-KCl buffer (pH 6.5) in the presence of different drugs concentrations: 10 μM (lane 1), 20 μM (2), 30 μM (3), 40 μM (4), 50 μM (5) and with no drug (lane 0). **B)** TSG4 (12 μM), in 10 mM MES, pH 6.5, 5 mM KCl, was incubated, as described above for 2HTR, in the presence of different drugs concentrations: 5 μM (lane 1), 10 μM (2), 20 μM (3), 30 μM (4), and with no drug (lane 0). Major bands are identified as single stranded DNA (ss), dimeric (D), tetrameric (T) and monomeric (M) G-quadruplex structures. **C-D)** Percentage of G-quadruplex structures formed (G_q%, see the caption of Fig. 4.2-1) in function of drug concentration (C (μM)) relative to the band shift assays reported in A) and in B) respectively. In the case of PIPER, intermolecular dimeric (P_D) and tetrameric (P_T) structures can be distinguished (the dashed line being their sum (P)). Intermediate bands between ss and M in (B) were not considered when calculating values reported in (D) (Rossetti *et al.* **2004**).

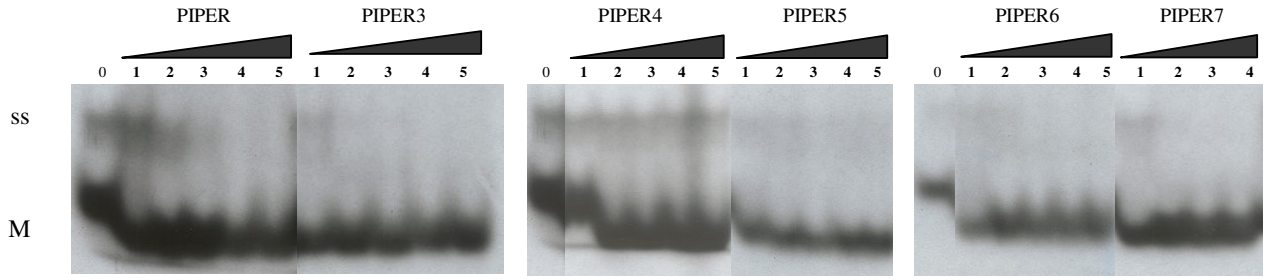

Fig. 4.2-3: G-quadruplex structures formation studied by native PAGE on TSG4 oligonucleotide in MES-KCl buffer (10 mM MES, pH 6.5, 50 mM KCl). 12 μM TSG4 was incubated in MES-KCl buffer in the presence of different drugs concentrations: 10 μM (lane 1), 20 μM (2), 30 μM (3), 40 μM (4), 50 μM (5) and with no drug (lane 0). It is evident the formation of monomeric G-quadruplex also in the absence of any drug (lane 0), differently from what happens at 5 mM KCl (Fig. 4.2-2(B)).

repeated in the same experimental conditions, except that TRAP buffer pH 7.5 was used (Fig. 4.2-4). Both PIPER4 and PIPER5 are unable to induce appreciable amount of intermolecular G-quadruplex structure (2HTR), while the behaviour of the other perylene derivatives is basically unchanged (Fig. 4.2-4(A,C)). Considering the formation of intramolecular G-quadruplex structure (TSG4), all perylene derivatives start to induce intramolecular G-quadruplex at higher concentration (Fig. 4.2-4(B,D)) with respect to the experiments carried out at pH 6.5 (Fig. 4.2-2(B,D)); also in this case, PIPER 4 and PIPER5 result the less efficient drugs, being unable to induce a canonical intramolecular G-quadruplex structure at the considered drugs concentrations.

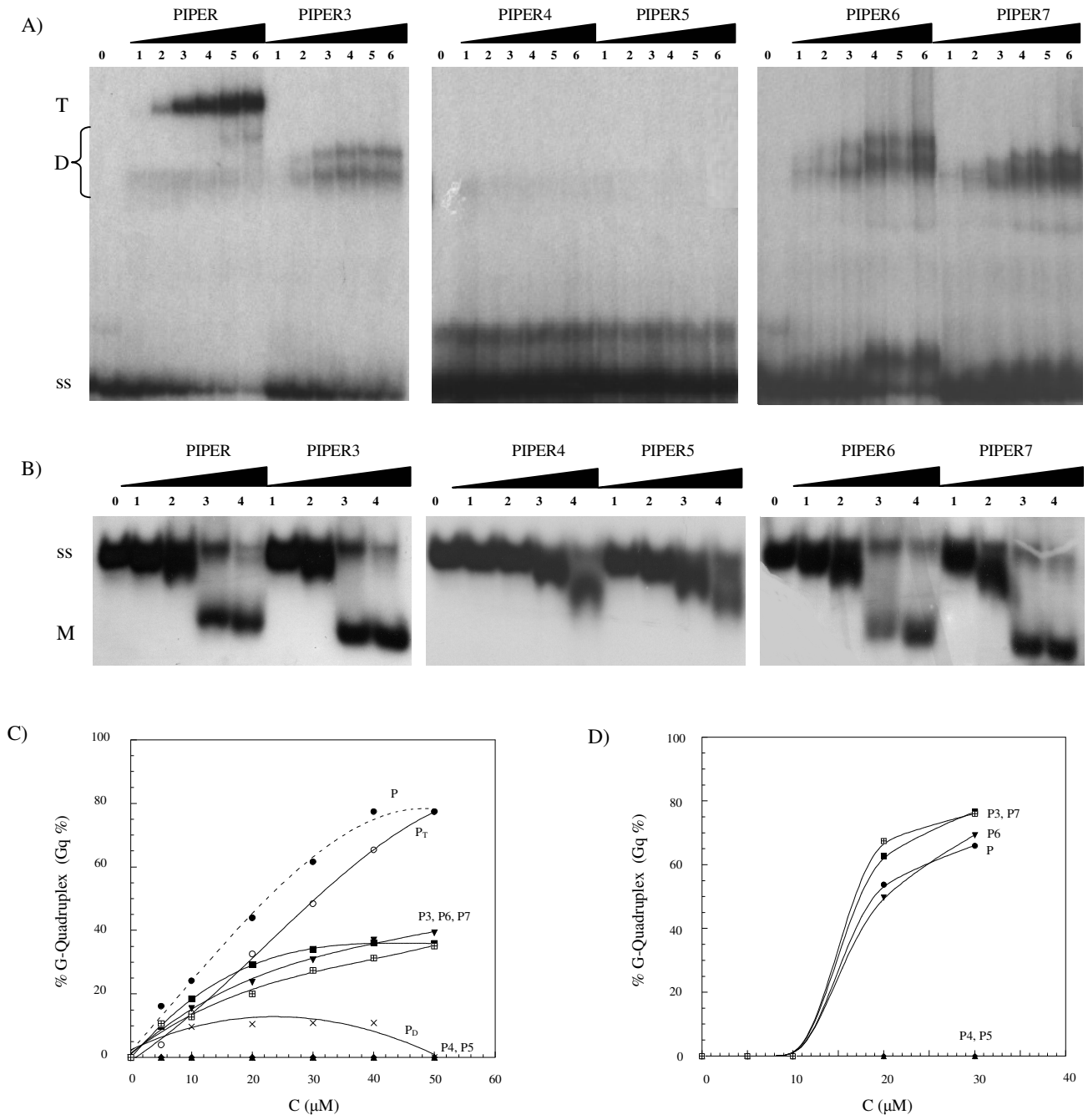

Fig. 4.2-4: G-quadruplex structures formation induced by the six perylene derivatives indicated, whose structures are reported in Fig. 4.1.a-1, studied by native PAGE; for details see the caption of Fig. 4.2-1/2. Samples containing 2HTR **(A)** or TSG4 **(B)**, were incubated as described in the legend of Fig. 4.2-2 except that they were incubated in TRAP Buffer, pH 7.5 (20 mM Tris-HCl (pH 7.5), 15 mM $MgCl_2$, 10 mM EDTA, 0.5% Tween20), 50 mM KCl in the case of 2HTR and 5 mM KCl in the case of TSG4, in the presence of different drugs concentrations: 5 μM (lane 1), 10 μM (2), 20 μM (3), 30 μM (4), 40 μM (5) and 50 μM (6) and with no drug (lane 0). **C-D)** Percentage of G-quadruplex structures formed (G_q%) in function of drug concentration (C (μM)) of the six perylene derivatives, relative to the band shift assays reported in A) and in B) respectively (Rossetti *et al.* **2004**).

4.3. Stabilization of preformed G-quadruplex and duplex DNA structures

4.3.a. FRET assays on a monomeric G-quadruplex

Fluorescence energy transfer can be used to reveal the formation of four-stranded DNA structures, and its stabilization by quadruplex-binding agents, as discussed in par. 3.3.c and reported by Mergny and coworkers (Mergny *et al.* **2001**, Koeppel *et al.* **2001**).

Curves obtained by FRET experiments on F21T sequence, performed as described in par. 3.3.c, are reported in Fig.4.3.a-1. R is the drug/DNA ratio defined as the ratio between the molar drugs concentration and the molar DNA concentration, expressed in oligonucleotides molecules. F21T is a 21-mer human telomeric sequence [$GGG(TTAGGG)_3$], whose ends are labelled by two fluorescent probes that form an acceptor/donor system (par. 3.3.c, Mergny *et al.* **2001**). The experimental conditions are identical to those used for the crystallization of the sequence [$AGGG(TTAGGG)_3$], whose structure was recently resolved as a new monomeric G-quadruplex structure (Parkinson *et al.* **2002**).

The change in shape of the melting curves when adding perylene derivatives suggests that, as a consequence of the binding with the drug molecules, the melting process looses its characteristic cooperativity and, at high R values, two melting steps appear in most cases. Nevertheless, the interactions between perylene derivatives and G-quadruplex seem to be very strong, with significant effects starting from very low concentrations (R=0.5).

It's interesting to note that most of perylene derivatives reach a sort of "saturation" at R=2; this could be due to the presence of two possible binding sites for each G-quadruplex: 5' and 3' external G-quartet planes. The appearance of two melting steps, quite evident in the case of

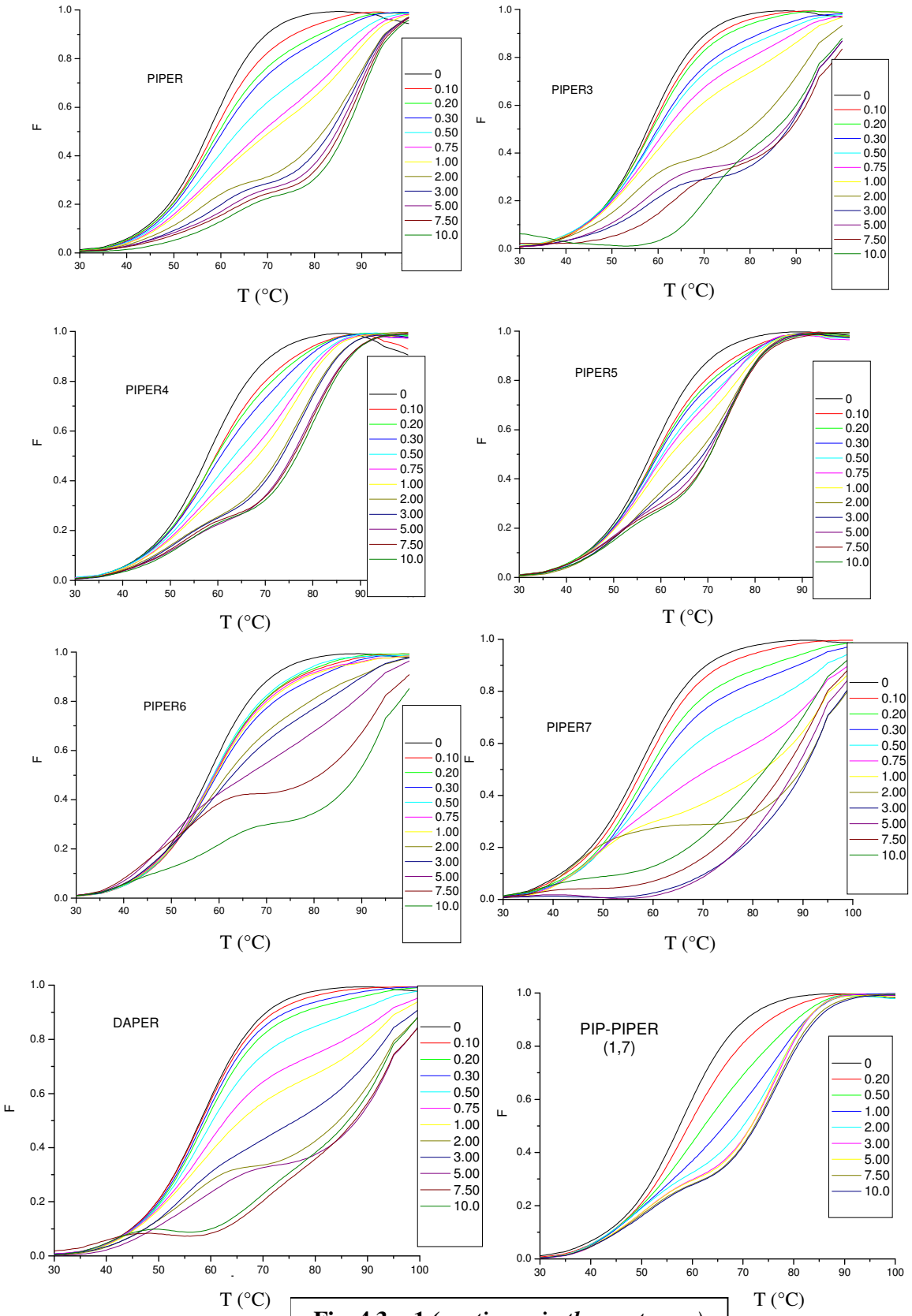

Fig. 4.3.a-1 ***(continues in the next page)***

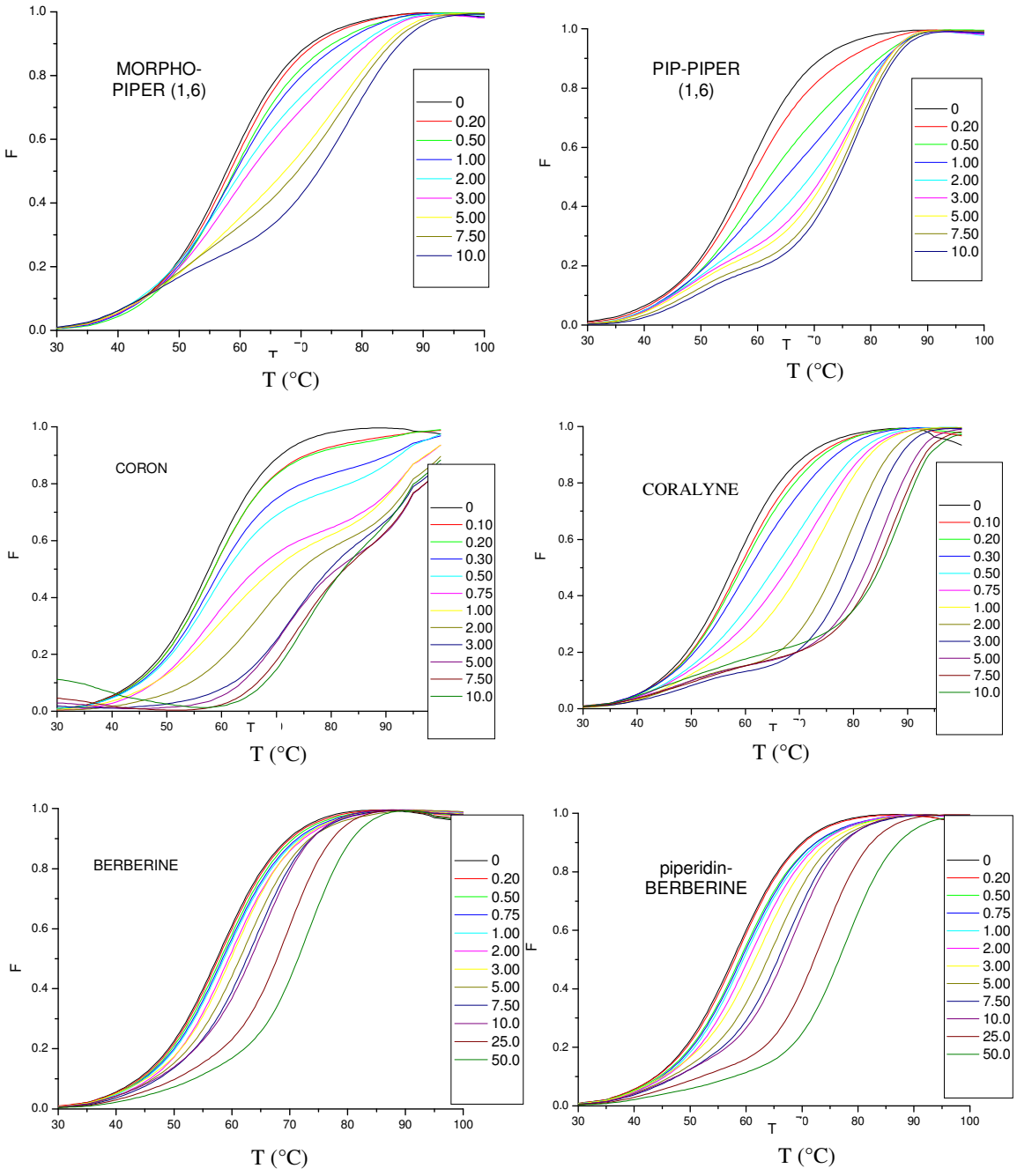

Fig. 4.3.a-1: Curves obtained by FRET experiments on F21T sequence. Legends show the drug/DNA ratios (R) as reported in par. 3.3.c. F is the relative fluorescence obtained after normalization and T is the temperature.

PIPER7, agrees with this model, too. The complexity of the melting curves could be also related to the change in the self-aggregation state of the ligand molecules with the increasing of the temperature.

Because of the biphasic nature of the FRET curves obtained in the case of perylene derivatives, it is not easy to determine the melting temperature of the drug-DNA complexes at each concentration, in particular at intermediate values of R. The presence of a first melting step could be due to an intermediate unfolding form, while it is reasonable to associate the second melting step to the final disruption of the G-quadruplex structure. For these reasons, in order to evaluate the different behaviour of the various drugs, the differences (ΔT) between the temperature corresponding to the second inflection point at R=10 for each derivative and the melting temperature of G-quadruplex without drugs (57.6±0.4°C) are reported in Tab.4.3.

Table 4.3

compound	ΔT(°C)
PIPER	33,2 ± 1,2
PIPER3	36,3 ± 0,6
PIPER4	22,2 ± 1,5
PIPER5	16,3 ± 1,3
PIPER6	36,4 ± 0,7
PIPER7	34,8 ± 1,0
CORON	36,4 ± 0,7
PIP-PIPER(1,7)	18,7 ± 0,8
PIP-PIPER(1,6)	19,5 ± 0,7
Morpho-PIPER	18,4 ± 1,8
DAPER	35.9 ± 0.7

It is evident that PIPER4, PIPER5 and the new perylene derivatives PIP-PIPER and Morpho-PIPER influence the G-quadruplex thermodynamic stability to a minor extent with respect to PIPER, PIPER3, PIPER6, PIPER7, DAPER and the new coronene derivative CORON.

Differently from perylene derivatives, berberine derivatives (berberine, coralyne and piperidin-berberine) show a continuous increasing of the melting temperature with the

increasing of drug/DNA ratio; the melting process is cooperative and appears monophasic at all drugs concentrations. In this case it is therefore possible to calculate the melting temperature (T_m) at each drug concentration. Since berberine and piperidin-berberine do not show a significant intrinsic fluorescence, it was possible to reach a drug concentration of 10μM, (R=50). A direct comparison of the increasing in the G-quadruplex melting temperature due to these two molecules is reported in Fig. 4.3.a-2. It is evident that the new added side chain increases the effect on G-quadruplex stability of the new compound piperidin-berberine with respect to natural berberine. Nevertheless, it is worth noting that coralyne, that has a fully aromatic core, is much more active than both the other two compounds (Fig. 4.3.a-3). In the case of coralyne, similarly to perylene derivatives, drug concentration was kept under 2μM because above this concentration the drug intrinsic fluorescence becomes significant.

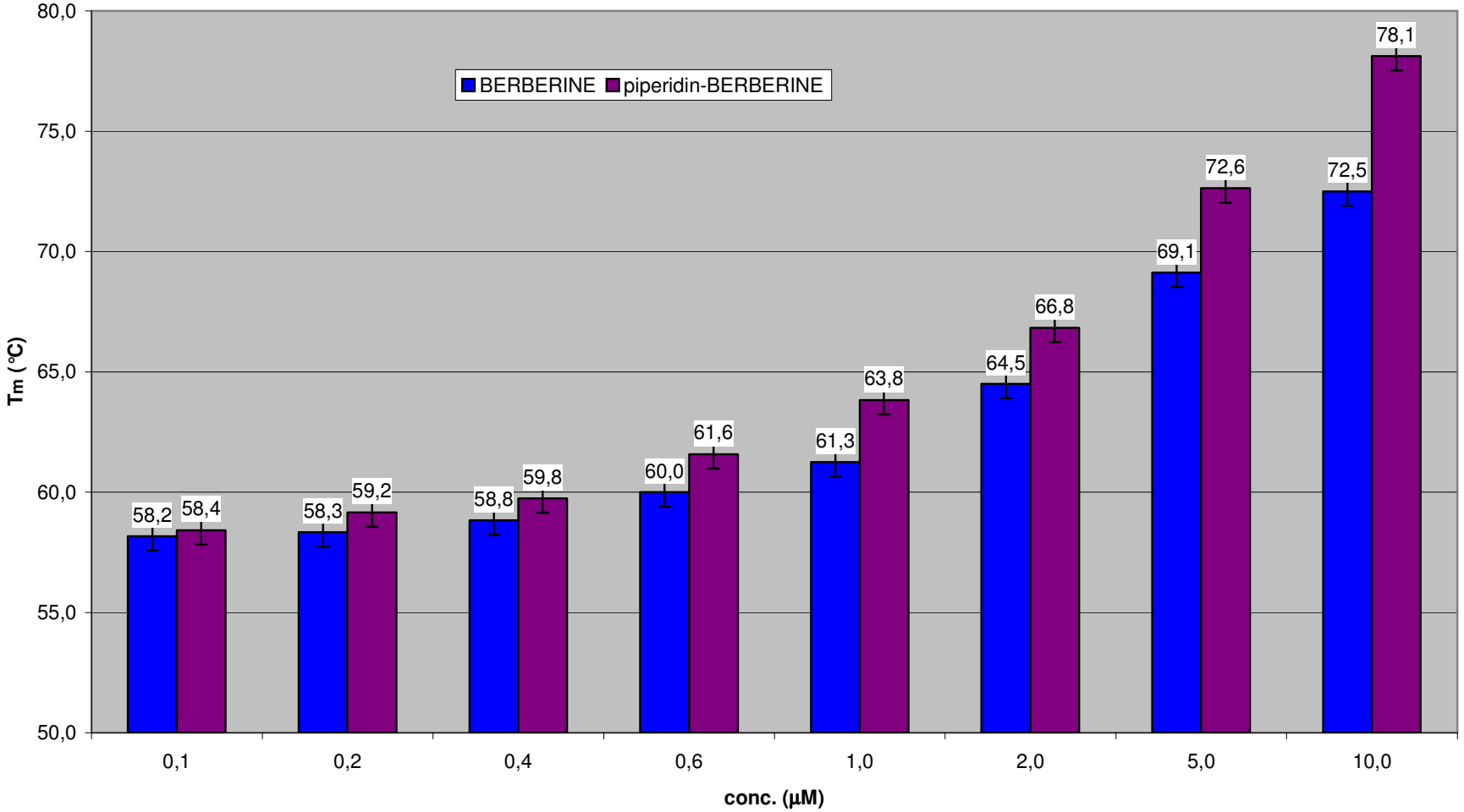

Fig. 4.3.a-2: Melting temperatures for F21T at increasing concentrations of berberine and piperidin-berberine, as derived from the first derivative of the melting curves reported in Fig. 4.3.a-1.

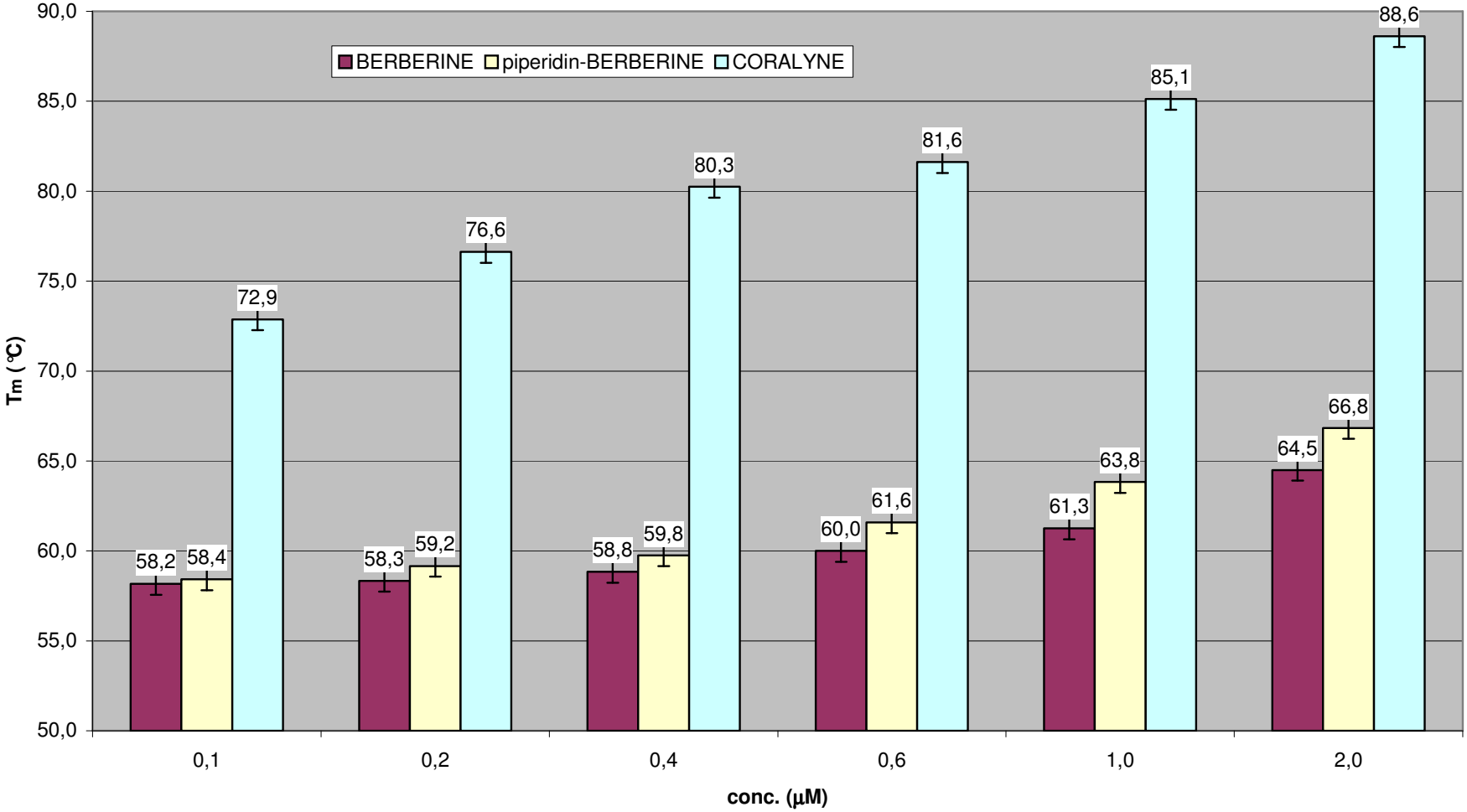

Fig. 4.3.a-3: Melting temperatures for F21T at increasing concentrations of berberine, piperidin-berberine and coralyne, as derived from the first derivative of the melting curves reported in Fig. 4.3.a-1.

4.3.b. Preliminary studies of selective interactions of one perylene derivative for G-quadruplex DNA with respect to duplex DNA by absorption spectroscopy and circular dichroism

The selectivity of G-quadruplex interacting compounds for G-quadruplex DNA with respect to duplex DNA is surely a topic of great interest for the possible biological applications of these molecules (Kerwin *et al.* **2002**, Kern *et al.* **2002**). As a preliminary study, UV/Vis absorption spectra of one perylene derivative (PIPER3) were performed in the presence of different concentrations of quadruplex and duplex DNA structures, as described in par. 3.3.b. The DNA/ligand ratio (R) is calculated considering phosphates concentration for both DNAs. The spectra reported in Fig. 4.3.b-1 (quadruplex) and 4.3.b-2 (duplex) show two interesting features: the increasing of the molar extinction coefficient and the change in the shape of the spectra, that become similar to those obtained for PIPER3 alone in organic solvent (see par. 4.1) at increasing concentration of DNA. Moreover, in both cases isobestic points can be observed, indicating the existence of an equilibrium between different species in solution. At the same DNA/ligand ratio (R), the hyperchromic effect is larger for G-quadruplex with respect to duplex DNA structures, above all for high values of R, as clearly evident from the graph reported in Fig. 4.3.b-3, suggesting a high selectivity of PIPER3 for quadruplex with respect to duplex DNA.

Another technique that appears suitable for this kind of study is circular dichroism (Cantor *et al.* **1980**, p. 409). In fact, because of their symmetry, perylene derivatives do not show dichroic spectra, although they have a strong absorption in the visible region (see Fig. 4.1.a-3). On the other hand, DNA alone does not present absorption bands in the visible region, so that the appearance of dichroic bands in this region when considering solutions at different drug/DNA ratios (Fig. 4.3.b-4) both for duplex and quadruplex DNA indicates that symmetric perylene chromophores interact with an asymmetric environment, represented by DNA

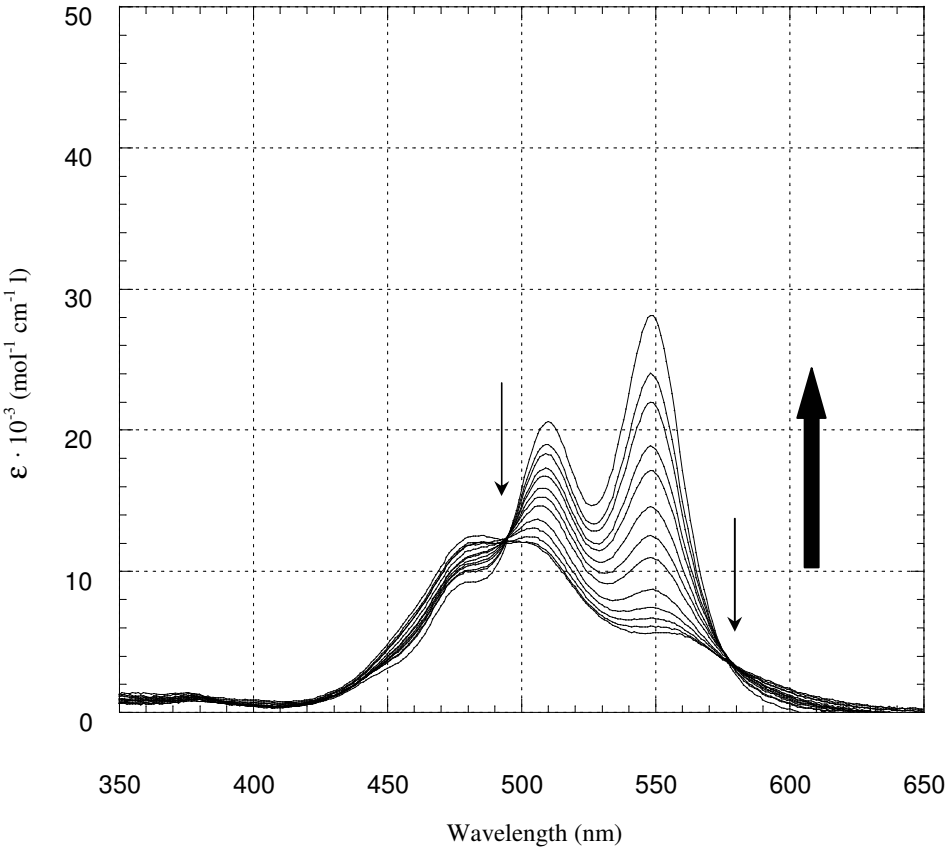

Fig. 4.3.b-1: Absorption spectra of samples containing PIPER3 10μM and oligonicleotide $(T_4G_4)_2$ at different concentrations, in MES buffer (10mM, pH 6.5). $(T_4G_4)_2$ was previously annealed in KCl 100mM. Thin arrows indicate isobestic points, large arrow indicates the increase in oligonucleotide concentration.

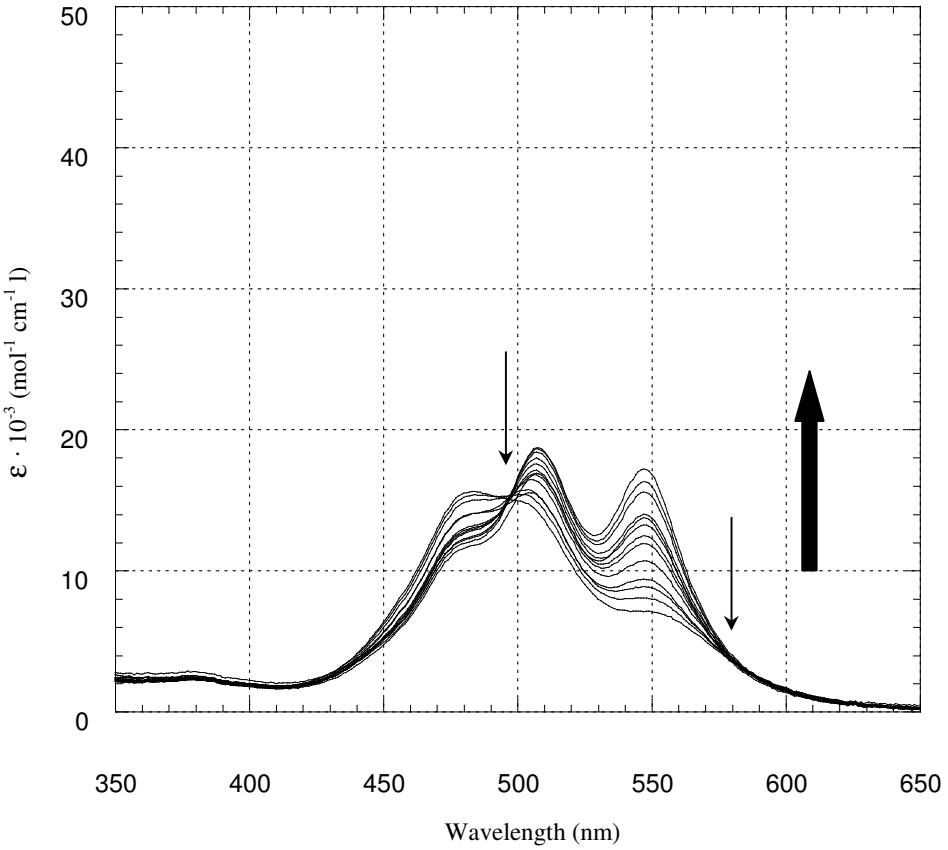

Fig. 4.3.b-2: Absorption spectra of samples containing PIPER3 10μM and canonical duplex DNA (Calf Thymus, CT) at different concentrations, in MES buffer (10mM, pH 6.5). Thin arrows indicate isobestic points, large arrow indicates the increase in oligonucleotide concentration.

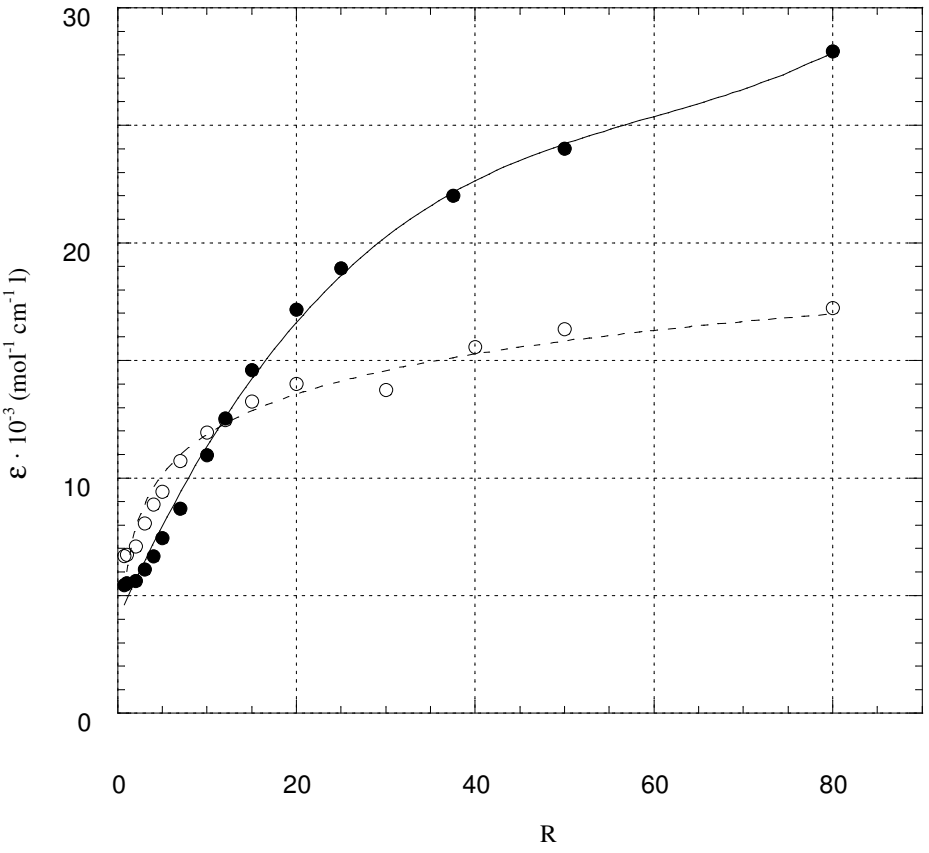

Fig. 4.3.b-3: PIPER3 (10μM) molar extintion coefficient (548nm) versus DNA/ligand concentration ratio (R). Used DNA was duplex CT, dotted line, and quadruplex $(T_4G_4)_2$, continuous line. R is calculated considering phosphates concentration for both DNAs.

structures. A complete titration in a suitable range of drug/DNA ratios and the consequent analysis could lead to a good approach for the evaluation and quantification of the interactions between drugs and different DNA structures.

These preliminary results are surely encouraging and absorption spectroscopy techniques appear a good method to evaluate binding constants for perylene derivatives with quadruplex and duplex DNA.

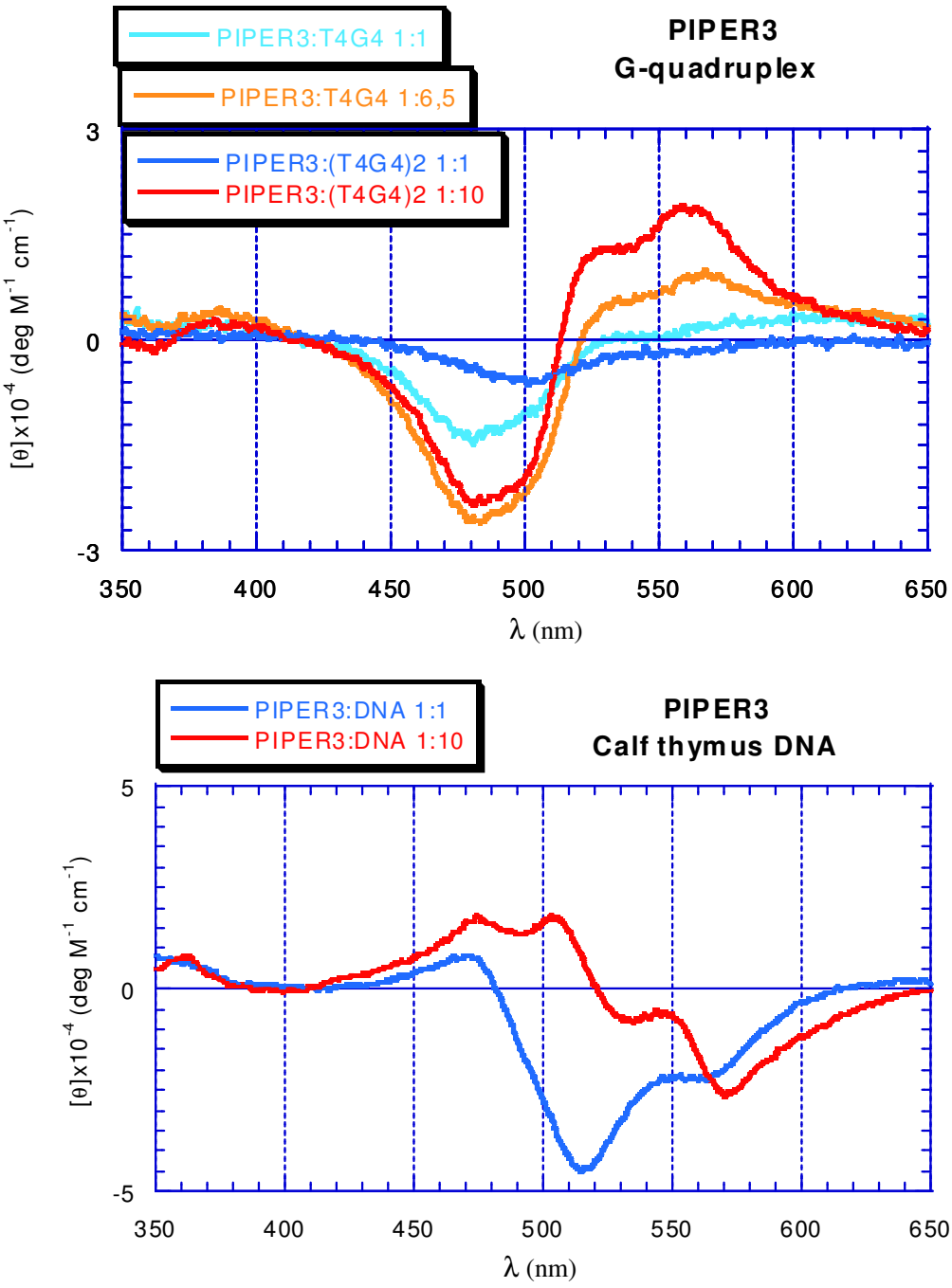

Fig. 4.3.b-4: Circular dichroism spectra of samples containing PIPER3 and different preformed DNA structures at 1:1 and 1:10 drug/DNA ratios. Sonicated calf thymus DNA was used as duplex model (bottom), while pre-annealed T_4G_4 and $(T_4G_4)_2$ oligonucleotides were considered as G-quarduplex models (top).

4.3.c. FRET assays on an autocomplementary decamer

Because of the great importance of the selectivity of the analysed drugs for G-quadruplex DNA with respect to duplex DNA, as discussed in the previous paragraph, the necessity to find a quicker method than the titrations of drugs binding sites carried out by absorption spectroscopy or circular dichroism emerges. Although the last ones are necessary to calculate the correct binding constants, a quicker evaluation of this selectivity could rely on using FRET techniques. If the same two fluorescent probes linked to the ends of the F21T oligonucleotide, used as G-quadruplex model, are linked to the ends of an autocomplementary sequence, according to the Watson and Crick base pairings, a method for the study of the interactions of the drugs with duplex DNA could be developed. In this case, it is necessary to define a "direction" of the sequence, so that the two fluorescent probes will be always at the same end of the DNA folded structure. It must be also considered that the unfolded structure would cause the separation of the two strands, differently from what happens in the case of monomeric G-quadruplex, since it consists of an intramolecular structure. In order to solve both these problems a polyethylenglycol linker was used to bind two autocomplementary decamer TATAGCTATA, with one probe at each end. For these reasons, the sequence F10D used in these FRET experiments was: 5'-FAM-dTATAGCTATA-$(CH_2\text{-}CH_2\text{-}O)_6$-dTATAGCTATA-TAMRA-3'. In this way, the folded structure, that is supposed to be a duplex DNA, will have the donor/acceptor system correctly positioned to give fluorescence transfer, while in the unfolded structure the two strands are always kept together, but the donor/acceptor distance is too large for energy transfer. The system so composed can seem quite different from a canonical duplex DNA, so that it was useful to try it on a classical DNA duplex binder as ethidium bromide (Cantor *et al.* **1980**, p. 445). In Fig. 4.3.c-1 the results of

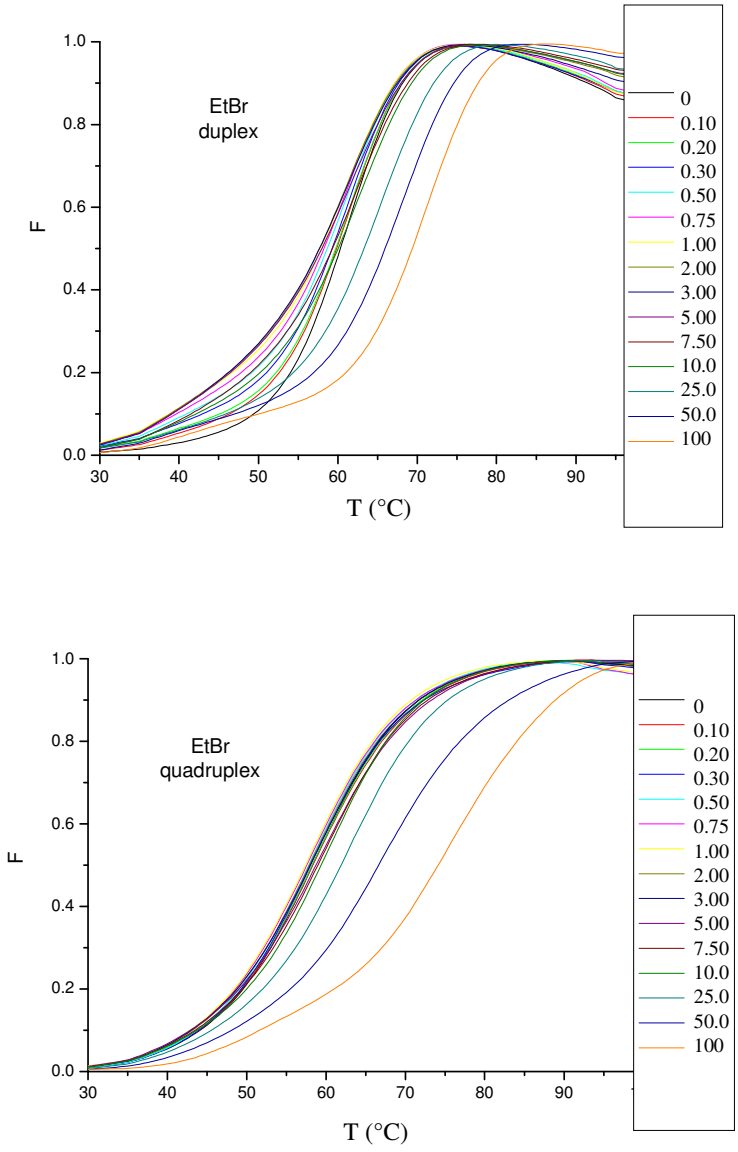

Fig. 4.3.c-1: Curves obtained by FRET experiments on F10D (top) and F21T (bottom) sequences at increasing concentrations of ethidium bromide. Legends show the drug/DNA ratios (R) as reported in par. 3.3.c. F is the relative fluorescence obtained after normalization and T is the temperature.

the FRET experiments with ethidium bromide at drug/DNA ratios up to 100 are reported. The melting curve of F10D without drug shows the typical sigmoid shape of a cooperative process and the corresponding melting temperature (T_m) is 60.7±0.4°C. Until R=10, a slight effect can be observed on the shape of the melting curves as an initial destabilizing effect that does not alter too much T_m values. Only at R = 25, 50 and 100, a net increasing of the melting temperature can be observed, with a ΔT_m of about +10°C at R=100. At the same concentrations, ethidium bromide show a similar behaviour with the G-quadruplex forming sequence F21T (Fig. 4.3.c-1, bottom): no significant effect until R=10 and increasing melting temperatures starting from R=25, with a maximum of about +15°C at R=100. This indicates that ethidium bromide can bind both to duplex and quadruplex DNA without particular selectivity for one of the two structures. These results agree with previous studies in which, although ethidium bromide has been reported to bind to G-quadruplexes, its affinity and specificity for this structure was found to be low (Perry *et al.* **1999**).

As for perylene derivatives, FRET experiments on F10D sequence were performed at the same drug/DNA ratios (R) used for F21T, and the curves obtained are reported in Fig.4.3.c-2. Maximum concentration is 2μM (R=10), because fluorescence of the perylene derivatives become significant above this concentration. It is worth noting that most of them show good interaction with G-quadruplex and even a sort of "saturation" under this concentration. On the contrary, with the major exception of PIPER7 and, to a minor extent, of DAPER (that is used for DNA precipitation, Liu *et al.* **1996**), all the other perylene derivatives show poor interactions with F10D duplex model. According to these results, they seem to show a good selectivity for G-quadruplex with respect to duplex DNA, as already suggested by titration with absorption spectroscopy of PIPER3 (that is however one of the few compounds that are able to slightly increase the melting temperature of F10D). It is also worth noting that

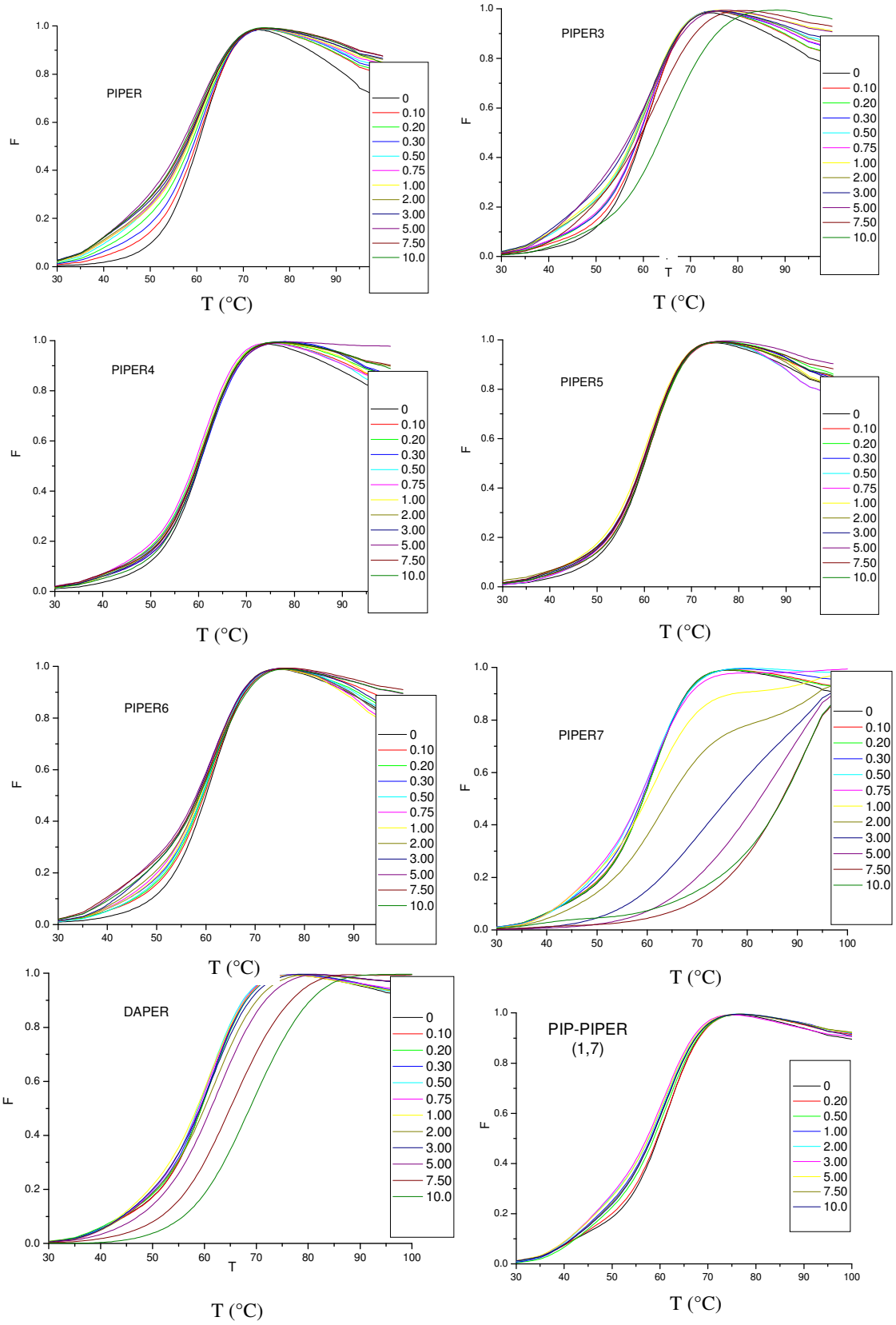

Fig. 4.3.c-2 ***(continues in the next page)***

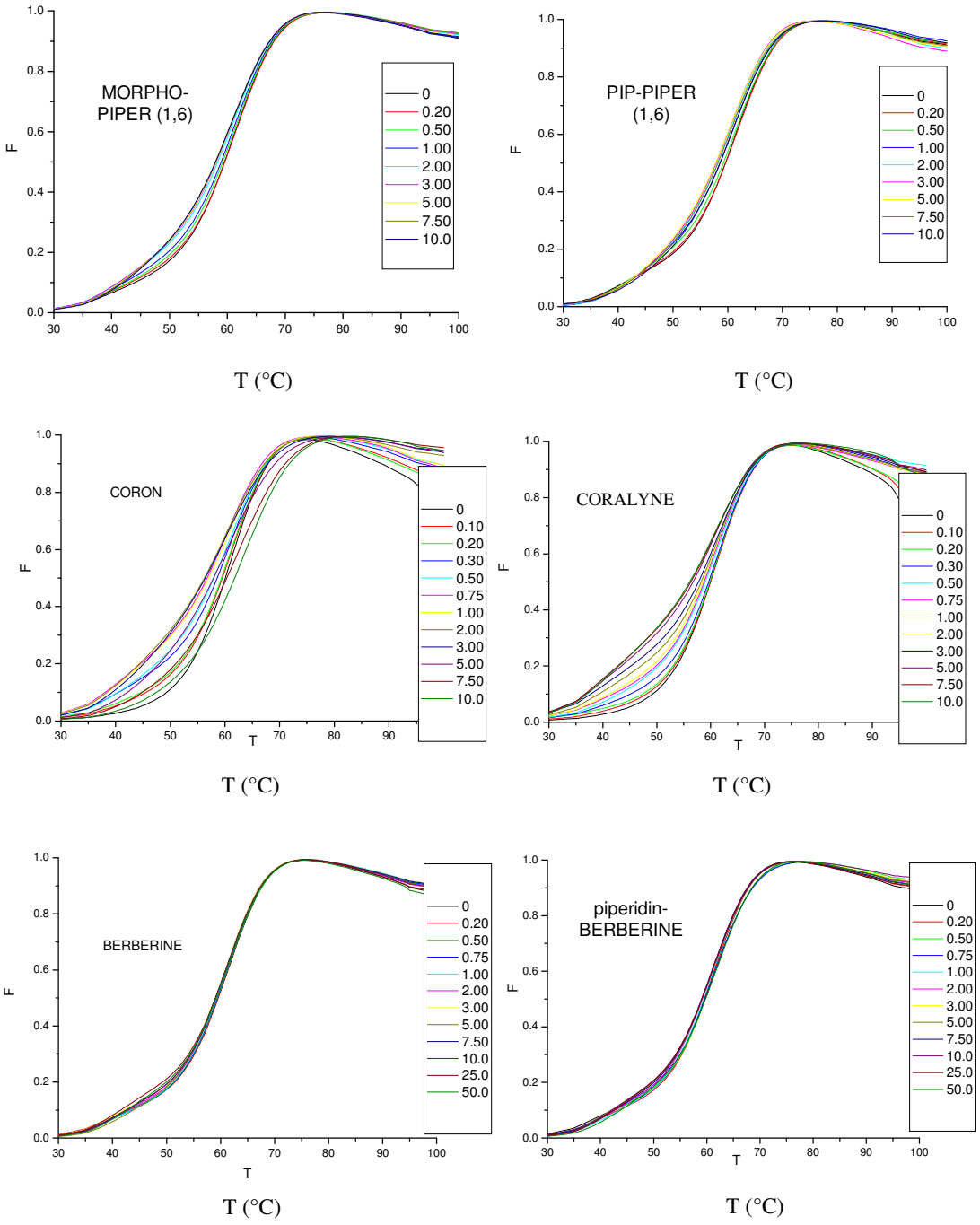

Fig. 4.3.c-2: Curves obtained by FRET experiments on F10D sequence. Legends show the drug/DNA ratios (R) as reported in par. 3.3.c. F is the relative fluorescence obtained after normalization and T is the temperature.

berberine and piperidin-berberine do not show interaction with F10D even at 50:1 drug/DNA ratio (Fig.4.3.c-2).

4.4. Different efficiency of the perylene diimides in telomerase inhibition

The efficiency of the studied compounds as telomerase inhibitors has been evaluated by Telomeric Repeat Amplification Protocol (TRAP) assays, as described in par. 3.3.d. The activity of a cellular extract containing telomerase on two different substrates has been evaluated at different drugs concentrations (Rossetti *et al.* **2002**, Rossetti *et al.* **2004**). In Fig. 4.4-1, the results of the experiments performed using the standard not telomeric TS oligonucleotide are reported. It is worth noting that after the synthesis of two telomeric repeats the DNA fragments are very similar to the oligonucleotide 2HTR, that was used in the electrophoretic mobility shift assays. PIPER is able to inhibit telomerase starting from a concentration of 40μM, while PIPER4 and PIPER5 are unable to inhibit the enzyme even at higher concentration. In the case of PIPER3, PIPER6 and PIPER7, on the contrary, the intensity and the number of bands clearly decrease with respect to the control, at a drug concentration in the range of 5-10μM.

TRAP assays were repeated using TSG4 oligonucleotide as telomerase substrate: it is able to form intramolecular G-quadruplex also before the telomerase synthesis. In fact, the KCl concentration used in the TRAP assay (68mM) allows the formation of G-quadruplex by TSG4 (Fig. 4.2-3). Nevertheless, a similar structure is not stable in the absence of a suitable concentration of G-quadruplex stabilizing molecules and it may be efficiently unfolded and extended by telomerase (Gomez *et al.* **2002**). The obtained results, in the presence of different perylene derivatives, are similar to those obtained using TS oligonucleotide (Fig. 4.4-2). PIPER3, PIPER6 and PIPER7 result the most efficient perylene derivatives in inhibiting telomerase, being active at a drug concentration in the range of 5-10μM.

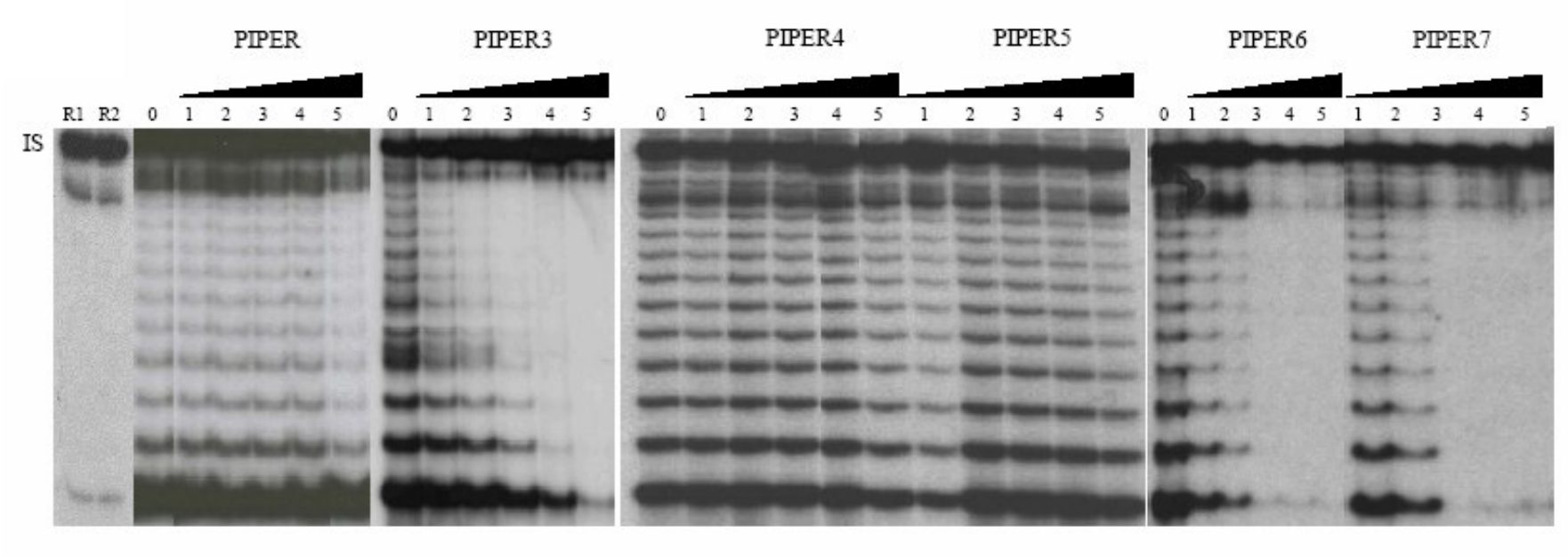

Fig. 4.4-1: Inhibition of human telomerase by different perylene derivatives, by Telomerase Repeat Amplification Protocol (TRAP) assay, using TS as substrate (par. 3.3.d). In lane 0 no drug was added, in lane R1 cell extract was not added, in lane R2 heat inactivation was performed by heating 10 μL extract at 75°C for 10 minutes prior to assaying 1 μL by TRAP analysis. The considered drugs concentrations were 10 μM (lane 1), 20 μM (2), 30 μM (3), 40 μM (4) and 50 μM (5). IS is a 130 bp "internal standard" to control the PCR amplification efficiency (Rossetti *et al.* **2004**).

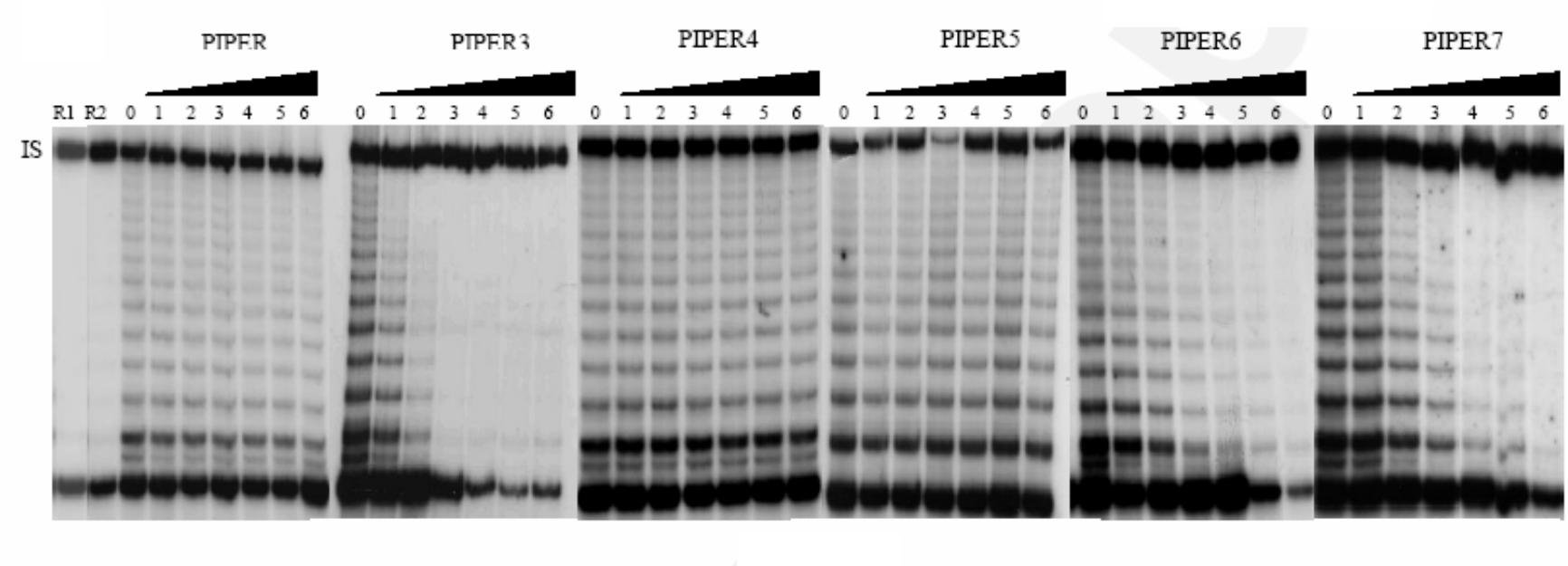

Fig. 4.4-2: Inhibition of human telomerase by different perylene derivatives, by Telomerase Repeat Amplification Protocol (TRAP) assay, using TSG4 as substrate (par. 3.3.d). The symbols used are the same as in Fig. 4.4-1. The considered drugs concentrations were 5 μM (lane 1), 10 μM (2), 20 μM (3), 30 μM (4), 40 μM (5) and 50 μM (6). (Rossetti *et al.* **2004**).

4.5. Structural models and energy calculations based on molecular modeling

Simulated annealing experiments, performed as described in par. 3.4, led to a set of 25 molecular structures for each studied compound, in which the ligand molecule is docked on the human G-quadruplex monomeric structure (Fig. 1.2-5, Parkinson *et al.* **2002**). The corresponding intermolecular energy values were used to calculate the average binding energies (and the relative standard deviations) reported in Tab. 4.5. Repeated experiments show a good reproducibility, suggesting that the number of structures generated was sufficient to be statistically significant.

Preliminary experiments performed on PIPER, using alternatively both external G-quartet planes of monomeric G-quadruplex structure to define the binding site, confirmed what was previously shown for acridine derivatives (Harrison *et al.* **2003**): the best binding energy values are obtained when using the more hydrophilic 3' G-quartet plane. If the hydrophobic 5' G-quartet surface is used (deleting the potassium ion present on this face), absolute values of binding energy are about 10% lower than the ones obtained in the other case. Moreover, drug molecules show a wide range of different positions on the 5' G-quartet surface: most of them have the side chains not fitted into the grooves but rather posed on the external phosphates backbone (Fig. 4.5-1). On the contrary, if the 3' G-quartet plane is considered, all the structures obtained, apart from few exceptions, show drug molecules in one of the two possible orthogonal orientations, with the side chains pointing towards two opposite grooves (Fig. 4.5-2). For these reasons the 3' G-quartet face was used as the binding site for the docking study of all the other compounds.

Ligand	Binding Energy			Hbonds/structure
PIPER (5')	-860	±	15	0.16
PIPER	-925	±	17	0.16
PIPER3(EXT)	-998	±	20	1.24
PIPER3(INT)	-933	±	13	0.44
PIPER3(MIX)	-963	±	22	0.88
PIPER3_medium	-964			
PIPER3(2CH)	-1867	±	22	1.56
PIPER2	-87	±	5	0.32
PIPER4	-936	±	14	0.36
PIPER5	-956	±	21	0.56
PIPER6	-963	±	12	0.20
PIPER7	-979	±	12	0.00
DAPER	-959	±	15	0.36
PIP-PIPER (1,7)	-937	±	26	0.36
PIP-PIPER (1,6)	-936	±	24	0.24
MORPHO-PIPER (1,6)	-944	±	33	0.40
CORON	-1729	±	40	0.28
BERBERINE	-432	±	8	0.00
CORALYNE	-455	±	10	0.00
Piperidin-BERBERINE	-862	±	44	0.20

Tab.4.5 Binding energies for complexes between the human monomeric G-quadruplex structure and the specified ligand, calculated as described in par. 3.4.

Notes:

- these calculations refer to the final 25 lowest energy structures for each experiment
- all energy values are expressed in kcal/mol
- (5') indicates experiments in which the binding pocket has been defined on the 5' G-quartet plane; in all the other simulations 3' G-quartet face was used
- Hbonds/structure is the medium number of H-bonds per structure, calculated dividing the total number of H-bonds for the number of structures (25)

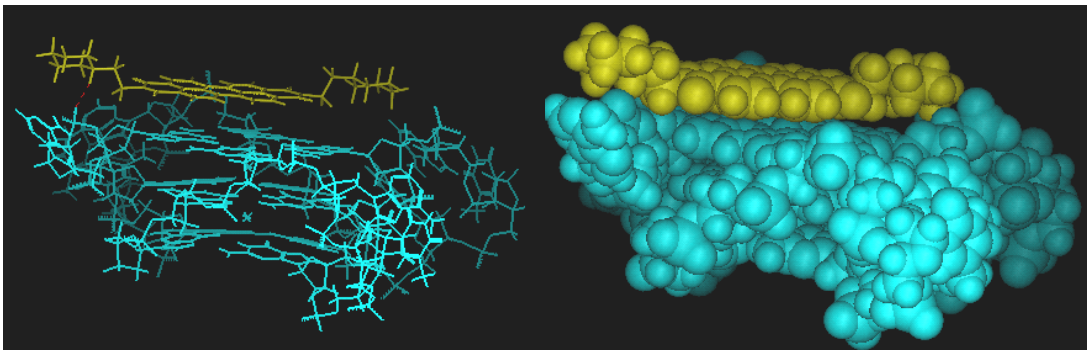

Fig. 4.5-1: PIPER molecule (yellow) stacked on the 5' G-quartet surface (DNA in blue). Sticks and lines (left) and CPK model (right).

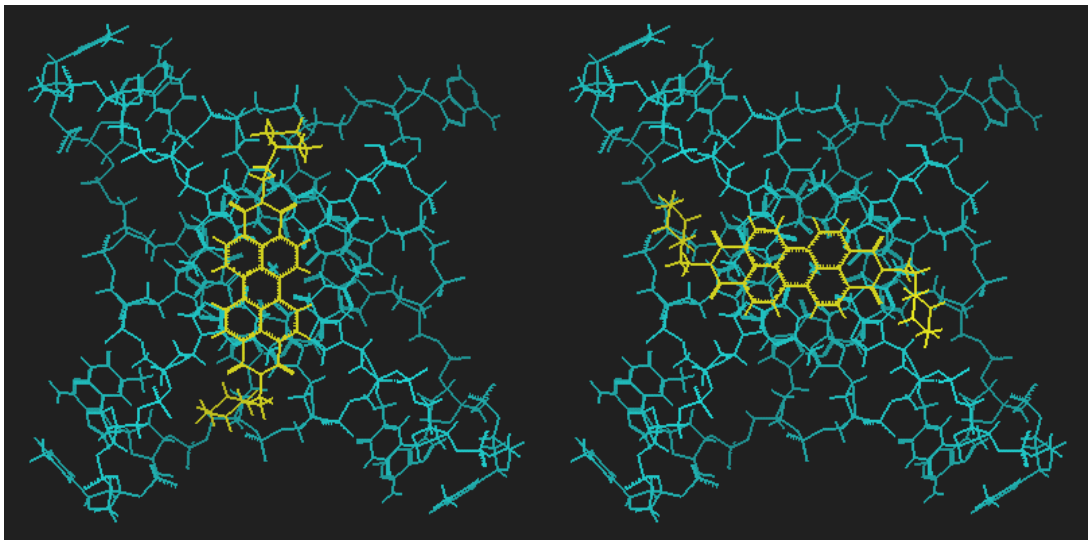

Fig. 4.5-2: The two possible orthogonal orientations of PIPER molecule (yellow) on the 3' G-quartet face (DNA in blue).

The case of PIPER3 is particular, since this molecule has a piperazine ring on the side chains; pK_a values reported for the two N atoms of the piperazine ring are about 11 and 5 respectively. This means that at a neutral pH only one nitrogen atom should be protonated on each ring; for this reason it was necessary to consider at least three different possible protonated forms for this molecule: the form with the two external (secondary) nitrogen atoms protonated (EXT), the form in which the protonated (tertiary) nitrogen atoms are internal (INT), and the form in which one is external and the other one internal (MIX). "PIPER3_medium" energy reported in Tab. 4.5 was calculated considering an occurrence of 25% for "EXT" and "INT" forms and 50% for "MIX" form, for obvious statistical reasons. A possible but rather unlikely PIPER3 structure with two positive charges per ring was also considered (2CH).

The main contribution to the binding energy is electrostatic, so that PIPER2 (no charge) has the lowest medium binding energy, while PIPER3(2CH) and CORON (4 charges per molecule, Fig.4.1.a-1) have the highest binding energies. It is worth noting that a PIPER3 molecule with four charges is quite unlikely, while 4 charged CORON (1 positive charge per piperidine ring) should be the most usual state.

Most of the structures obtained for PIPER on the 3' G-quartet face show the ligand molecule in a position analogue to the one represented in Fig. 4.5-3: one side chain is well fitted into one of the four grooves (regardless of which one), while the other one is free to move, since it can't reach the opposite groove. In someway the two chains seem to be too "short" to fit into both the opposite grooves simultaneously. Indeed DAPER and PIPER5, that have longer side chains than PIPER, manage to fit into them properly as shown in Fig.4.5-4. Binding energies for these compounds are actually slightly higher (in absolute value) than the ones for PIPER/PIPER4 (Tab. 4.5). This would suggest that the longer the chain, the better the binding to the G-quadruplex. Actually the fundamental parameter seems to be the distance between

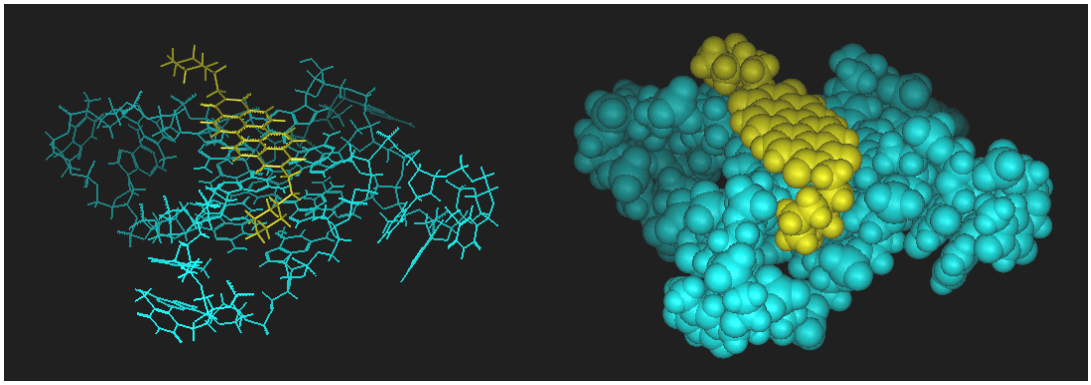

Fig. 4.5-3: PIPER molecule (yellow) stacked on the 3' G-quartet surface (DNA in blue). Sticks and lines (left) and CPK model (right).

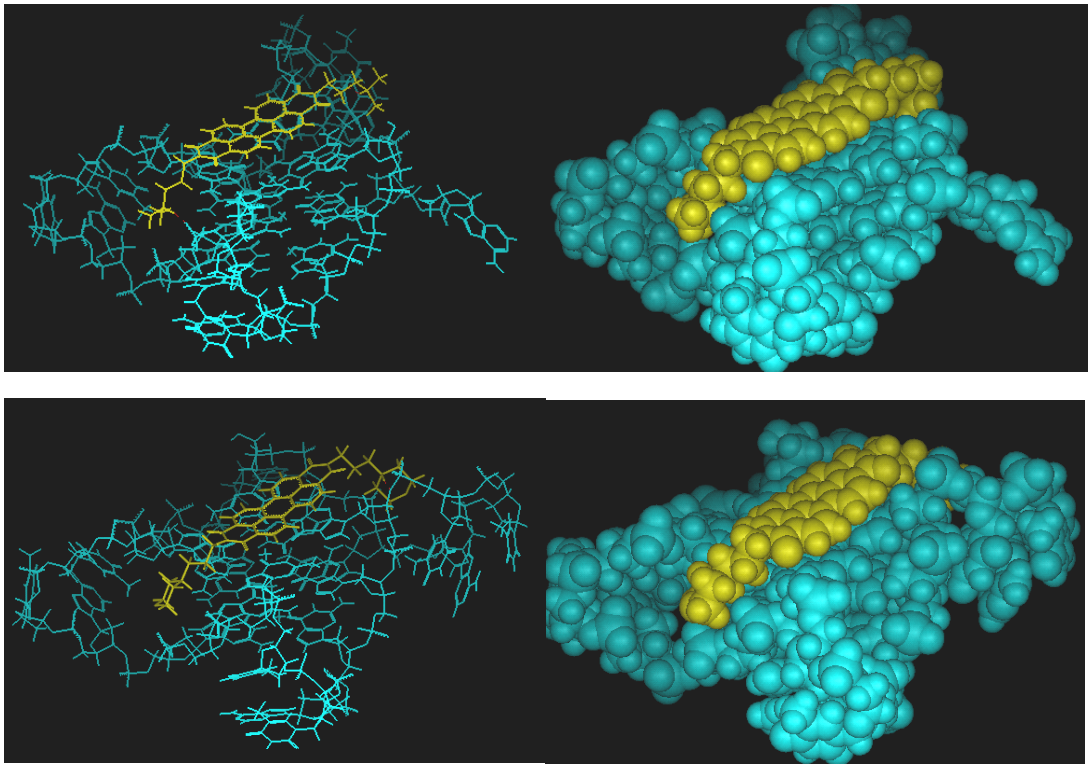

Fig. 4.5-4: DAPER (top) and PIPER5 (bottom) fit both opposite grooves. Sticks and lines (left) and CPK model (right). Ligands are yellow and DNA blue.

the positively charged nitrogen atom and the aromatic core. In fact, PIPER6 and PIPER7 show calculated binding energies close to the ones of PIPER5/DAPER. These two compounds have not the nitrogen atom directly linked to the side chain: this means that the distance of the nitrogen atom from the aromatic core is roughly the same as in the case of PIPER5, that is characterized by a propyl linker (Fig. 4.1.a-1).

Hydrogen bonds are occasionally formed between the N-H group on the side chains of perylene derivatives and several acceptor groups on the DNA, mainly oxygen atoms of the phosphate groups (see Fig. 4.5-2/4) and more rarely oxygen atoms on the ribose rings or nitrogen atoms on the guanine bases. The number of H-bonds formed per structure increases when a positive charge is put on the external nitrogen atom of the piperazine ring of PIPER3 (EXT, MIX and 2CH forms), because the other N atom (tertiary and not protonated) can act as an acceptor group, with the possibility of multiple H-bonds (Fig. 4.5-5). In these cases the best binding energy values are reached indeed (Tab. 4.5).

As for the new perylene and coronene derivatives, CORON shows a strong binding to G-quadruplex, mainly due to the electrostatic interactions (Tab. 4.5). As deeply discussed in chapter 5, it is important to underline that for several reasons it is not correct to compare the binding energies obtained for molecules that present a different scaffold. The model reported in Fig. 4.5-6 shows that at least two side chains fit into two consecutive grooves, while one or both of the others are free to move. The new highly water soluble perylene derivatives show a behaviour and binding energies very similar to PIPER and previous perylene derivatives (see Tab. 4.5), despite a slight distortion of the aromatic plane due to the presence of the lateral rings (Fig. 4.5-7 for PIP-PIPER(1,7)). These compounds were considered protonated only on the side chains piperidine rings (on the major axis of perylene).

Finally, berberine, its analogue coralyne and its derivative piperidin-berberine were considered. The models obtained for berberine and piperidin-berberine are reported in Fig.

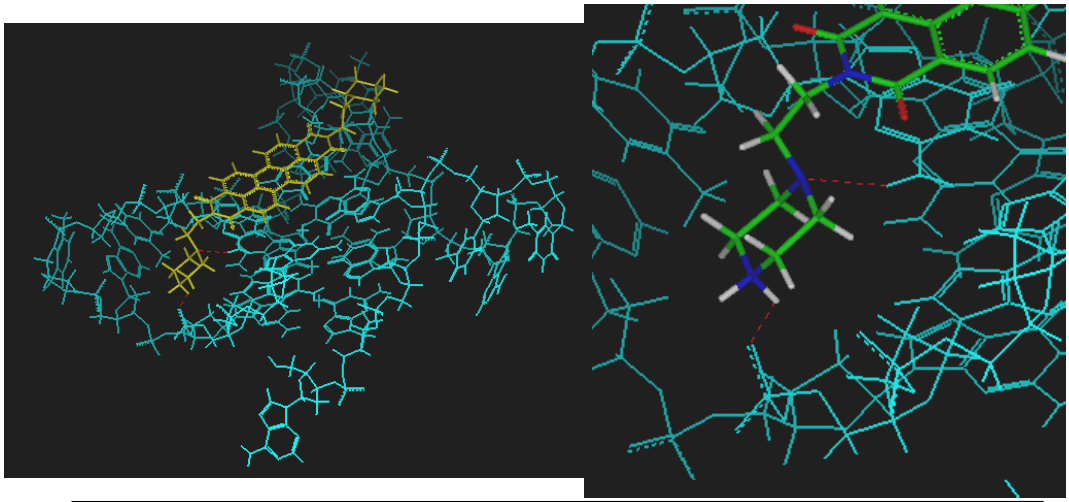

Fig. 4.5-5: multiple H-bonds (red dashed line) formed by PIPER3(EXT). Detail coloured according to atom types on the right.

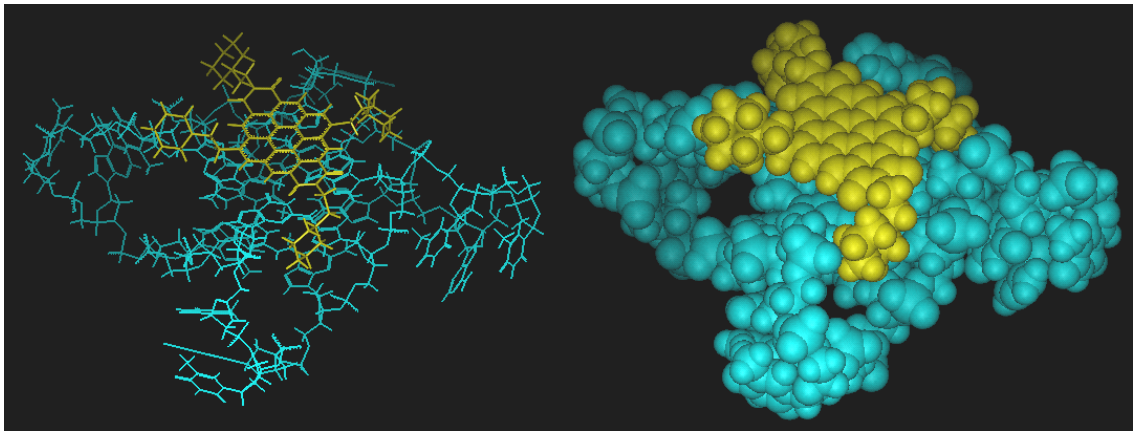

Fig. 4.5-6: Complex between CORON (yellow) and G-quadruplex (blue). Sticks and lines (left) and CPK model (right).

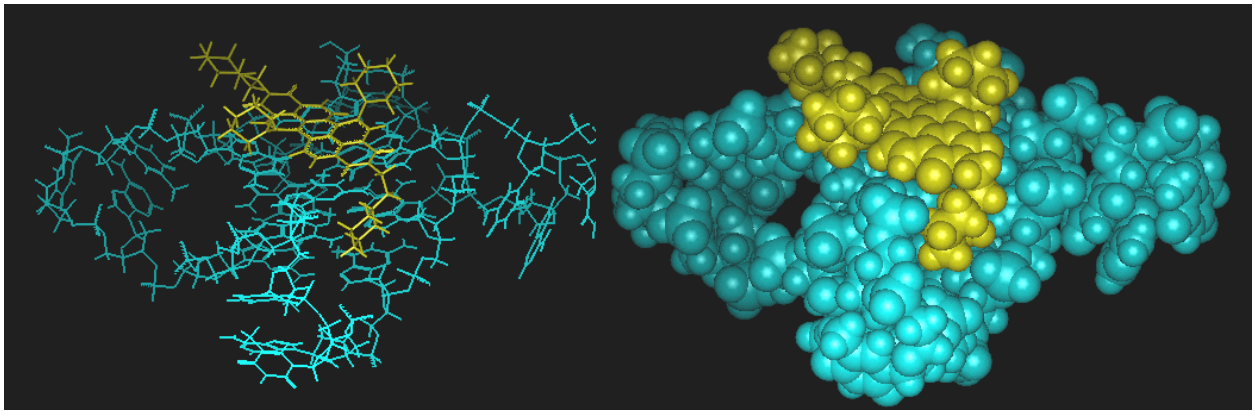

Fig. 4.5-7: Complex between PIP-PIPER(1,7) (yellow) and G-quadruplex (blue). Sticks and lines (left) and CPK model (right).

4.5-8 and 4.5-9 respectively. Berberine stacks on the terminal G-tetrad of the G-quadruplex structure; the new side chain of piperidin-berberine is suitable to interact with one of the four grooves of the G-quadruplex, increasing the binding energy and leading to possible formation of H-bonds (Tab. 4.5).

Although the molecular modeling studies reported here give surely interesting information on the molecular features of the complexes between the studied drugs and the parallel monomeric G-quadruplex structure, several limitations can be observed in this method, mainly related to the absence of explicit water molecules, the rigidity of the DNA structure and the strong effect of the positive charges on the ligand molecule. Several attempts (described in the following section) have been made to try to solve these problems, but it is clear, as discussed in chapter 5, that the binding energy values must not be considered as absolute values, but rather as a relative ranking that can be correct only in a series of homologue molecules, whose structures are similar.

Further simulations: A first approach in order to better reproduce the real environment in which the drug-DNA complexes exist was tried by defining a water-box around the lowest energy and most frequently repeated structures, and performing further minimization and molecular dynamics, taking into account explicit water molecules. These experiments were performed solvating the selected structure from the previous simulated annealing, defining a layer of water molecules of 20Å centred on the ligand molecule, through the "soak" function inside the InsightII Package. This creates a sphere around the complex of about 1500 water molecules, which makes following calculations very slow. First of all, 500 steps of minimization of the whole complex according the usual Polak-Ribiere conjugate gradient method were performed. Then, a 10ps dynamics at 300K was performed. In this phase, only an interface of 7Å from the ligand molecule was completely free to move, while restrains

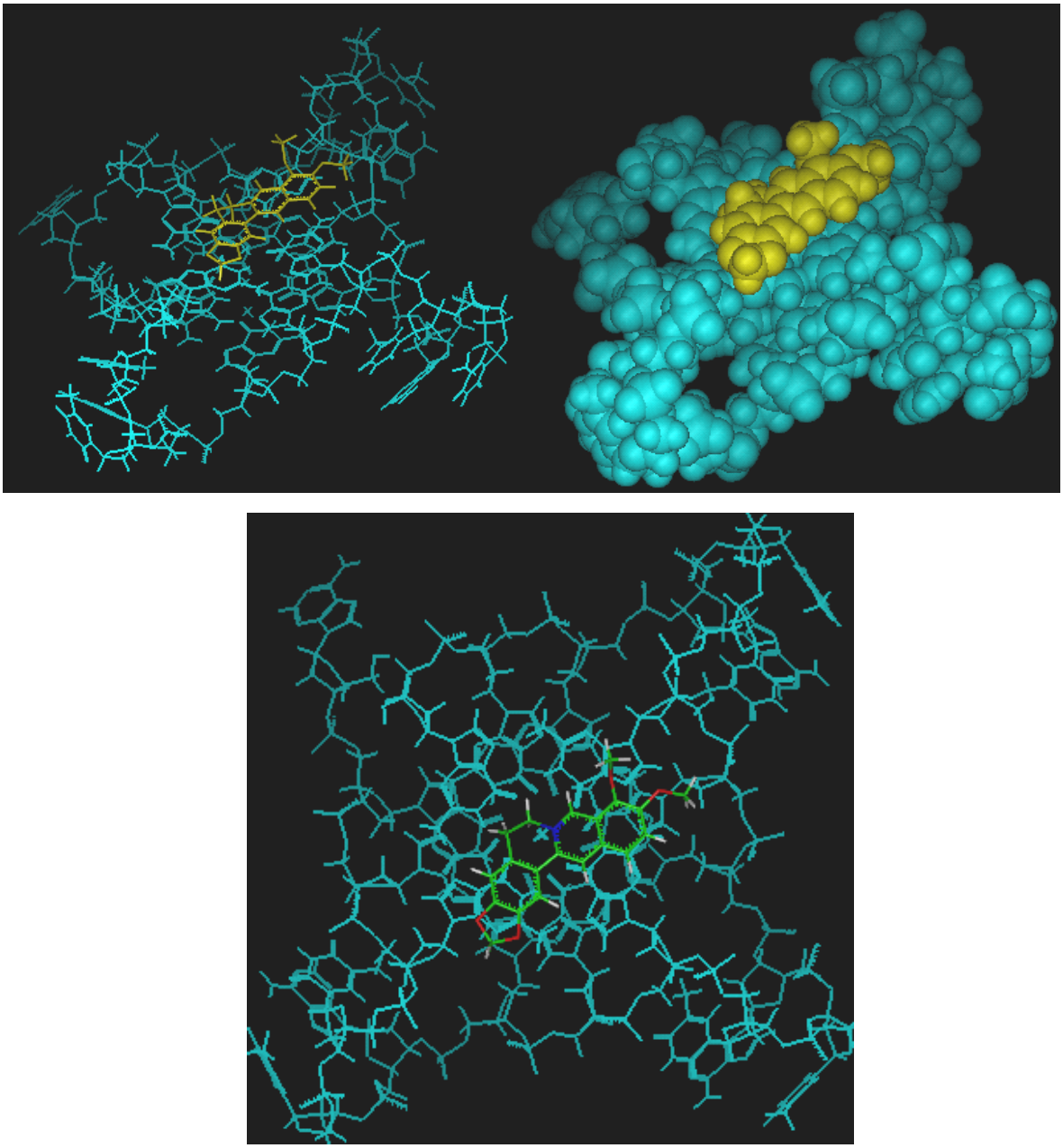

Fig. 4.5-8: Model obtained for the complex between berberine (yellow and atom-type coloured) and monomeric G-quadruplex (blue). Sticks and lines (top left), CPK model (top right) and top view (bottom), that evidences the superimposing of the berberine aromatic moiety on the G-tetrad: positive charged nitrogen atom is at the centre of the G-tetrad.

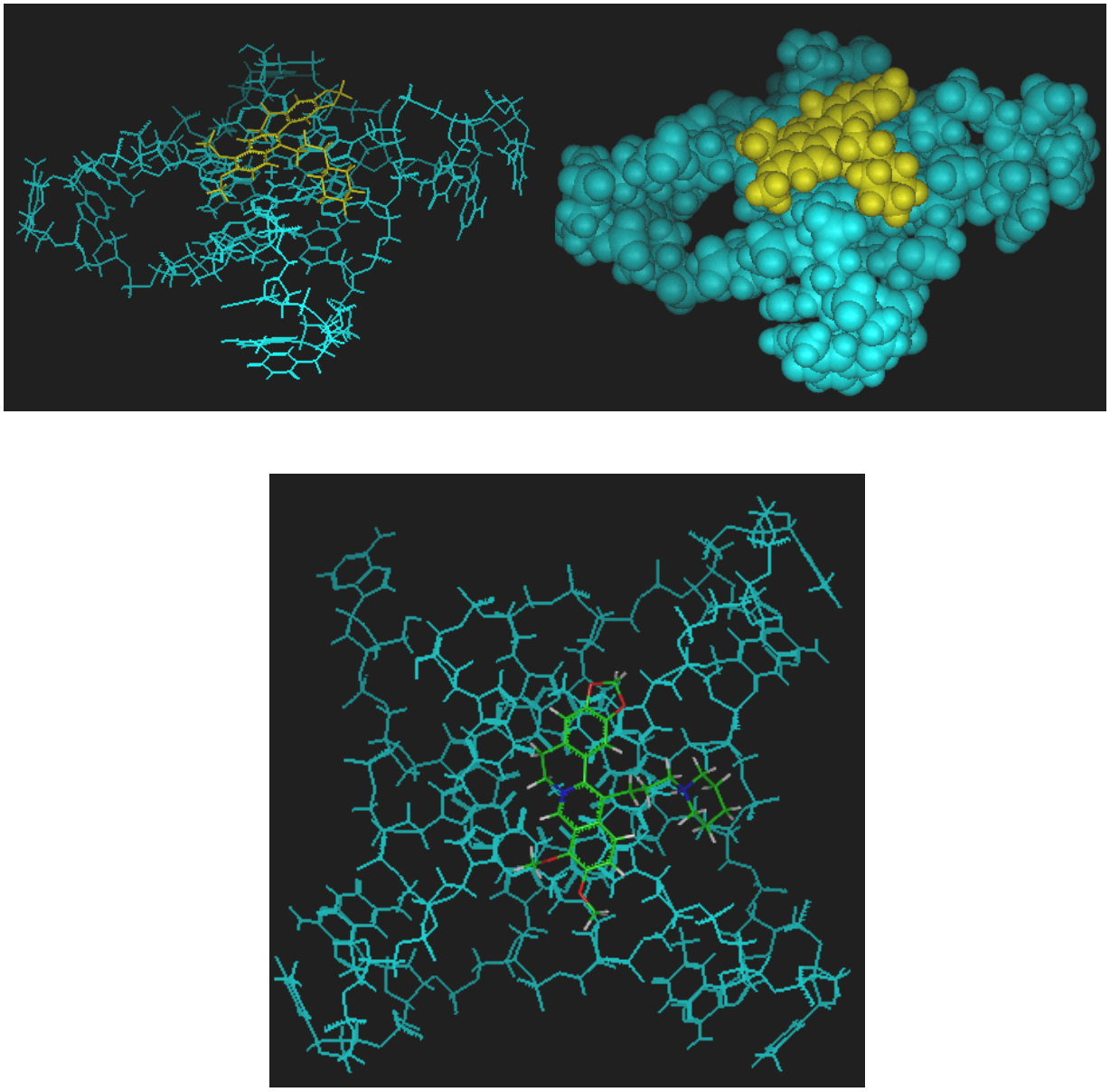

Fig. 4.5-9: Model obtained for the complex between piperidin-berberine (yellow and atom-type coloured) and monomeric G-quadruplex (blue). Sticks and lines (top left), CPK model (top right) and top view (bottom). It is evident that the position of the new side chain is suitable to interact with one of the four grooves of the G-quadruplex.

were applied to the rest of water molecules to avoid dispersion of the solvation sphere during the dynamics. Successively, one frame every 200fs was considered for minimization, so that 50 structures were minimized. The minimization was performed in three steps: 500 steps of PR conjugate gradient on the whole structure, 2000 steps with restraints on all water molecules except those belonging to a new defined interface of 8Å from the ligand molecule, a final 500 steps of minimization taking fix all the water molecules, so that only the ligand molecule was free to move. DNA was fully constrained during the whole process. These calculations took a long time and preliminary results on PIPER and DAPER molecules did not show significant variations with respect to the models previously obtained, so that they were not performed on the other molecules.

In order to consider flexible DNA, a binding pocket within 5 Å from the ligand in the best positions was defined, so that the guanine residues involved in the interactions with drugs could be free to move, while so far the DNA has been fully constrained. Different levels of tethering were considered during the following simulated annealing, that was identical to the second step of the previous simulated annealing. Unfortunately, it was not possible to find a value of the tethering parameter suitable for these experiments. If it is too low in fact, no change in the final structure was observed. If too high, on the other hand, the movable G-quartet lose its characteristic H-bonds pattern.

An analogue problem was found when G-quadruplex structures of different topology or duplex DNA structures were taken into account. Also in this case in fact, excessive flexible DNA led to improbable structures, while too rigid DNA did not allow ligand molecules to interact with DNA bases, in particular terminal G-quartets, since they are not available for interactions with drug molecules, as in the case of the open structure used in the previous simulations.

Finally, an attempt to better calculate charges distribution of ligand molecules, that seems such a critical feature, was made by semiempirical calculations with the Mopac module of InsightII. The final energy values obtained with this method did not differ from the previous ones, calculated with the standard charges distribution according to the CVFF force field.

4.6. Preliminary biochemical studies on the new compounds

Preliminary results obtained by PAGE show that berberine and its analogues are able to induce G-quadruplex dimeric structures on 2HTR oligonucleotide (Fig. 4.6-1(A)), with a different extent (Fig. 4.6-1(B)). Coralyne shows the best efficiency in inducing the G-quadruplex, in agreement with FRET results (Fig. 4.3.a-3). Furthermore coralyne shows a higher telomerase inhibition activity (starting from a concentration above 50μM) than the two other compounds, as derived by preliminary TRAP assays, performed using TSG4 as substrate, reported in Fig. 4.6-2(A). It is worth noting that while berberine derivatives are able to stabilize a preformed G-quadruplex structure at 50mM potassium ions concentration (as studied by FRET assay, par. 4.3.a), they are not able to induce an analogue monomeric G-quadruplex structure at 5mM potassium ions concentration (Fig. 4.6-1(C)). The different ability to induce inter and intramolecular G-quadruplex structures was previously observed for telomestatin and a porphyrin derivative (Kim *et al.* **2003**); this selectivity was correlated with different biological effects of the two compounds.

In Fig. 4.6-2(B), TRAP assay for CORON is also reported. This compound shows telomerase inhibition starting from a concentration of 50μM, similarly to PIPER (Fig. 4.4-1/2). Since the two new side chains and the larger aromatic area of CORON, with respect to PIPER, would be expected to improve the electrostatic and hydrophobic interactions with G-quadruplex DNA, a possible explanation of the moderate inhibitory activity of CORON could relay on the influence of the same molecular features on the self-aggregation processes for this new molecule. In fact, these processes have been shown to be very important in determining the efficiency of the perylene diimides in inducing and stabilizing G-quadruplexes and in inhibiting telomerase (chapter 5). In particular, CORON shows a behaviour in aqueous solution similar to that of PIPER4 and PIPER5 (Fig. 4.1.a-5). In fact, in the absorption spectra

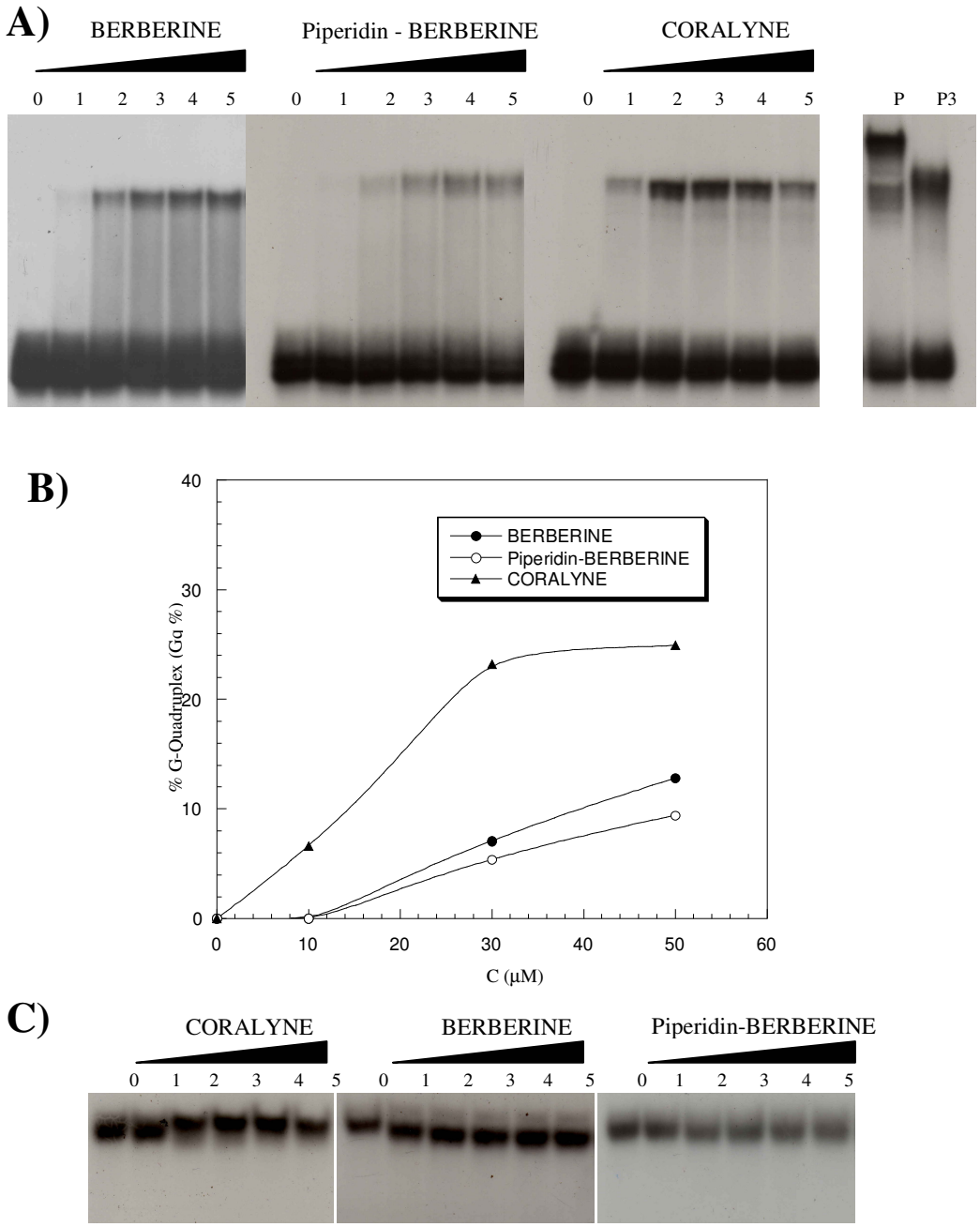

Fig. 4.6-1: A) G-quadruplex structures formation induced on 2HTR oligonucleotide by berberine and its derivatives (Fig. 4.1.b-1) studied by native PAGE (PolyAcrylamide Gel Electrophoresis) according to the experimental procedure described in par. 3.3.a. Experiments were performed at 12 μM oligonucleotide (2HTR) concentration in MES-KCl buffer (pH 6.5) at increasing concentrations of the berberine derivatives and with no drug (lane 0). In lane P and P3, 2HTR was incubated with 30 μM PIPER and PIPER3 respectively. Drugs concentrations: 10 μM (lane 1), 30 μM (2), 50 μM (3), 70 μM (4) and 100 μM (5). **B)** Percentage of G-quadruplex structures formed (G_q%, see the caption of Fig. 4.2-1) in function of drug concentration (C (μM)) relative to the band shift assays reported in A). **C)** Same as in A) but using TSG4 oligonucleotide and a 5mM KCl-10mM MES buffer (pH 6.5).

A)

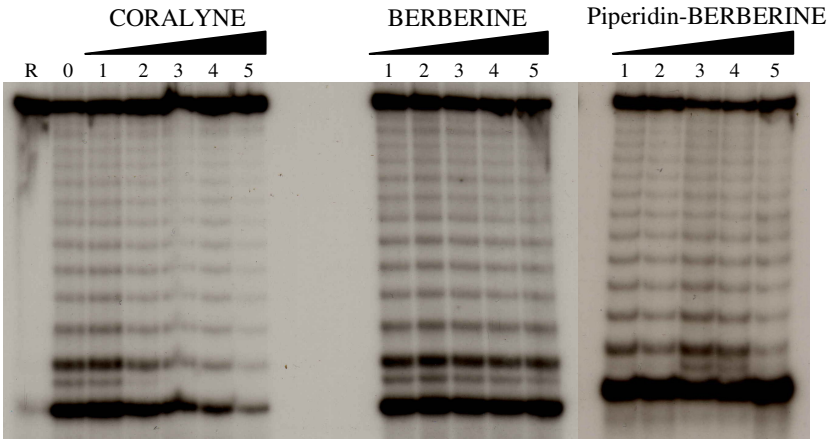

B)

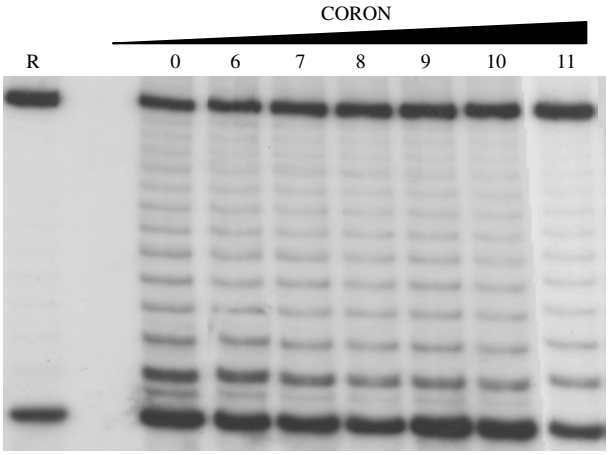

Fig. 4.6-2: A) Inhibition of human telomerase by berberine and its derivatives (Fig. 4.1.b-1) by Telomerase Repeat Amplification Protocol (TRAP) assay, using TSG4 as substrate (par. 3.3.d). In lane 0 no drug was added, in lane R cell extract was not added. The considered drugs concentrations were 30 μM (lane 1), 50 μM (2), 70 μM (3), 100 μM (4) and 130 μM (5). **B)** TRAP assay on CORON: 10 μM (6), 20 μM (7), 30 μM (8), 40 μM (9), 50 μM (10) and 100 μM (11).

both at pH 6.5 and at pH 7.5, there is no isobestic point and a strong hypochromic effect with respect to the DMSO spectrum can be observed, suggesting the formation of more than one type of multimeric aggregates.

5. Discussion

Among the different investigated compounds (par. 4.1), perylene diimides with two hydrophilic side chains (Fig. 4.1.a-1) have been studied in detail, since they represent a series of compounds in which, maintaining unchanged the stacking interactions due to the perylene aromatic core, it is possible to compare the effect of different side chains linked to the same aromatic moiety (Rossetti *et al.* **2002**, Rossetti *et al.* **2004**). They have been investigated in their ability to induce G-quadruplex DNA structures by PAGE method (par. 4.2) and to inhibit human telomerase by TRAP assays (par. 4.4). Preliminary results on the stabilization of preformed G-quadruplex and duplex DNA structures by one of these compounds by means of absorption spectroscopy and circular dichroism are also reported (par. 4.3.b). FRET assays (par. 4.3.a/c) have been performed to study the interactions of all the analyzed compounds with a pre-annealed G-quadruplex monomeric structure and with a model of duplex DNA. In order to elucidate some molecular features of the complexes between the investigated compounds and the human monomeric parallel G-quadruplex structure resolved by Neidle and coworkers (Parkinson *et al.* **2002**), simulated annealing experiments have been performed (par. 4.5). Finally, preliminary results of PAGE and TRAP assays on recently synthesized perylene, berberine and coronene derivatives are reported (par. 4.6).

The results obtained by PAGE measurements of PIPER2 (Fig. 4.2-1) show with good evidence that a strong decrease of electrostatic interactions between the drug and DNA does not allow the formation of any G-quadruplex structure. Since PIPER2 should be able to establish stacking interactions with the G-tetrads, these data confirm the essential role of the electrostatic interactions between the side chains of the drugs and DNA grooves. In fact, the quaternization of the nitrogen atom on the pyridine ring of PIPER2 (par. 3.1.a) led to the fully

charged nitrogen atom of PIPER7, which shows an activity comparable to the best perylene derivatives. As for the other perylene diimides, the results reported in this thesis allow to establish that both the efficiency in forming G-quadruplex structures, as derived by PAGE (par. 4.2), and the telomerase inhibition, as derived by two different TRAP assays (par. 4.4), depend on the features of the perylene derivatives side chains. In all cases, a fundamental molecular feature appears to be the distance between charged nitrogen atoms in the side chains and the aromatic moiety of the drugs. This finding is consistent with the threading intercalation model proposed for this kind of molecules by Hurley and coworkers (Fedoroff *et al.* **1998**, par. 1.6.a), in which the drug is stacked on the terminal G-tetrad, so that the distance defined above is surely of great importance in optimizing the interactions with the phosphates in the DNA grooves. In fact, the compounds having the longest distance between the positively charged nitrogen atom on the side chains and the aromatic moiety (PIPER3, PIPER5, PIPER6 and PIPER7) are the most efficient in inducing dimeric G-quadruplex structures at pH 6.5 (Fig. 4.2-1/2). When the distance is shorter (PIPER and PIPER4), a different behaviour is observed: PIPER4 is barely efficient in inducing dimeric G-quadruplex structures, while PIPER is the only compound able to induce tetrameric G-quadruplex.

Another important aspect to be considered is the "self-association" of the drugs in water solution, probably correlated to the pK_a values and the basicity of the side chains, as recently reported by Kerwin and coworkers (Kerwin *et al.* **2002**, Kern *et al.* **2002**). The absorption spectra of perylene diimides (par. 4.1.a) put in evidence a more complex aggregation for morpholine containing perylene derivatives (PIPER4 and PIPER5) with respect to the other compounds at pH 6.5. Increasing the pH to 7.5, PIPER behaviour changes, becoming very similar to that of PIPER4 and PIPER5. Anyway, the complexity of these processes does not allow to find a simple correlation with PAGE results and to develop a structural model. With regard to this, it should be noted that as previously suggested by Kerwin *et al.* (**2002**), at the

moment it is not possible to establish if the binding of the drugs to the G-quadruplex DNA occurs from monomeric or aggregated ligands. In the first case, the drug multimerization should be competitive with respect to the monomeric drug binding to the G-quadruplex (par. 1.6.a).

The length and the basicity of the six perylene derivatives side chains play a synergistic role in determining the activity of the drugs. In fact, PIPER4 and PIPER5, that have the same side chains basicity, result the most inefficient compounds in inducing G-quadruplex structures at pH 7.5 (Fig. 4.2-4), evidencing the important role of the drugs self aggregation. But it is worth noting that, at pH 6.5, PIPER4 is still the less efficient perylene derivative in inducing G-quadruplex structures, while PIPER5, characterized by a longer side chain, results so efficient as the other perylene derivatives (Fig. 4.2-2), pointing out an important role also for the distance between charged nitrogen atoms in the side chains and the aromatic moiety of the drugs.

According to TRAP assays performed using either TS or TSG4 oligonucleotides as telomerase substrate (par. 4.4), PIPER3, PIPER6 and PIPER7 result the most efficient perylene derivatives in inhibiting telomerase. A quantitative correlation with PAGE results is tempting, but not possible. In fact, in the case of TS, after the synthesis of two telomeric repeats the DNA fragments are very similar to the oligonucleotide 2HTR, that was used in the electrophoretic mobility shift assays, but the concentrations of telomeric repeats having different length can not be evaluated. On the other hand, in the case of TSG4, where the sequence is exactly the same used in one of the PAGE assays, the ability of telomerase to unfold the G-quadruplex structure formed at the TRAP buffer potassium concentration (Gomez *et al.* **2002**) makes difficult to establish a correlation with the behaviour of perylene diimides studied by PAGE at different potassium concentrations, but always in the absence of the destabilizing effect of telomerase (par. 4.2).

Nevertheless, the comparison between the results derived from PAGE (par. 4.2) and absorption spectroscopy (par. 4.1.a) in TRAP buffer and those obtained from the two different TRAP assays (par. 4.4) allows to establish that the same drugs molecular features which determine the G-quadruplex formation strikingly influence also the ability of these compounds to inhibit telomerase. In fact PIPER3, PIPER6 and PIPER7 result the most efficient perylene derivatives, while PIPER, PIPER4 and PIPER5 appear definitively less efficient. These results suggest that a too short side chain and/or a weak basicity of side chain amines give rise to a poor inhibitory activity, probably due to the different thermodynamic stabilization of the complexes between these drugs and G-quadruplex DNA structures.

In order to study in depth these thermodynamic aspects, FRET assay on a human monomeric G-quadruplex forming sequence has been considered (par. 4.3.a). Although it is not possible to use ΔT_m values to access binding affinities when the temperature dependence of binding constant has not been first characterized (Canzonetta *et al.* **2002**, Bostock-Smith *et al.* **1999**), the results reported for these experiments confirm weaker interactions of PIPER4 and PIPER5 with monomeric G-quadruplex with respect to the other perylene diimides (Tab. 4.3). The compounds that arise most the G-quadruplex melting temperature (PIPER, PIPER3, PIPER6, PIPER7) are the same that show the highest efficiency in inducing G-quadruplex structures as derived by PAGE (par. 4.2) and in inhibiting telomerase (par. 4.4), with the major exception of PIPER, that show a poor telomerase inhibition. These results suggest a good correlation between these different techniques. FRET results on CORON show a good efficiency in increasing the melting temperature of G-quadruplex DNA, at least comparable to the best perylene diimides, while the new perylene derivatives (PIP-PIPER and MORPHO-PIPER) show a behaviour similar to PIPER4 and PIPER5. Finally, FRET experiments allowed the evaluation of berberine, its analogue coralyne and its derivative piperidine-berberine, underlining the improvement of the last compound with respect to berberine itself, due to the

new piperidine containing side chain, but also showing the best interactions for coralyne, due to its full aromatic core.

Since the selectivity of G-quadruplex interacting compounds for G-quadruplex DNA with respect to duplex DNA is a topic of great interest for the possible biological applications of these molecules, preliminary studies using absorption spectroscopy (par. 4.3.b) and FRET assays (par. 4.3.c) have been reported. In particular, absorption and circular dichroic spectra were registered for PIPER3 in the presence of different concentrations of pre-annealed G-quadruplexes and calf thymus DNA (par. 4.3.b). The stronger increasing of the molar extinction coefficients in the case of quadruplex with respect to duplex DNA suggests a high selectivity for this compound. These results and the presence of dichroic bands in the visible region indicate that a complete titration in a suitable range of drug/DNA ratios and the consequent analysis could be considered a good approach for the evaluation and quantification of the interactions between drugs and different DNA structures. FRET assays on a fluorescence labelled autocomplementary decamer (par. 4.3.c) suggest a good selectivity for G-quadruplex with respect to duplex DNA for all the investigated compounds, with the major exception of PIPER7.

Molecular modeling studies have been performed to elucidate the structural aspects at the molecular level in the formation of complexes between monomeric G-quadruplex DNA and the analysed compounds (par. 4.5). These studies confirmed the "threading intercalation" model proposed for this kind of molecules by Hurley and coworkers (Fedoroff *et al.* **1998**), in which the drug is stacked on the terminal G-tetrad, stabilized by π–π interactions with the central aromatic core, while the side chains interact with the G-quadruplex grooves. For perylene diimides two possible orthogonal orientations are possible, while CORON can interact simultaneously with the four grooves. As for the series of perylene diimides, the energy calculations based on these simulations confirm that the distance between charged

nitrogen atoms in the side chains and the aromatic moiety of the drugs is surely of great importance in optimising the interactions with the phosphates in the DNA grooves. In fact, the compounds in which this distance is longer (PIPER3, PIPER5, PIPER6, PIPER7, DAPER) show higher binding energies than the compounds in which this distance is shorter (PIPER, PIPER4). The relative ranking obtained for this series of compounds is comparable to their efficiency in inducing the monomeric G-quadruplex in TSG4 (par. 4.2) and in inhibiting telomerase (par. 4.4), with the major exceptions of PIPER4 and PIPER5. For these molecules in fact, the fundamental contribution of the weaker basicity of the morpholine ring is not correctly taken into account. This is due to the fact that the simulated annealing method (as all the classical docking methods) takes into account only one ligand molecule, that can be fully protonated or not protonated. Furthermore, the "self-aggregation" processes are not considered. For these reasons, the system is not able to explain the different behaviour of PIPER4 and PIPER5, for which the self-aggregation seems much more important than for all the other compounds, as suggested by absorption spectroscopy measurements (par. 4.1.a), contributing to determine a poor activity both to induce G-quadruplex formation and to inhibit telomerase.

The "threading intercalation" model is also confirmed for the other classes of recently synthesized molecules, with the possibility of simultaneous interaction of the four side chains of CORON with the four grooves of the G-quadruplex (par. 4.5). It would be tempting to compare the binding energies obtained for these molecules to the ones obtained for perylene diimides, but this is not correct. In fact, the CVFF force field used in these simulations and, similarly, all the other force field available in the InsightII software are not suitable for a correct evaluation of the interactions between aromatic systems (Chessari *et al.* **2002**). A more complex treatment should be applied, such as the density functional theory (Grimme **2004**), but this is not possible at the moment in commercially available simple docking softwares.

For these reasons, and in any case with the limitations illustrated above and in par. 4.5, a comparison between the relative binding energies is correct only in a series of homologous molecules, such the perylene diimides. Another important parameter is the amount of total charges per molecule, which must be the same for a correct comparison.

Both these aspects are evident if we consider the three compounds berberine, piperidin-berberine and coralyne (Fig. 4.1.b-1). They look similar, but they are different exactly for the two aspects mentioned above: coralyne has a different aromatic system with respect to the other two molecules, while piperidin-berberine has a positive charge more than the other two molecules. Piperidin-berberine (with two charges) would be expected to be much more efficient in binding to G-quadruplex structure than berberine and coralyne (one positive charge per molecule), while these two molecules should not be very different one from the other in terms of binding energies (Tab. 4.5). Although it is necessary to be cautious, as discussed above, when considering ΔT_m obtained by FRET assays as a parameter to evaluate binding affinities, the melting temperatures reported in Fig. 4.3.a-3 suggest a very different ranking among these compounds. Coralyne shows melting temperatures much higher than the other two compounds, probably due to its full aromatic core, while the new side chain of piperidin-berberine increases only slightly the G-quadruplex melting temperature with respect to berberine.

6. Conclusions and perspectives

The results reported in this thesis show that different molecular features contribute to determine the efficiency of G-quadruplex interactive compounds in inducing and stabilizing different G-quadruplex structures. In particular, when the π–π interactions are the same in a series of homologues compounds, which are characterized by the same aromatic core, such as perylene diimides, the length and the basicity of the side chains play a main role in determining the behaviour of the different compounds. The same molecular parameters deeply influence the ability of these compounds to inhibit human telomerase. Molecular modeling studies have elucidated some of these experimental results and FRET assays look promising as a quick method to evaluate G-quadruplex binding and selectivity with respect to duplex DNA. Absorption spectroscopy and circular dichroism will be used to quantify the interactions of the studied compounds with duplex and quadruplex DNA structures; the reported preliminary results illustrate the potentiality of these methods. PAGE and TRAP analysis will be extended to all the recently synthesized new compounds.

It is worth noting that the synthetic strategies developed to obtain the new perylene and coronene derivatives result in a great versatility: different side chains can be added to the new coronene moiety, with the possibility of achieving selectivity towards different G-quadruplex structures, as has been shown for perylene diimides. Moreover, it is possible to add two different kinds of side chains (one type on the imidic nitrogen atoms and a different one directly linked to the aromatic moiety), since they are added in two different steps. This is very interesting since some G-quadruplex structures have four identical grooves (where the side chains mainly interact), while others have grooves of different dimensions. Furthermore, by means of intermediate compounds, it will be possible to obtain asymmetric molecules.

Finally, the reported berberine analogues and derivatives represent a new interesting class of G-quadruplex interacting compounds and telomerase inhibitors, structurally related to natural products.

All the information obtained so far on the interactions between the studied compounds and G-quadruplexes as well as the techniques used for these studies and the synthetic strategies reported in this thesis will be used to design new and more efficient G-quadruplex interactive compounds and telomerase inhibitors.

7. References

- Alberti, P.; Ren, J.; Teulade-Fichou, M.P.; Guittat, L.; Riou, J.F.; Chaires, J.; Helene, C.; Vigneron, J.P.; Lehn, J.M.; Mergny, J.L. "Interaction of an acridine dimer with DNA quadruplex structures" *J. Biomol. Struct. Dyn.* **2001**, *19*, 505.
- Allsopp, R.C.; Chang, E.; Kashefiaazam, M.; Rogaev, E.I.; Piatyszek, M.A.; Shay, J.W.; Harley, C.B. "Telomere shortening is associated with cell division *in vitro* and *in vivo*" *Exp. Cell Res.* **1995**, *220*, 194.
- Baumann, P.; Cech, T.R. "Pot1, the putative telomere end-binding protein in fission yeast and humans" *Science* **2001**, *292*, 1171.
- Bianco, A.; Cavarischia, C.; Guiso, M. "The heck coupling reaction using aryl vinyl ketones: Synthesis of flavonoids" *Eur. J. Org. Chem.* **2004**, 2894.
- Bodnar, A.G.; Ouellette, M.; Frolkis, M.; Holt, S.E.; Chiu, C.P.; Morin, G.B.; Harley, C.B.; Shay, J.W.; Lichtsteiner, S.; Wright, W.E. "Extension of life-span by introduction of telomerase into normal human cells" *Science*, **1998**, *279*, 349.
- Bostock-Smith, C.E.; Searle, M.S. "DNA minor groove recognition by bis-benzimidazole analogues of Hoechst 33258: insights into structure-DNA affinity relationships assessed by fluorescence titration measurements" *Nucleic Acids Res.* **1999**, *27*, 1619.
- Cantor, C.R.; Schimmel, P.R. "Techniques for the study of biological structure and function" *Biophysical Chemistry* **1980**, Vol. II.
- Canzonetta, C.; Caneva, R.; Savino, M.; Scipioni, A.; Catalanotti, B.; Galeone, A. "Circular dichroism and thermal melting differentiation of Hoechst 33258 binding to the curved (A_4T_4) and straight (T_4A_4) DNA sequences" *Biochim. Biophys. Acta* **2002**, *1576*, 136.
- Chen, Q.; Kuntz, I.D.; Shafer, R.H. "Spectroscopic recognition of guanine dimeric hairpin quadruplexes by a carbocyanine dye" *Proc. Natl. Acad. Sci. USA* **1996**, *93*, 2635.
- Chessari, G.; Hunter, C.A.; Low, C.M.; Packer, M.J.; Vinter, J.G.; Zonta, C. "An evaluation of force-field treatments of aromatic interactions" *Chemistry* **2002**, *8*, 2860.

- Crnugelj, M.; Hud, N.V.; Plavec, J. "The solution structure of d($G_4T_4G_3$): a bimolecular quadruplex with a novel fold" *J. Mol. Biol.* **2002**, *320*, 911.
- Crossland, R.K.; Servis, K.L. "Facile synthesis of methanesulfonate esters" *J. Org. Chem.* **1970**, *35*, 3195.
- de Lange, T.; Shiue, L.; Myers, R.M.; Cox, D.R.; Naylor, S.L.; Killery, A.M.; Varmus, H.E. "Structure and variability of human chromosome ends" *Mol. Cell. Biol.* **1990**, *10*, 518.
- Fang, G.; Cech, T.R. "Characterization of a G-quartet formation reaction promoted by the beta-subunit of the Oxytricha telomere-binding protein" *Biochemistry* **1993**, *32*, 11646.
- Fedoroff, O.Y.; Rangan, A.; Chemeris, V.V.; Hurley, L.H. "Cationic porphyrins promote the formation of i-motif DNA and bind peripherally by a nonintercalative mechanism" *Biochemistry* **2000**, *39*, 15083.
- Fedoroff, O.Y.; Salazar, M.; Han, H; Chemeris, V.V.; Kerwin, S.M.; Hurley, L.H. "NMR-Based model of a telomerase-inhibiting compound bound to G-quadruplex DNA" *Biochemistry* **1998**, *37*, 12367.
- Feng, J.L.; Funk, W.D.; Wang, S.S.; Weinrich, S.L.; Avilion, A.A.; Chiu, C.P.; Adams, R.R.; Chang, E.; Allsopp, R.C.; Yu, J.H.; Le, S.Y.; West, M.D.; Harley, C.B.; Andrews, W.H.; Greider, C.W.; Villeponteau, B. "The RNA component of human telomerase" *Science* **1995**, *269*, 1236.
- Franceschin, M.; Alvino, A.; Ortaggi, G.; Bianco, A. "New hydrosoluble perylene and coronene derivatives" *Tetrahedron Lett.* **2004**, *45*, 9015.
- Galderisi, U.; Cascino, A.; Giordano, A. "Antisense oligonucleotides as therapeutic agents" *J. Cell Physiol.* **1999**, *181*, 251.
- Gan, Y.; Lu, J.; Johnson, A.; Wientjes, M.G.; Schuller, D.E.; Au, J.L. "A quantitative assay of telomerase activity" *Pharmaceutical Res.* **2001**, *18*, 488.
- Ghosh, A.K.; Bhattacharyya, F.K.; Ghosh, D.K. "Leishmania donovani: amastigote inhibition and mode of action of berberine" *Exp. Parasitol.* **1985**, *60*, 404.
- Gomez, D.; Mergny, J.L.; Riou, J.F. "Detection of telomerase inhibitors based on g-quadruplex ligands by a modified telomeric repeat amplification protocol assay" *Cancer Res.* **2002**, *62*, 3365.
- Grand, C.L.; Han, H.; Munoz, R.M.; Weitman, S.; Von Hoff, D.D.; Hurley, L.H.; Bearss, D.J. "The cationic porphyrin TMPyP4 down-regulates c-MYC and human

telomerase reverse transcriptase expression and inhibits tumor growth *in vivo*" *Mol. Cancer Ther.* **2002**, *1*, 565.

- Griffith, J.D.; Comeau, L.; Rosenfield, S.; Stansel, R.M.; Bianchi, A.; Moss, H.; de Lange, T. "Mammalian telomeres end in a large duplex loop" *Cell* **1999**, *97*, 503.
- Grimme, S. "Accurate description of van der Waals complexes by density functional theory including empirical corrections" *J. Comput. Chem.* **2004**, *25*, 1463.
- Hahn, W.C.; Stewart, S.A.; Brooks, M.W.; York, S.G.; Eaton, E.; Kurachi, A.; Beijersbergen, R.L.; Knoll, J.H.M.; Meyerson, M.; Weinberg, R.A. "Inhibition of telomerase limits the growth of human cancer cells" *Nature Med.* **1999**, *5*, 1164.
- Haider, S.M.; Parkinson, G.N.; Neidle, S. "Crystal structure of the potassium form of an *Oxytricha nova* G-quadruplex" *J. Mol. Biol.* **2002**, *320*, 189.
- Halvorsen, T.L.; Leibowitz, G.; Levine, F. "Telomerase activity is sufficient to allow transformed cells to escape from crisis" *Mol. Cell. Biol.* **1999**, *19*, 1864.
- Han, H.; Bennett, R.J.; Hurley, L.H. "Inhibition of unwinding of G-quadruplex structures by Sgs1 helicase in the presence of N,N'-bis[2-(1-piperidino)ethyl]-3,4,9,10-perylenetetracarboxylic diimide, a G-quadruplex-interactive ligand" *Biochemistry* **2000**, *39*, 9311.
- Han, H.; Cliff, C.L.; Hurley, L.H. "Accelerated assembly of G-quadruplex structures by a small molecule" *Biochemistry* **1999**, *38*, 6981.
- Han, H.; Langley, D.R.; Rangan, A.; Hurley, L.H. "Selective interactions of cationic porphyrins with G-quadruplex structures" *J. Am. Chem. Soc.* **2001**, *123*, 8902.
- Harley, C.B.; Futcher, A.B.; Greider, C.W. "Telomeres shorten during ageing of human fibroblasts" *Nature* **1990**, *345*, 458.
- Harrison, R.J.; Cuesta, J.; Chessari, G.; Read, M.A.; Basra, S.K.; Reszka, A.P.; Morrell, J.; Gowan, S.M.; Incles, C.M.; Tanious, F.A.; Wilson, W.D.; Kelland, L.R.; Neidle, S. "Trisubstituted acridine derivatives as potent and selective telomerase inhibitors" *J. Med. Chem.* **2003**, *46*, 4463.
- Harrison, R.J.; Gowan, S.M.; Kelland, L.R.; Neidle, S. "Human telomerase inhibition by substituted acridine derivatives" *Bioorg. Med. Chem. Lett.* **1999**, *9*, 2463.
- Henderson, E.; Hardin, C.C.; Walk, S.K.; Tinoco I. Jr.; Blackburn, E.H. "Telomeric DNA oligonucleotides form novel intramolecular structures containing guanine-guanine base pairs" *Cell* **1987**, *51*, 899.
- Hiyama, E.; Hiyama, K. "Telomerase as tumor marker" *Cancer Lett.* **2003**, *194*, 221.

- Incles, C.M.; Schultes, C.M.; Neidle, S. "Telomerase inhibitors in cancer therapy: current status and future directions" *Curr. Opin. Investig. Drugs* **2003**, *4*, 675.
- Karlseder, J. "Telomere repeat binding factors: keeping the ends in check" *Cancer Lett.* **2003**, *194*, 189.
- Karlseder, J.; Smogorzewska, A.; de Lange, T. "Senescence induced by altered telomere state, not telomere loss" *Science* **2002**, *295*, 2446.
- Kern, J.T.; Kerwin, S.M. "The aggregation and G-quadruplex DNA selectivity of charged 3,4,9,10-perylenetetracarboxylic acid diimides" *Bioorg. Med. Chem. Lett.* **2002**, *12*, 3395.
- Kern, J.T.; Thomas, P.W.; Kerwin, S.M. "The relationship between ligand aggregation and G-quadruplex DNA selectivity in a series of 3,4,9,10-perylenetetracarboxylic acid diimides" *Biochemistry* **2002**, *41*, 11379.
- Kerwin, S.M.; Chen, G.; Kern, J.T.; Thomas, P.W. "Perylene diimide G-quadruplex DNA binding selectivity is mediated by ligand aggregation" *Bioorg. Med. Chem. Lett.* **2002**, *12*, 447.
- Kim, J.H.; Chung, J.N.; Paik, Y.K.; Park, J.; Kim, E.D.; Lee, Y.S.; Kim, S.E. "Preparation of protoberberine derivatives as antifungal agents" *Patent* US 6008356 (**1999**)
- Kim, M.Y.; Gleason-Guzman, M.; Izbicka, E.; Nishioka, D.; Hurley, L.H. "The different biological effects of telomestatin and TMPyP4 can be attributed to their selectivity for interaction with intramolecular or intermolecular G-quadruplex structures" *Cancer Res.* **2003**, *63*, 3247.
- Kim, M.Y.; Vankayalapati, H.; Shin-Ya, K.; Wierzba, K.; Hurley, L.H. "Telomestatin, a potent telomerase inhibitor that interacts quite specifically with the human telomeric intramolecular G-quadruplex" *J. Am. Chem. Soc.* **2002**, *124*, 2098.
- Kim, N.W.; Piatyszek, M.A.; Prowse, K.R.; Harley, C.B.; West, M.D.; Ho, P.L.C.; Coviello, G.M.; Wright, W.E.; Weinrich, S.L.; Shay, J.W. "Specific association of human telomerase activity with immortal cells and cancer" *Science* **1994**, *266*, 2011.
- Kim, N.W.; Wu, F. "Advances in quantification and characterization of telomerase activity by the telomeric repeat amplification protocol (TRAP)" *Nucleic Acid Res.* **1997**, *25*, 2595.
- Kipling, D. "The telomere", Oxford University Press (**1995**).

- Koeppel, F.; Riou, J.F.; Laoui, A.; Mailliet, P.; Arimondo, P.B.; Labit, D.; Petitgenet, O.; Helene, C.; Mergny, J.L. "Ethidium derivatives bind to G-quartets, inhibit telomerase and act as fluorescent probes for quadruplexes" *Nucleic Acids Res.* **2001**, *29*, 1087.
- Latimer, L.J.; Payton, N.; Forsyth, G.; Lee, J.S. "The binding of analogues of coralyne and related heterocyclics to DNA triplexes" *Biochem. Cell Biol.* **1995**, *73*, 11.
- Liu, Z. R.; Rill, R. L. "N,N'-bis[3,3'-(dimethylamino)propylamine]-3,4,9,10-perylenetetracarboxylic diimide, a dicationic perylene dye for rapid precipitation and quantitation of trace amounts of DNA" *Analytical Biochemistry* **1996**, *236*, 139.
- Lue, N.F. "Adding to the ends: what makes telomerase processive and how important is it?" *Bioessays* **2004**, *26*, 955.
- Lundblad, V. "Telomere maintenance without telomerase" *Oncogene* **2002**, *21*, 522.
- Makarov, V.L.; Hirose, Y.; Langmore, J.P. "Long G tails at both ends of human chromosomes suggest a C strand degradation mechanism for telomere shortening" *Cell* **1997**, *88*, 657.
- Mergny, J.L., Helene, C. "G-quadruplex DNA: a target for drug design" *Nat. Med.* **1998**, *4*, 1366.
- Mergny, J.L.; Lacroix, L.; Teulade-Fichou, M.P.; Hounsou, C.; Guittat, L.; Hoarau, M.; Arimondo, P.B.; Vigneron, J.P.; Lehn, J.M.; Riou, J.F.; Garestier, T.; Helene, C. "Telomerase inhibitors based on quadruplex ligands selected by a fluorescence assay" *Proc. Natl. Acad. Sci. USA* **2001**, *98*, 3062.
- Mergny, J.L.; Maurizot, J.C. "Fluorescence resonance energy transfer as a probe for G-quartet formation by a telomeric repeat" *Chembiochem.* **2001**, *2*, 124.
- Mergny, J.L.; Riou, J.F.; Mailliet, P.; Teulade-Fichou, M.P.; Gilson, E. "Natural and pharmacological regulation of telomerase" *Nucleic Acids Res.* **2002**, *30*, 839.
- Mitkin, O.D.; Kombarov, R.V.; Yurovskaya, M.A. "Indoles from 3-nitropyridinium salts:1 an extension of the transformation method on 5-substituted indoles" *Tetrahedron* **2001**, *57*, 1827.
- Morin, G.B. "The human telomere terminal transferase enzyme is a ribonucleoprotein that synthesizes TTAGGG repeats" *Cell* **1989**, *59*, 521.
- Naasani, I.; Seimiya, H.; Yamori, T.; Tsuruo, T. "FJ5002: a potent telomerase inhibitor identified by exploiting the disease-oriented screening program with COMPARE analysis" *Cancer Research* **1999**, *59***,** 4004Nakamura, T.M.; Morin, G.B.;

Chapman, K.B.; Weinrich, S.L.; Andrews, W.H.; Lingner, J.; Harley, C.B.; Cech, T.R. "Telomerase catalytic subunit homologs from fission yeast and human" *Science* **1997**, *277*, 955.

- Negri, R.; Costanzo, G.; Saladino, R.; Di Mauro, E. "One-step, one-lane chemical DNA sequencing by N-methylformamide in the presence of metal ions" *Biotechniques* **1996**, *21*, 910.
- Neidle, S.; Parkinson, G. "Telomere maintenance as a target for anticancer drug discovery" *Nat. Rev. Drug Discov.* **2002**, *1*, 383.
- Neidle, S.; Parkinson, G.N. "The structure of telomeric DNA" *Curr. Opin. Struct. Biol.* **2003**, *13*, 275.
- Osiadacz, J.; Majka, J.; Czarnecki, K.; Peczynska-Czoch, W.; Zakrzewska-Czerwinska, J.; Kaczmarek, L.; Sokalski, W.A. "Sequence-selectivity of 5,11-dimethyl-5H-indolo[2,3-b]quinoline binding to DNA. Footprinting and molecular modeling studies" *Bioorg. Med. Chem.* **2000**, *8*, 937.
- Parkinson, G.N.; Lee, M.P.; Neidle, S. "Crystal structure of parallel quadruplexes from human telomeric DNA" *Nature* **2002**, *417*, 876.
- Perry, P.J.; Jenkins, T.C. "Recent advances in the development of telomerase inhibitors for the treatment of cancer" *Expert Opin. Invest. Drugs* **1999**, *8*, 1981.
- Phan, A.T.; Gueron, M.; Leroy, J.L. "The solution structure and internal motions of a fragment of the cytidine-rich strand of the human telomere" *J. Mol. Biol.* **2000**, *299*, 123.
- Phan, A.T.; Mergny, J.L. "Human telomeric DNA: G-quadruplex, i-motif and Watson-Crick double helix" *Nucleic Acids Res.* **2002**, *30*, 4618.
- Rangan, A.; Fedoroff, O.Y.; Hurley, L.H. "Induction of duplex to G-quadruplex transition in the c-myc promoter region by a small molecule" *J. Biol. Chem.* **2001**, *276*, 4640.
- Read, M.; Harrison, R.J.; Romagnoli, B.; Tanious, F.A.; Gowan, S.H.; Reszka, A.P.; Wilson, W.D.; Kelland, L.R.; Neidle, S. "Structure-based design of selective and potent G quadruplex-mediated telomerase inhibitors" *Proc. Natl. Acad. Sci. USA* **2001**, *98*, 4844.
- Read, M.A.; Neidle, S. "Structural characterization of a guanine-quadruplex ligand complex" *Biochemistry* **2000**, *39*, 13422.

- Read, M.A.; Wood, A.A.; Harrison, J.R.; Gowan, S.M.; Kelland, L.R.; Dosanjh, H.S.; Neidle, S. "Molecular modeling studies on G-quadruplex complexes of telomerase inhibitors: structure-activity relationships" *J. Med. Chem.* **1999**, *42*, 4538.
- Reddel, R.R.; Bryan, T.M.; Murnane, J.P. "Immortalized cells with no detectable telomerase activity. A review." *Biochemistry (Mosc).* **1997**, *62*, 1254.
- Ren, J.; Chaires, J.B. "Sequence and structural selectivity of nucleic acid binding ligands" *Biochemistry* **1999**, *38*, 16067.
- Rezler, E.M.; Bearss, D.J.; Hurley, L.H. "Telomere inhibition and telomere disruption as processes for drug targeting" *Annu. Rev. Pharmacol. Toxicol.* **2003**, *43*, 359.
- Rhodes, D.; Giraldo, R. "Telomere structure and function" *Curr. Opin. Struct. Biol.* **1995**, *5*, 311
- Riou, J.F.; Guittat, L.; Mailliet, P.; Laoui, A.; Renou, E.; Petitgenet, O.; Megnin-Chanet, F.; Helene, C.; Mergny, J.L. "Cell senescence and telomere shortening induced by a new series of specific G-quadruplex DNA ligands" *Proc. Natl. Acad. Sci. USA* **2002**, *99*, 2672.
- Rohr, U.; Kohl, C.; Mullen, K.; van de Craats, A.; Warman, J. "Liquid crystalline coronene derivatives" *J. Mater. Chem.* **2001**, *11*, 1789.
- Rohr, U.; Schlichting, P.; Bohm, A.; Gross, M.; Meerholz, K.; Brauchle, C.; Mullen, K. "Liquid crystalline coronene derivatives with extraordinary fluorescence properties" *Angew. Chem. Int. Ed.* **1998**, *37*, 1434.
- Rossetti, L.; Franceschin, M.; Bianco, A.; Ortaggi, G.; Savino, M. "Perylene diimides with different side chains are selective in inducing different G-quadruplex DNA structures and in inhibiting telomerase" *Bioorg. Med. Chem. Lett*. **2002,** *12***,** 2527.
- Rossetti, L.; Franceschin, M.; Schirripa, S.; Bianco, A.; Ortaggi, G.; Savino, M. "Selective interactions of perylene derivatives having different side chains with inter- and intramolecular G-quadruplex structures. A correlation with telomerase inhibition" *Bioorg. Med. Chem. Lett*. **2005**, *15*, 413.
- Saldanha, S.N.; Andrews, L.G.; Tollefsbol, T.O. "Assessment of telomere length and factors that contribute to its stability" *Eur. J. Biochem.* **2003**, *270*, 389
- Schaffitzel, C.; Berger, I.; Postberg, J.; Hanes, J.; Lipps, H.J.; Pluckthun, A. "In vitro generated antibodies specific for telomeric guanine-quadruplex DNA react with *Stylonychia lemnae* macronuclei" *Proc. Natl. Acad. Sci. USA* **2001**, *98*, 8572.

- Shay, J.W.; Wright, W.E. "Telomerase: a target for cancer therapeutics" *Cancer Cell* **2002**, *2*, 257.
- Shin-ya, K.; Wierzba, K.; Matsuo, K.; Ohtani, T.; Yamada, Y.; Furihata, K.; Hayakawa, Y.; Seto, H. "Telomestatin, a novel telomerase inhibitor from *Streptomyces anulatus*" *J. Am. Chem. Soc.* **2001**, *123*, 1262.
- Siddiqui-Jain, A.; Grand, C.L.; Bearss, D.J.; Hurley, L.H. "Direct evidence for a G-quadruplex in a promoter region and its targeting with a small molecule to repress c-MYC transcription" *Proc. Natl. Acad. Sci. USA* **2002**, *99*, 11593.
- Simonsson, T. "G-quadruplex DNA structures-variations on a theme" *Biol. Chem.* **2001**, *382*, 621.
- Sonogashira, K.; Tohda, Y.; Hagihara, N. "Convenient synthesis of acetylenes. Catalytic substitutions of acetylenic hydrogen with bromo alkenes, iodo arenes, and bromopyridines" *Tetrahedron Lett.*, **1975**, 4467.
- Stansel, R.M.; de Lange, T.; Griffith, J.D. "T-loop assembly in vitro involves binding of TRF2 near the 3' telomeric overhang" *EMBO J.* **2001**, *20*, 5532.
- Strahl, C.; Blackburn, E.H. "Effects of reverse transcriptase inhibitors on telomere length and telomerase activity in two immortalized human cell lines" *Mol. Cell. Biol.* **1996**, *16*, 53.
- Teulade-Fichou, M.P.; Carrasco, C.; Guittat, L.; Bailly, C.; Alberti, P.; Mergny, J.L.; David, A.; Lehn, J.M.; Wilson, W.D. "Selective recognition of G-quadruplex telomeric DNA by a bis(quinacridine) macrocycle" *J. Am. Chem. Soc.* **2003**, *125*, 4732.
- Wang, S.S.; Zakian, V.A. "Telomere-telomere recombination provides an express pathway for telomere acquisition" *Nature* **1990**, *345*, 456.
- Wang, Y.; Patel, D.J. "Solution structure of the human telomeric repeat d[$AG_3(T_2AG_3)_3$]" *Structure* **1993**, *1*, 263.
- Watson, J.D. "Origin of concatemeric T7 DNA" *Nat. New Biol.* **1972**, *239*, 197.
- Watson, J.D.; Hopkins, N.; Roberts, J.; Steiz, J.; Weiner, A. "Molecular Biology of the Gene", Benjamin-Cummings (**1987**).
- White, L.K.; Wright, W.E.; Shay, J.W. "Telomerase inhibitors" *Trends Biotechnol.* **2001**, *19*, 114.
- Williamson, J.R. "G-quartet structures in telomeric DNA" *Annu. Rev. Biophys. Biomol. Struct.* **1994**, *23*, 703.

- Williamson, J.R. “Guanine quartets” *Curr. Opin. Struct. Biol.* **1993**, *3*, 357.
- Williamson, J.R.; Raghuraman, M.K.; Cech, T.R. “Monovalent cation-induced structure of telomeric DNA: the G-quartet model” *Cell* **1989**, *59*, 871.
- Wright, W.E.; Tesmer, V.M.; Huffman, K.E.; Levene, S.D.; Shay, J.W. “Normal human chromosomes have long G-rich telomeric overhangs at one end” *Genes Dev.* **1997**, *11*, 2801
- Wu, H.L.; Hsu, C.Y.; Liu, W.H.; Yung, B.Y. “Berberine-induced apoptosis of human leukemia HL-60 cells is associated with down-regulation of nucleophosmin/B23 and telomerase activity” *Int. J. Cancer.* **1999**, *81*, 923.
- Zahler, A.M.; Williamson, J.R.; Cech, T.R.; Prescott, D.M. “Inhibition of telomerase by G-quartet DNA structures” *Nature* **1991**, *350*, 718.
- Zee-Cheng, K.Y.; Cheng, C.C. “Practical preparation of coralyne chloride” *J. Pharm. Sci.* **1972**, *61*, 969.
- Zhang, R.X. “Laboratory studies of berberine used alone and in combination with 1,3-bis(2-chloroethyl)-1-nitrosourea to treat malignant brain tumors” *Chinese Med. J.* **1990**, *103*, 658.
- Zhang, X.; Mar, V.; Zhou, W.; Harrington, L.; Robinson, M.O. “Telomere shortening and apoptosis in telomerase-inhibited human tumor cells” *Genes Dev.* **1999**, *13*, 2388.

8. Figure Index

9. Acknowledgments

I would like to express my gratitude to professor Neidle who hosted me in his group, and to all the members of the Cancer Research UK Biomolecular Structure Group, at the School of Pharmacy of the University of London, where I could perform all FRET experiments and molecular modeling studies. In particular, I would like to thank Christoph Schultes for his patience and help in teaching me all I needed to know and Irene, for her kindness and attention towards me.

Now, I beg pardon to the English reader, but I would like to express my acknowledgments in my own language, to fully and correctly express my feelings.

Ringraziamenti

Chi fa ricerca, o lo ha fatto per un periodo abbastanza lungo della propria vita, sa che questo non è un lavoro come un altro. Fare ricerca è un lavoro senza orario, che non finisce quando si esce dal laboratorio. Può essere entusiasmante, quando si hanno risultati interessanti, frustrante quando non se ne hanno, ma in ogni caso totalizzante. Per questo motivo, in questi "ringraziamenti", vita professionale e personale rimarranno indissolubilmente legate, com'è giusto che sia.

Non a caso, quindi, il primo grazie va a persone non direttamente legate al mio lavoro di tesi, ma che per me sono così importanti: Marco, Mauro e Fabiana. È impossibile misurare quanto grande sia questo "grazie" e contare i piccoli e grandi episodi che ci sono dietro; semplicemente non potrei immaginare questi anni senza di loro. Hanno condiviso con me successi e sconfitte, momenti di entusiasmo e di delusione, hanno partecipato delle mie gioie, mi hanno sostenuto nei momenti difficili, mi hanno criticato con affetto quando è stato necessario, ma, cosa che ho apprezzato più di tutte, mi hanno sopportato in momenti in cui risultavo insopportabile perfino a me stesso. A Fabiana va un grazie "doppio", per la sua preziosa consulenza sul molecular modeling.

Un grazie di cuore agli amici di sempre: Roberta, a cui mi unisce una profonda amicizia,

Francesco, Manuel, con cui ho potuto vivere in parallelo tante tappe fondamentali delle mie scelte professionali, Federica e Davide. Con loro ho passato innumerevoli serate rilassanti e divertenti, piacevoli vacanze e immancabili capodanni.

Alla mia famiglia "allargata" (mamma, papà, Laura e Luciana) vorrei rivolgere un ringraziamento particolare, per avermi sostenuto, non solo economicamente, in tutti questi anni, senza interferire nelle mie scelte. Con il tempo abbiamo reciprocamente imparato, a volte non senza aspre discussioni, che non sempre possiamo realizzare le aspettative reciproche, ma che questo non ci impedisce di volerci bene. Oggi ci vediamo forse meno spesso, ma stiamo davvero bene insieme, e se sono riuscito a realizzare alcuni sogni lo devo sicuramente al loro sostegno.

Un doveroso grazie ai professori Ortaggi, Bianco e Savino, che hanno seguito strettamente il mio lavoro di ricerca in questi anni. Non sono mancati momenti di incomprensione, ma spesso proprio da questi sono nati nuovi slanci e nuove idee. Hanno creduto nel mio lavoro e mi hanno dato la possibilità di lavorare in maniera autonoma, in un contesto di collaborazione estremamente piacevole.

Un profondo grazie ad Antonello Alvino, Anna D'Ambrosio e Stefano Schirripa, il cui contributo è stato fondamentale per lo sviluppo, rispettivamente, della sintesi di derivati perilenici e coronenici, dei derivati della berberina e dello studio biofisico dei complessi DNA-perilendiimmidi.

Ringraziare Luigi Rossetti solo per i saggi biologici sarebbe davvero riduttivo. Prima "maestro", poi amico e collega, ha seguito costantemente il mio lavoro di ricerca, aiutandomi in molti momenti fondamentali. Grazie al suo costante buonumore, ha il merito di continuare a mantenere nel "lab9" di Biologia Molecolare l'ambiente di lavoro più piacevole tra i vari laboratori in cui ho avuto occasione di lavorare. A questo clima hanno contribuito e continuano a contribuire molte persone, ma la presenza di Rosella mi manca in maniera particolare.

Un ringraziamento alla dottoressa Galli per l'analisi elementare di tutti i composti sintetizzati, al signor Piccioni per gli spettri NMR a 300 MHz e al dottor Dorio per la spettrometria di massa.

Un grazie a tutte le persone del Dipartimento di Chimica con cui ho piacevolmente interagito in questi anni. In particolare: Andrea Masotti, con cui, continuando a dividere studio, laboratorio e impegni didattici, non mancano occasioni di utile scambio di idee; il professor Barteri, che condivide con me la passione per la "Chimica dei Sistemi Biologici"; i professori De Santis, Guiso e Bonadies, che sono stati sempre disponibili ad un proficuo confronto sulle materie di propria competenza; Antonella Dimitrio, che, oltre ad essere estremamente efficiente nel proprio lavoro, possiede la capacità di regalare un sorriso ad ogni persona e una umanità, che la rendono davvero insostituibile; Annamaria, che, spesso come me ancora al lavoro alle otto e mezzo di sera, ha piacevolmente alleggerito con la sua simpatia le lunghe giornate di lavoro e mi ha più volte pazientemente aiutato, a dipartimento ormai chiuso, a regolare lo stillicidio di interminabili colonne cromatografiche; Alessia, Cristiana, Claudia, Carolina, Angela, Raffaella e Diana, che in modi e momenti diversi hanno contribuito a rendere divertenti e produttivi questi anni di lavoro.

Un grazie alle persone che, all'interno della Società Chimica Italiana, hanno apprezzato il mio entusiasmo e la mia iniziativa. In particolare, Henriette Molinari, che è la prima persona all'interno della SCI con cui ho cominciato a collaborare, il professor Bonora e tutti i membri del Consiglio Direttivo della Divisione di Chimica dei Sistemi Biologici, che continuano ad apprezzare il mio lavoro, e i membri del Consiglio Direttivo del Gruppo Giovani, insieme ai quali ho il piacere di portare avanti iniziative interessanti e stimolanti non solo per i giovani chimici, ma per tutte le persone che, in tempi davvero difficili in questo campo, si dedicano attivamente alla diffusione della cultura e della ricerca scientifica.

Un grazie particolare a Stefano che ha saputo dare un gusto speciale alla mia permanenza a Londra e, nel contempo, un motivo di rimpianto al momento della mia partenza.

Infine, un pensiero speciale va a Francesco, il cui gesto tragico e disperato ha rappresentato per me insieme momento di dolorosa riflessione, punto di partenza di tanti percorsi ed elemento con cui mi sono dovuto costantemente confrontare in questi anni. E in questo confronto, soprattutto nei momenti più difficili, ho spesso trovato un motivo per non demordere, energia per superare le difficoltà e in ultima analisi, quasi paradossalmente, l'amore per quella vita che egli, forse per un solo drammatico momento, ha irrevocabilmente disprezzato fino all'estremo.

Printed in Rome on Wednesday, 09 March 2005